AD NUMBER

ADB011646

LIMITATION CHANGES

TO:

Approved for public release; distribution is unlimited.

FROM:

Distribution authorized to U.S. Gov't. agencies only; Test and Evaluation; 16 MAR 1976. Other requests shall be referred to Naval Weapons Center, China Lake, CA 93555.

AUTHORITY

NWC Notice dtd 18 Jan 1978

NWC TP 5857

Measurement of Near-Field Blast Effects of Fluidically Encased Explosive Charges

by
Andre deKlerk
Denver Research Institute
for the
Propulsion Development Department

MAY 1976

Naval Weapons Center
CHINA LAKE, CALIFORNIA 93555

Naval Weapons Center

AN ACTIVITY OF THE NAVAL MATERIAL COMMAND

R. G. Freeman, III, RAdm., USN ..... Commander
G. L. Hollingsworth ..... Technical Director

FOREWORD

This final report describes an experimental investigation to determine the near-field blast effects of fluidically encased explosives. This investigation was conducted by the Denver Research Institute during the period September 1973 through May 1975. The work was sponsored by the Naval Weapons Center (NWC), China Lake, California, under Navy Contract N00123-72-C-0267 and supported by the Naval Air Systems Command under AirTask A350-3500/008B/5F32-352-500.

Dr. L. H. Smith, Mr. J. A. Weeks and Mr. R. R. Coates of NWC have reviewed this report for technical accuracy.

The effort reported herein is part of a continuing investigation and conclusions reached are subject to revision as work progresses. This report is released for information at the working level and does not necessarily reflect the views of NWC.

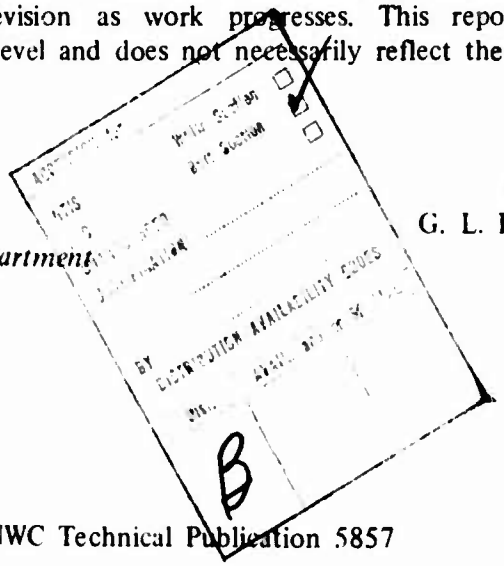

Released by
G. W. LEONARD, *Head*
Propulsion Development Department
9 April 1976

Under authority of
G. L. HOLLINGSWORTH
Technical Director

NWC Technical Publication 5857

Published by ..... Technical Information Department
Collation ..... Cover, 51 leaves
First printing ..... 175 unnumbered copies

UNCLASSIFIED

SECURITY CLASSIFICATION OF THIS PAGE (When Data Entered)

19 REPORT DOCUMENTATION PAGE	READ INSTRUCTIONS BEFORE COMPLETING FORM
1. REPORT NUMBER (18) NWC TP 5857 ✓	2. GOVT ACCESSION NO. / 3. RECIPIENT'S CATALOG NUMBER
4. TITLE (and Subtitle) (6) MEASUREMENT OF NEAR-FIELD BLAST EFFECTS OF FLUIDICALLY ENCASED EXPLOSIVE CHARGES•	5. TYPE OF REPORT & PERIOD COVERED (9) Final Rept. • Sept 1973–May 1975
	6. PERFORMING ORG. REPORT NUMBER
7. AUTHOR(s) (12) Andre deKlerk	8. CONTRACT OR GRANT NUMBER(s) (15) N00123-72-C-0267 ✓
9. PERFORMING ORGANIZATION NAME AND ADDRESS (16) Denver Research Institute ✓ University of Denver Denver, Colorado 80210	10. PROGRAM ELEMENT, PROJECT, TASK AREA & WORK UNIT NUMBERS Air Task A350-3500/008B/ 5F32-352-500
11. CONTROLLING OFFICE NAME AND ADDRESS Naval Weapons Center China Lake, California 93555	12. REPORT DATE (11) May 1976
	13. NUMBER OF PAGES 100 (12) 105 p.
14. MONITORING AGENCY NAME & ADDRESS (if different from Controlling Office)	15. SECURITY CLASS. (of this report) UNCLASSIFIED
	15a. DECLASSIFICATION/DOWNGRADING SCHEDULE

16. DISTRIBUTION STATEMENT (of this Report)

Distribution limited to U.S. Government agencies only; test and evaluation; 16 March 1976. Other requests for this document must be referred to the Naval Weapons Center.

17. DISTRIBUTION STATEMENT (of the abstract entered in Block 20, if different from Report)

18. SUPPLEMENTARY NOTES

19. KEY WORDS (Continue on reverse side if necessary and identify by block number)

EXPLOSIVE BLAST EFFECTS
FLUIDIC ENCASEMENT MATERIALS
PEAK PRESSURE
POSITIVE IMPULSE

20. ABSTRACT (Continue on reverse side if necessary and identify by block number)

See back of form.

DD FORM 1 JAN 73 1473 EDITION OF 1 NOV 65 IS OBSOLETE
S/N 0102-014-6601

UNCLASSIFIED 108 600
SECURITY CLASSIFICATION OF THIS PAGE (When Data Entered)

(U) *Measurement of Near-Field Blast Effects of Fluidically Encased Explosive Charges,* by Andre deKlerk, Denver Research Institute. China Lake, Calif., Naval Weapons Center, May 1976, 100 pp. (NWC TP 5857, publication UNCLASSIFIED.)

(U) A specialized explosive test facility for measuring near-field blast behavior of fluidic encased explosives was built and calibrated during this program. The primary pressure-time measurement system incorporated metallic Hopkinson bars to permit measurement and comparison of the blast effectiveness within the particulate environment generated by various fluidic encasement materials surrounding the explosive charges. The surrounding materials investigated included water, ethylene glycol, glycerol, glass, leaded glass and solder. A very substantial enhancement in both peak pressure and positive impulse was realized, especially for the higher density surrounding materials, i.e., glass, leaded glass and solder.

CONTENTS

INTRODUCTION

OBJECTIVES

The basic objectives of this program were to (1) build a test facility for measuring blast effectiveness and (2) empirically establish the comparative blast effectiveness of several types of fluidic encasement materials (surrounds).

PROCEDURE

Two different test facilities were constructed for determining the pressure-time history generated by encased test charges. The first facility consisted of a steel tank with Hopkinson pressure bars and a piezoelectric pressure gauge mounted radially along the circumference of the tank, as shown in Fig. 1. The explosive charge was centrally suspended inside the tank. Following a series of tests which utilized both bare charges and liquid surrounds, the steel tank started to rupture. Even though the tank was repaired and strengthened, it was felt that a more blast resistant test facility would be required to evaluate the remaining solid surround charges. A second facility was therefore constructed by modifying an existing test arena previously used for vaporific damage (VADAM) studies. This 4-foot-thick, reinforced concrete test arena is shown in Fig. 2. The Hopkinson bars and a piezoelectric pressure gauge were positioned in an existing central opening in the structure and were protected from the blast by a 3-inch-thick armor plate shield. Five instrumentation ports were placed 4 inches apart on a horizontal line to facilitate the mounting of the pressure gauges and Hopkinson pressure bars. The same charge standoff was retained at the second site to provide a comparison with data collected previously in the tank.

The fluidic surround materials used in the test series consisted of water, ethylene glycol, glycerol, glass, leaded glass and solder. Each material was test fired in five differing charge-to-mass ratios.

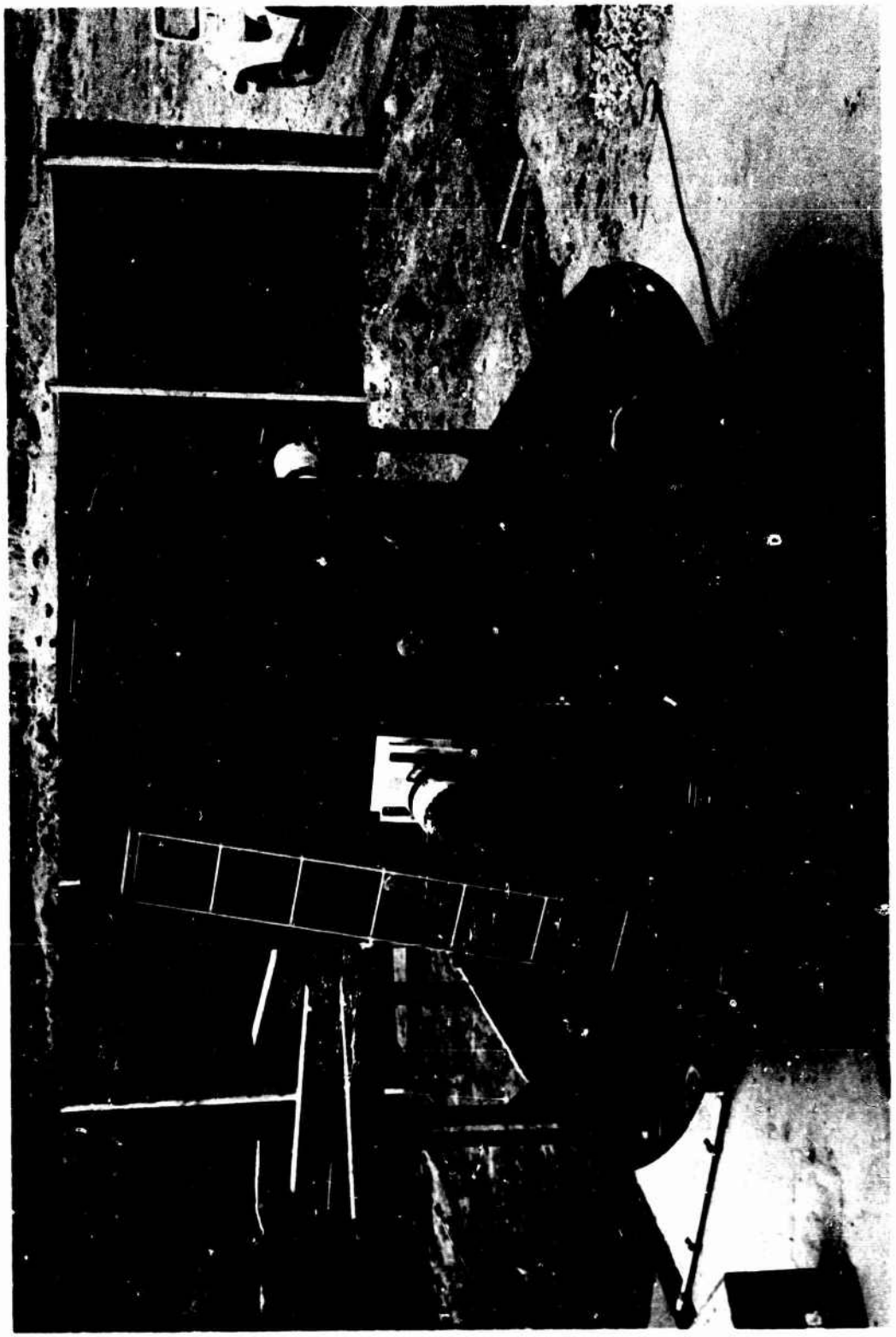

FIGURE 1. Tank Test Facility.

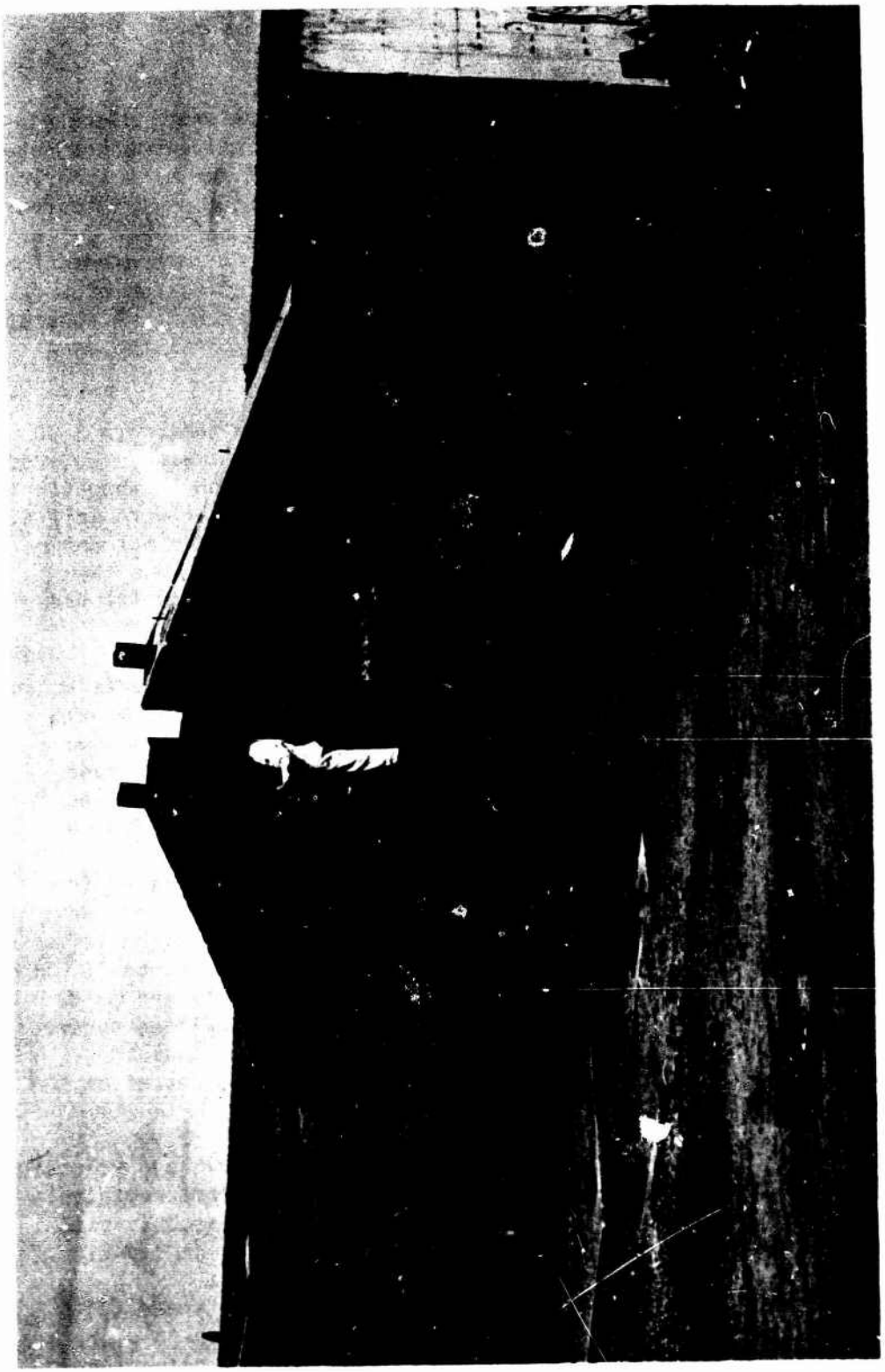

FIGURE 2. VADAM Test Facility.

FACILITY DESCRIPTION

PHYSICAL FACILITIES

A 6-foot diameter tank (Fig. 1), made of 3/4-inch steel plate was constructed to form the initial test facility. All explosive charges were suspended from the top of the tank and in the case of the bare spherical charges, the charge centerline coincided with the height of the instrumentation ports. When firing bare as well as encased pentolite cylinders, the lower edge of the charge was aligned with the instrumentation ports in each case to allow for the slight downward deflection of the blast wave due to initiating the cylinders at the upper end. A concrete, steel-clad, conically shaped blast deflector situated below the tank nullified the effects of ground reflections.

Twelve stainless steel flanges were welded to the tank with a 30 degree spacing between each flange. These flanges and their associated components formed the instrumentation ports, one of which is shown in Fig. 3. Nylon inserts having a 1/2-inch internal diameter were initially intended to encase the impact end of the Hopkinson pressure bar and permit a flush mounting of the bar with the inside surface of the tank wall. However, due to coupling problems encountered between the bar and the tank, it was eventually decided that the best data were realized when the pressure bars were positioned 1/16 of an inch behind the nylon insert. With this arrangement the nylon inserts acted as an orifice and directed the blast wave onto the impact end of the Hopkinson pressure bars. Inserts made from either nylon or lead were used to house the piezoelectric pressure transducers. In this case, however, the inserts were threaded internally using a 1/2-20 thread size. The piezoelectric pressure gauge assembly is shown in Fig. 4.

The suspension system for the Hopkinson bars was fabricated from wood and designed to assure the longest possible delay for shock wave transmission to the Hopkinson bars. One such suspension system is shown in Fig. 5. However, this system was later modified since it was very sensitive to wind gusts which caused the bars to sway and be deflected away from the instrumentation port exit. The modified system used the same wooden stands lowered by approximately 8 inches to accommodate a two point suspension system where the bars rested on two adjustable holders machined out of aluminum.

A make-screen chronometer was used to measure the average velocity imparted to an impulse plug by the blast wave. To generate repeatable data, the plug velocities had to be high enough to consistently break both of the screens without incurring any large velocity degradation. This resulted in 1/2-inch diameter aluminum impulse plugs having a length-to-diameter ratio approaching unity. Two problem areas immediately became apparent. One, due to the short length-to-diameter ratio, binding occurred between the impulse plug and the nylon insert.

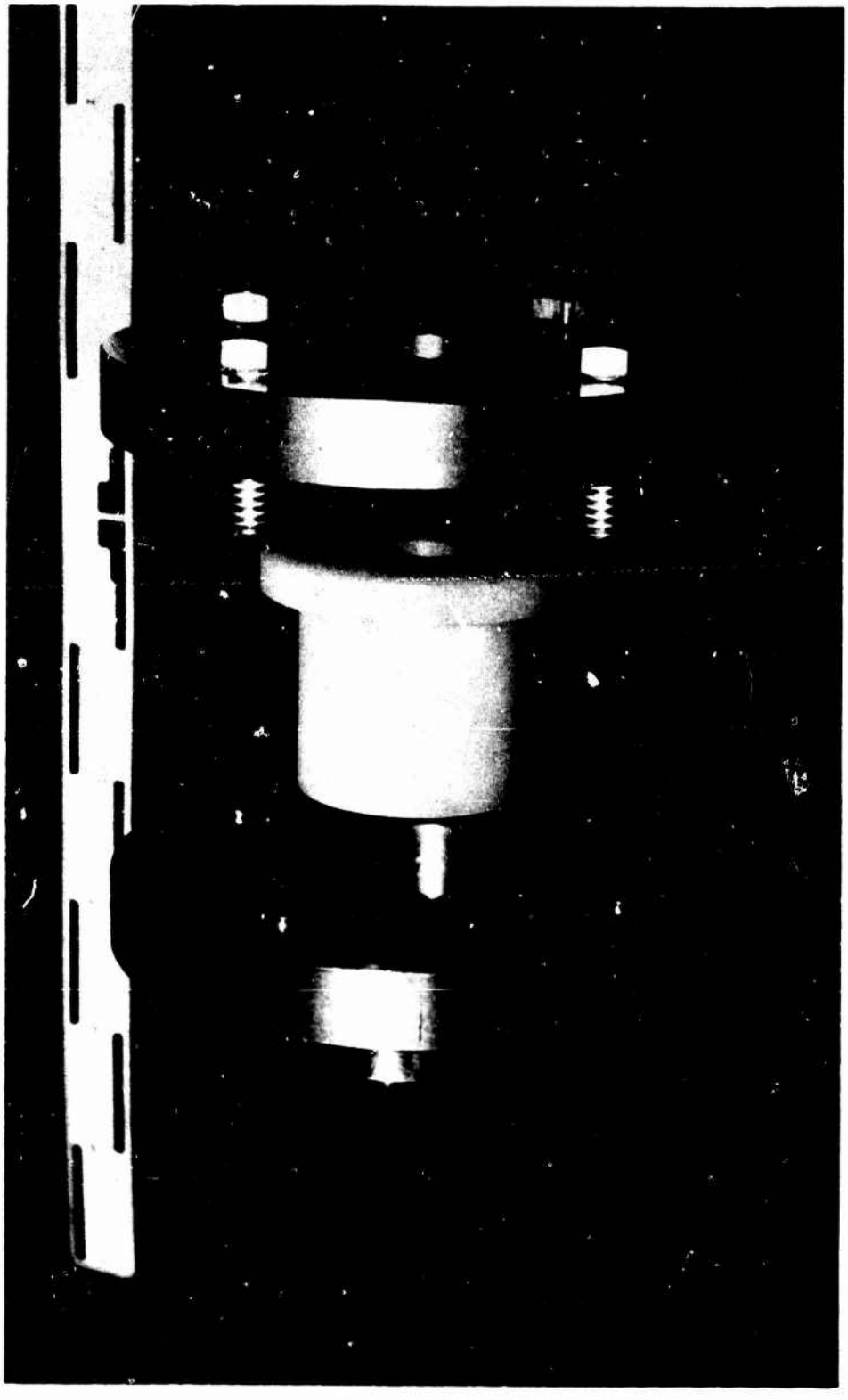

FIGURE 3. Expanded View of Instrumentation Port.

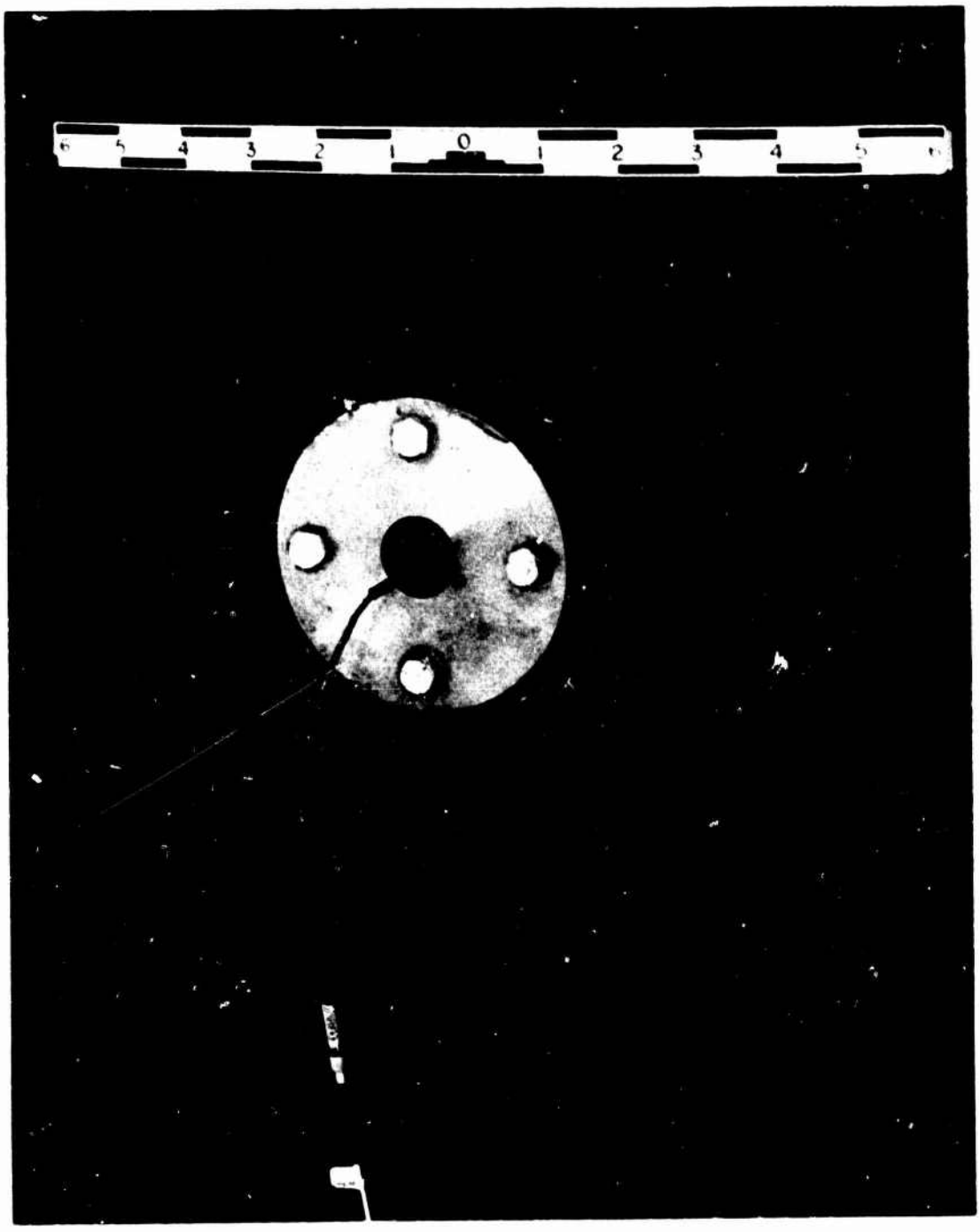

FIGURE 4. Piezoelectric Pressure Gauge Mounted in a Nylon Insert.

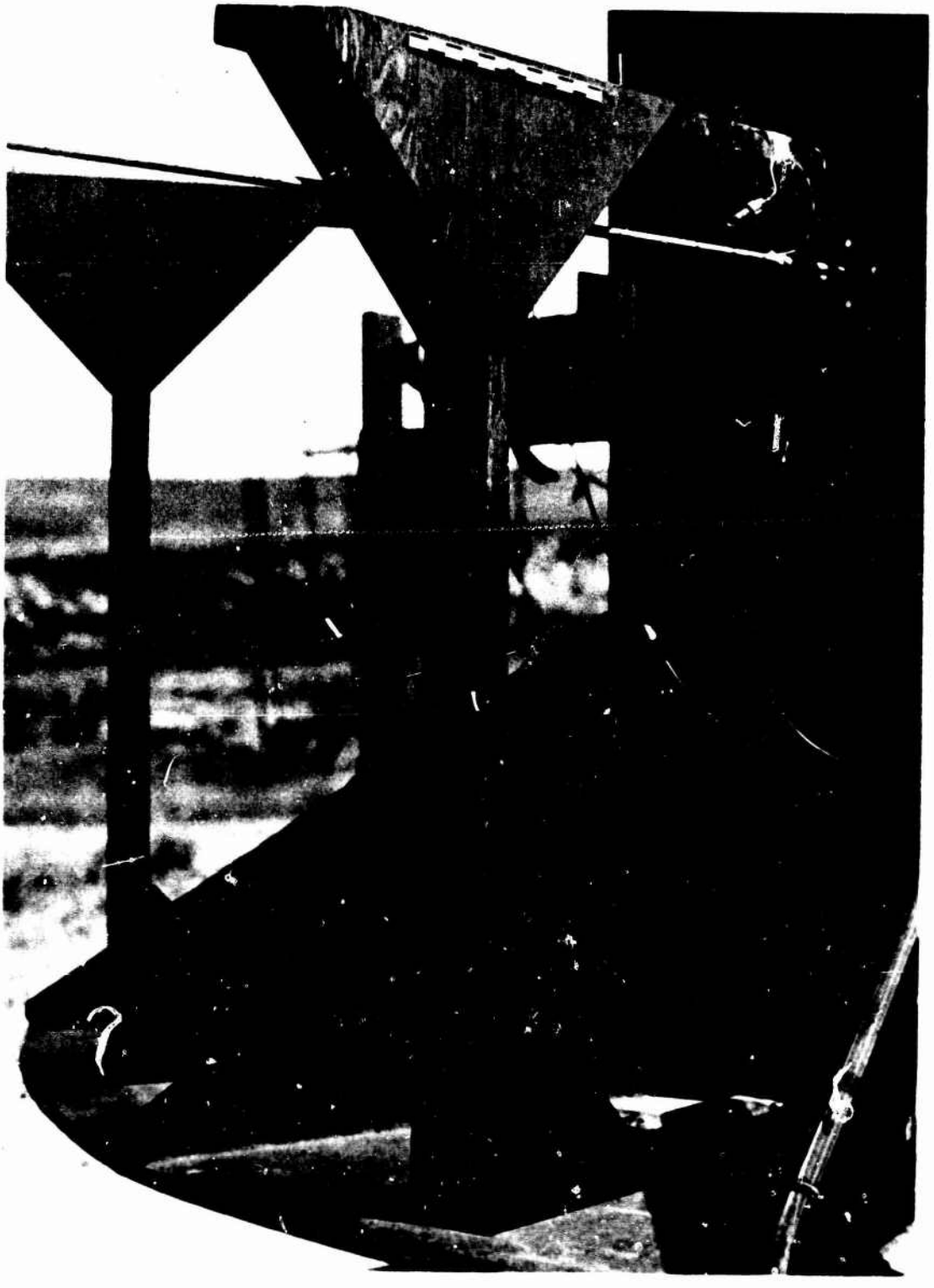

FIGURE 5. Hopkinson Bar Suspension Stand.

Two, because of the short plug length the trapped segment of impulse could only be on the order of 5 microseconds in length. To circumvent these problems, a prototype impulse trap was constructed which consisted of a string of suspended steel balls connected to the inside blast environment of the tank by means of a momentum transfer bar. By monitoring the excursion of the steel balls using a high speed camera, the incremental impulse shape could be calculated. Due to its flimsy construction, the prototype failed to produce the desired results. While the construction of such a system is possible, it would be fairly costly. Therefore this scheme was abandoned.

A moving vane trigger was mounted on a wooden dowel and inserted through one of the vacant stainless steel flanges containing a nylon insert with a one-inch internal diameter. This trigger and its associated circuitry was used to trigger the Tektronix 555 oscilloscopes on which the pressure-time curves were displayed.

The steel tank test facility was temporarily abandoned after firing only two of the test charges having solid surrounds due to the development of an 18-inch-long visible crack. The crack was symmetrically situated in a vertical direction above and below the instrumentation port line. It was repaired, however, by means of an inner and outer weld. The tank was further strengthened by the following structural modification. Two 9-inch-wide, 1/2-inch-thick steel bands were welded to the tank wall at locations 3-inches above and 3-inches below the ports. Twelve vertical stiffeners (6-inch by 48-inch by 3/4-inch) were then welded to the tank wall as well as to the twelve gussets that are mounted between the tank wall and skirt.

This modification to the tank appeared to solve the problem of possible rupture. A series of 15 liquid encased test charges were subsequently fired without incurring any visible adverse effects to the structure.

Since a series of 14 test charges having surrounds made of dense solids remained to be fired, it was mutually decided by personnel from Denver Research Institute (DRI) and NWC to construct a new test arena. A primary structure in existence at DRI fulfilled the basic requirements needed for this facility. The site chosen was the VADAM test facility illustrated in Fig. 2. This steel-clad concrete barricade is 34 feet long, 17 feet high and 4 feet thick with a throat 11 feet high and 4 feet wide in the center. A sheet of 3-inch-thick armor plate 63 inches wide and 106 inches high was bolted and welded across the throat of the barricade. The armor plate was also supported from below by a steel structure resting on the foundation shelf of the barricade. A slot 7 inches wide and 27 inches long, which had been cut in the armor plate, was positioned so that it ran horizontally part way across the throat of the barricade at a height of approximately 40 inches above the floor of the throat. A sheet of 3/4-inch-thick steel plate was bolted across the entire sheet of armor plate and to the barricade. The steel plate is shown in its final configuration in Fig. 6.

Five 1-inch diameter holes, spaced 4 inches apart on a horizontal line, were drilled in the 3/4-inch steel plate to provide instrumentation ports as shown in Fig. 7. The center hole was located approximately 24 inches from the edge and 51 inches from the bottom of the 3/4-inch steel plate. This positioned the instrumentation ports approximately 10 feet above ground level. Since the charge standoff distance was 36 inches the effects of ground reflections could be ignored. Two different types of inserts were constructed: one for the Hopkinson pressure bars, the other for the piezoelectric pressure transducers. The pressure bar ports, machined from high tensile strength steel bolts, formed an orifice with a 1/2-inch diameter and a 1 1/2-inch length. The Hopkinson pressure bars were supported at two points, the rear support being fixed, and the front one adjustable, both vertically and horizontally. The bars and supports are illustrated in Fig. 8. The impact end of each Hopkinson pressure bar was placed at a distance of 1/8-inch behind the exit of its corresponding instrumentation port. This increase in separation distance from the 1/16-inch distance used in the tank facility was required due to flexure of the steel plate assembly which resulted in contact between the pressure bars and the steel plate at the smaller separation distance when the larger charge sizes were fired. The piezoelectric pressure gauge insert was machined out of Lexan and tapped for a 1/2-20 thread. Provision was made to position a fragment stripper in front of the piezoelectric pressure transducer to protect it against possible damage. This fragment stripper, shown in Fig. 7, consisted of a 1/2-inch diameter steel bolt mounted approximately 6 inches in front of the insert holding the pressure gauge.

A boom was constructed to facilitate the suspension of the test charges at a constant standoff distance of 36 inches. The moving vane trigger was supported on a movable stand, located in a position 180 degrees away from the instrumentation ports, with respect to the charge position.

FIGURE 6. VADAM Test Fixture.

FIGURE 7. Instrumentation Ports and Fragment Stripper.

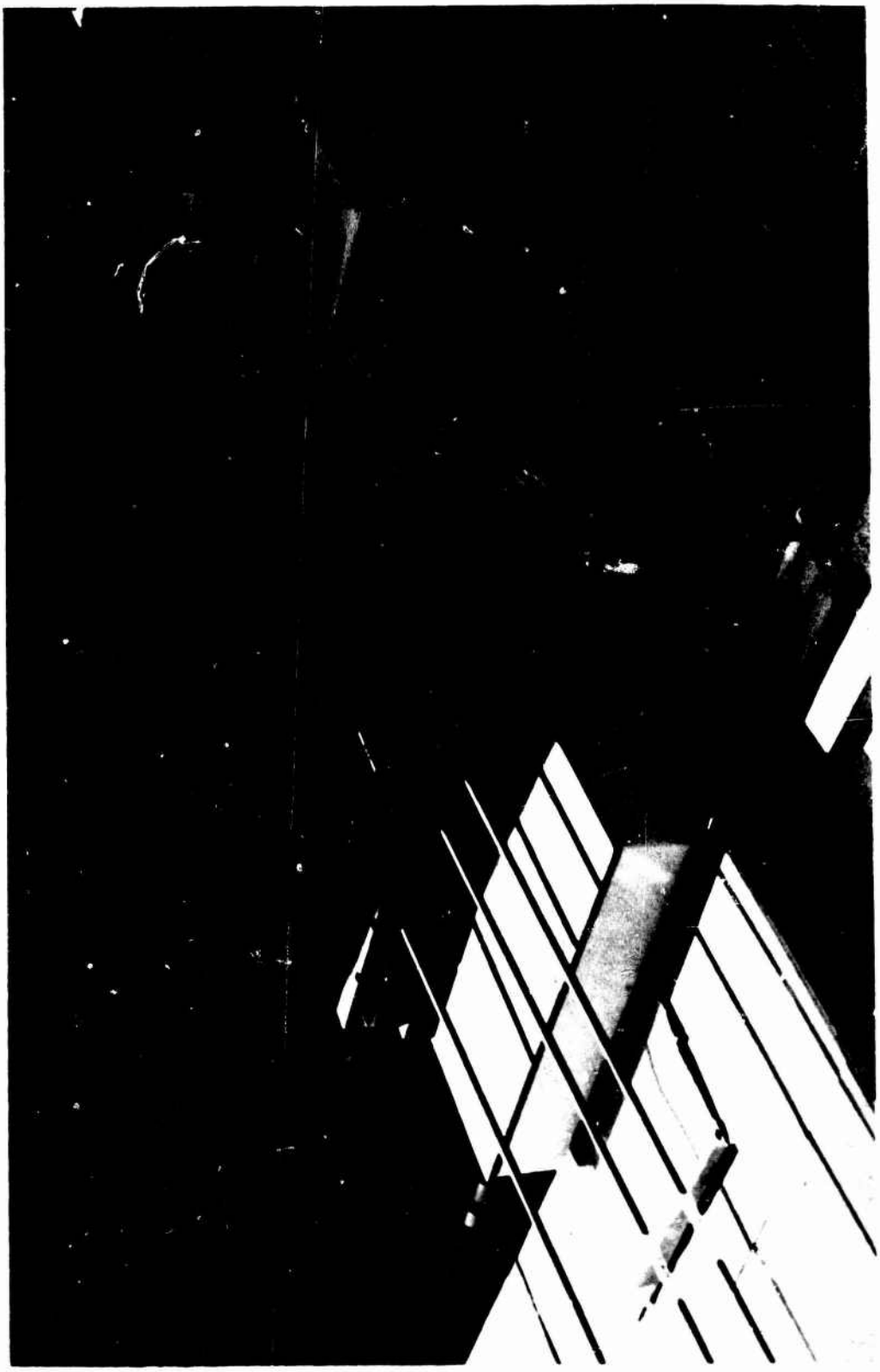

FIGURE 8. Hopkinson Pressure Bars on the Suspension Stand.

INSTRUMENTATION

Hopkinson pressure bars were used at both test facilities to measure the pressure-time history of the blast effects caused by fluidically encased explosive test charges.

The pressure bars were manufactured from 1/2-inch diameter bar stock using predominantly steel and aluminum bars. Occasionally a yellow brass bar also was employed. At the tank test facility aluminum Hopkinson bars were used for all the measurements involving encased charges. This necessitated the frequent replacement of the bars due to cratering and/or shear failure of the impact face. Extreme shear failures occurred during the firing of two test charges involving solid surrounds. It was therefore decided that steel should be employed as the primary bar material at the VADAM test facility, since all the surrounds would be solids. Hopkinson bar lengths were increased from 72 inches to approximately 116 inches to permit the measurement of longer duration impulses. Several 116 inch long 2024-T4 aluminum bars were also fabricated for use in the VADAM test facility. As expected, the bars made from 2024-T4 aluminum were more resistant to damage than the 6061-T6. (The average yield-strength of 2024-T4 aluminum is 68,000 lb/in^2.) Two types of steel bars were employed. The first, manufactured from hot rolled steel was heat treated to a yield strength of 170,000 lb/in^2 and the second made from Vasco Max 300, was heat treated to a yield strength of 150,000 lb/in^2.

Each Hopkinson bar had a single strain gauge attached at a distance of approximately 6 inches from the impact face of the bar. The strain gauges used were supplied by Micro-Measurements and were of two types: the first, CEA-06-250 UW-120, was used on the steel bars; and the second, CEA-13-250 UW-120, was used on the aluminum bars. Each Hopkinson bar was electrically grounded. Two 6-inch-long pieces of microdot coaxial cable were used to connect the strain gauge to the amplifier leads. The center conductor of each coaxial cable was connected to a copper tab on the strain gauge and the two braided shields to the system ground point. The input leads to the amplifiers consisted of a twisted pair, foil shielded cable which has the advantage of both low noise characteristics and low capacitance. Both gauge connections and gauge lead wire design are illustrated in Fig. 9 and Fig. 10. The high density fluidic surrounds caused a tremendous amount of damage to the aluminum Hopkinson pressure bars. In some instances the impact faces of the aluminum bars were actually sheared off. While the bar is still usable, experience has shown that whenever a bar sustains damage to that extent the strain gauge connection pads are also destroyed which results in a loss of data. In Fig. 11 the left hand bar was made of hot rolled steel that had been heat treated. All the other bars were manufactured from aluminum alloys.

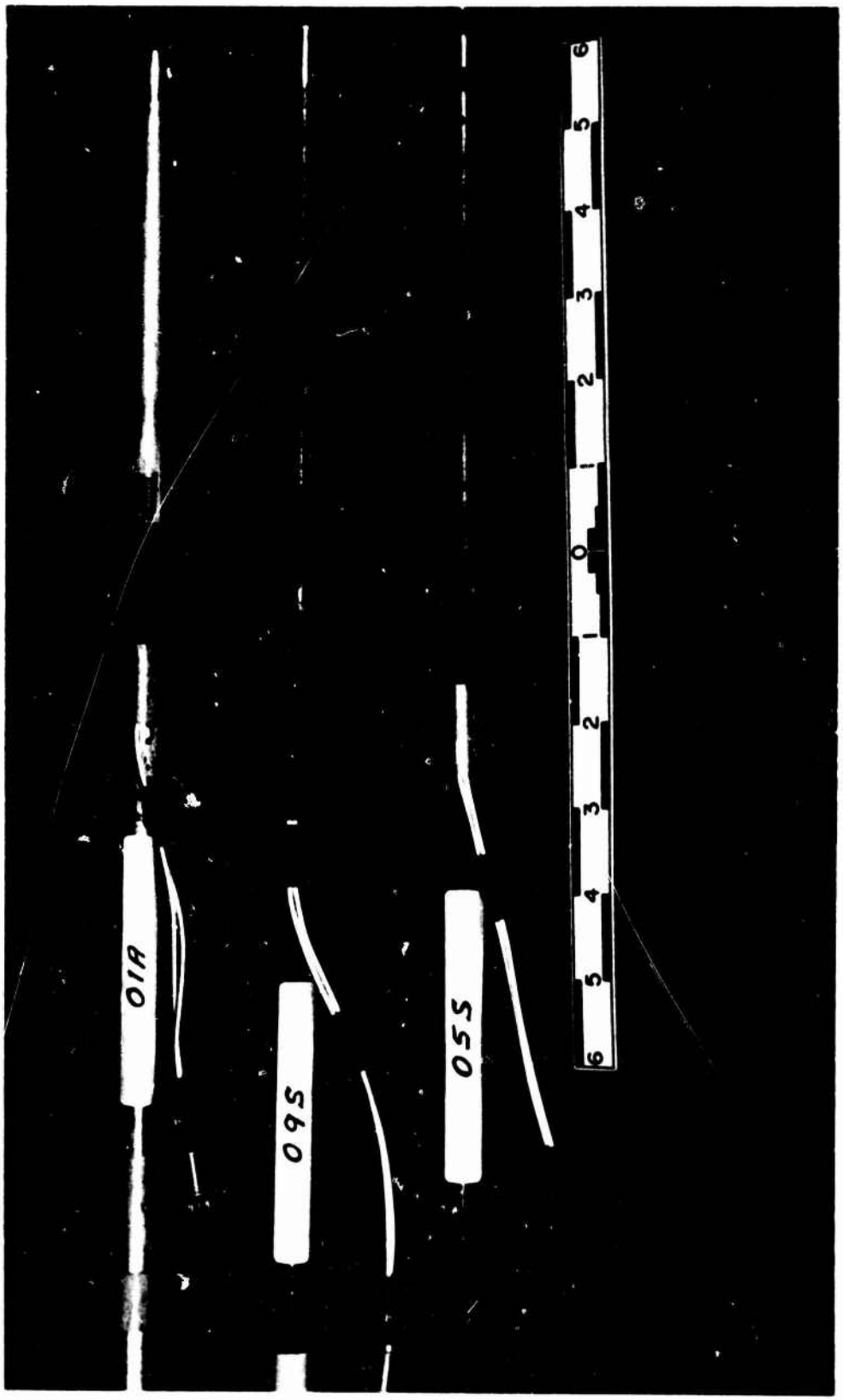

FIGURE 9. Strain Gauges and Gauge Connection on Hopkinson Pressure Bars.

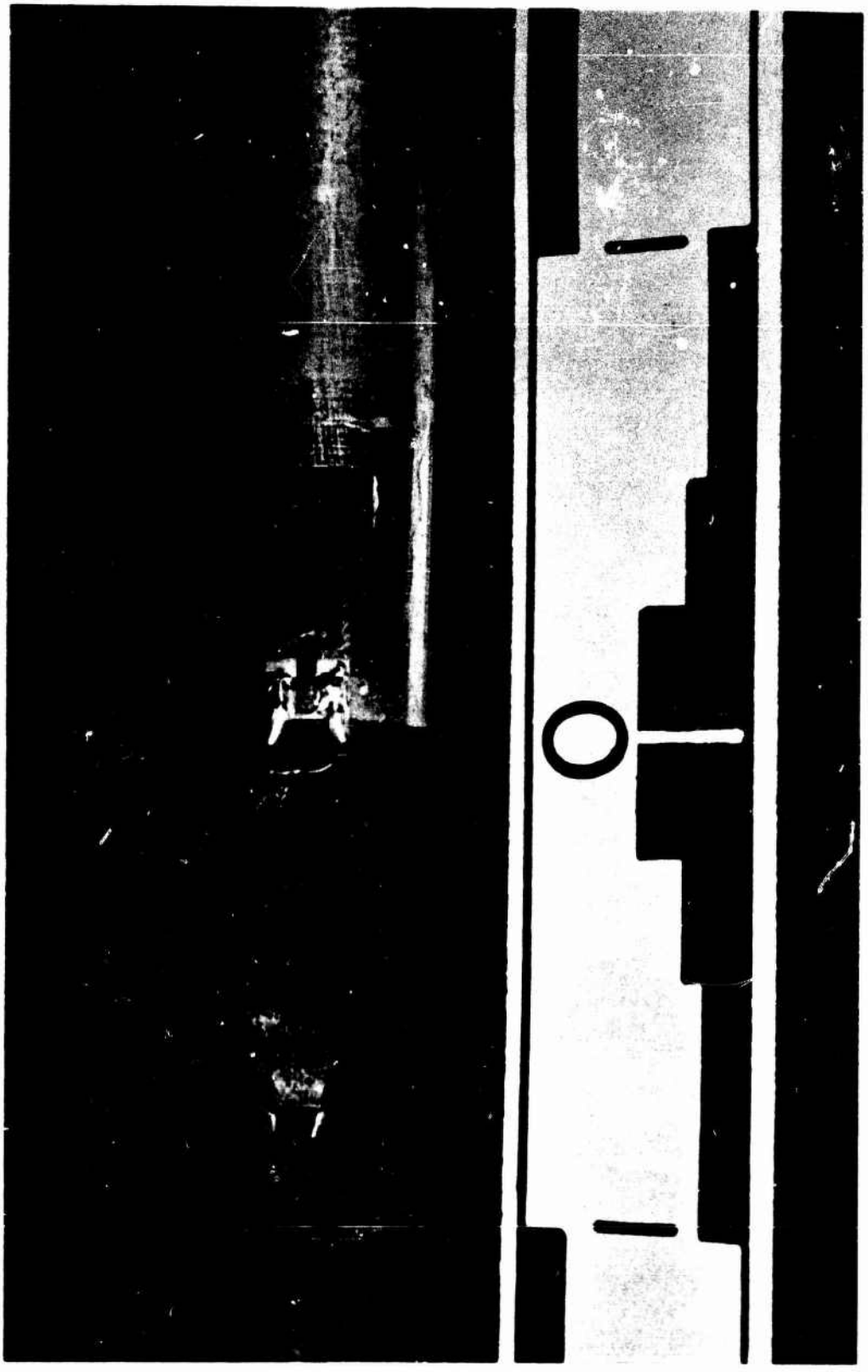

FIGURE 10. Strain Gauge and Lead Assembly.

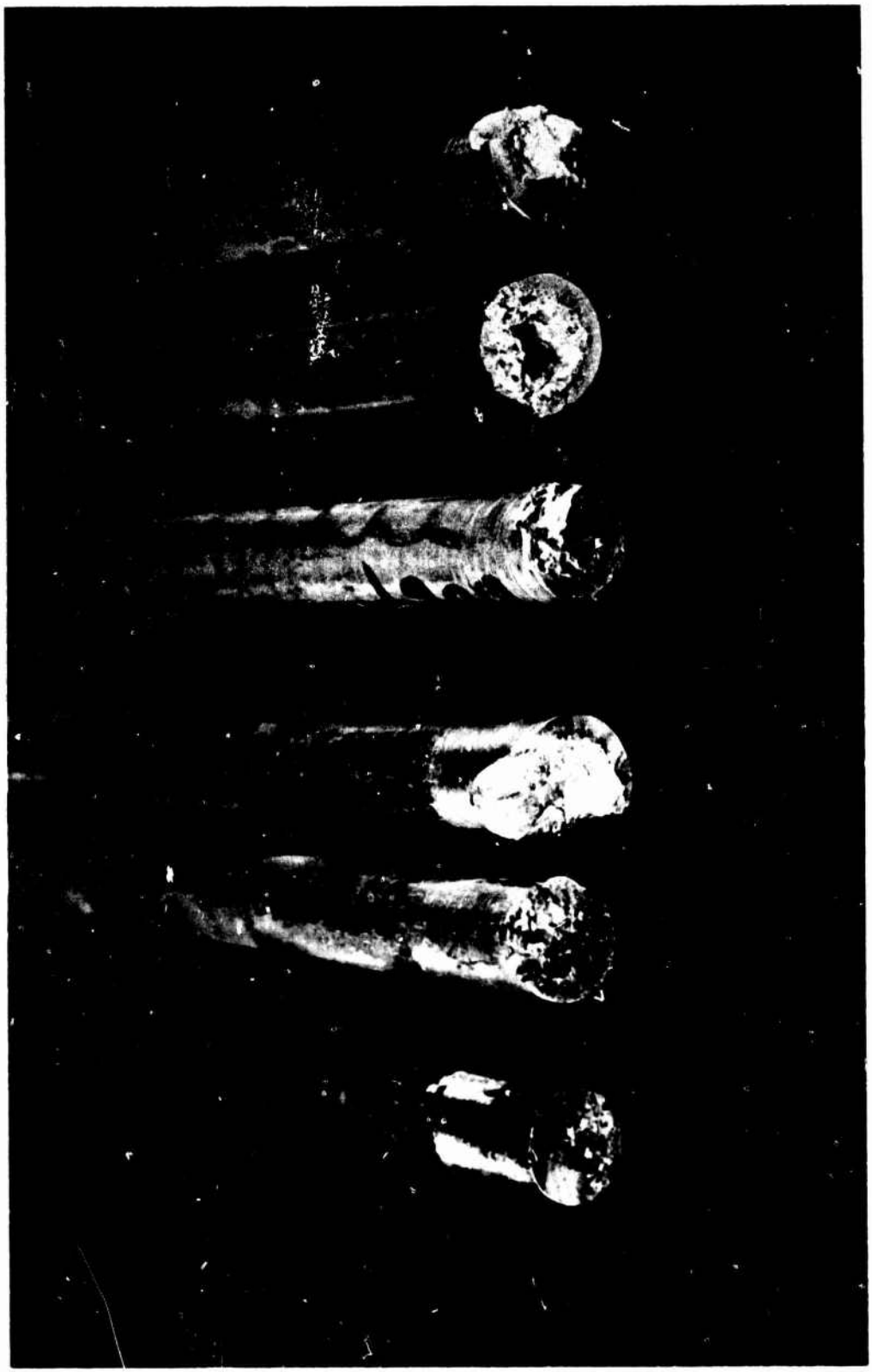

FIGURE 11. Impact Face Damage on the Hopkinson Pressure Bars.

One 72-inch long, yellow brass (type 360) Hopkinson bar was also incorporated into the pressure monitoring instrumentation at the VADAM facility. This Hopkinson bar was mounted behind a fragment stripper in order to monitor the air blast that is associated with the detonation of a fluidically encased explosive charge.

A block diagram representation of the strain gauge amplifiers for the Hopkinson bars is shown in Fig. 12. Three such amplifiers were used during each test shot. All supply voltages were regulated to minimize any drift in amplifier parameters as well as to reduce any cross-talk between the three data channels. The detailed circuit diagram is shown in Fig. 13. Metal film resistors were used throughout the construction of these amplifiers to minimize the effects of thermal changes. The differential input stage reduces the system response to common mode signals such as 60 cycle pickup from the power cables. The emitter follower serves as a buffer between the differential input stage and the operational amplifier stage. The 120A operational amplifier has an adjustable bandwidth capability thereby allowing a rise time of 500 nano-seconds at the output of this stage. However, the output of the 120A operational amplifier is fed to a voltage follower to reduce the effects of capacitive loading due to the long coaxial cables employed at the tank test facility. This last stage could have been eliminated at the VADAM test arena since the cable lengths were relatively short. This, however, was not necessary since the system bandwidth was preset to give a 4 microsecond rise time which resulted in a large reduction of background noise. (The background noise of the system is approximately 10 millivolts peak-to-peak.) The output of the 120A operational amplifier was also fed to a low-pass filter which has a preset rise time of 50 microseconds. This averaging filter reduces the spiky behavior of the data caused by particulate impacts and improves the ease of data reduction. Even though it appears that the filter would cause a loss of data, this is not the case, since any short rise time data (such as peak pressures) normally can be picked up from the raw data signal displayed simultaneously on the upper beam of the dual beam oscilloscopes. It must also be remembered that any realistic target, i.e., one of finite mass and dimensions, will act as a low-pass filter when being subjected to a short rise time, short duration impulse.

It was found that the firing line radiated an enormous interference signal following the detonation of the electrical blasting cap. To solve this problem the firing line was terminated by a 2 ohm resistor which had little if any effect on the function capability of the blasting cap.

CHARGE CONFIGURATION

When firing spherical charges for test or calibration purposes, the explosive charges were suspended in hairnets. This technique was also employed whenever bare pentolite cylinders were detonated. All cylindrical test charges were center-point initiated at the upper end

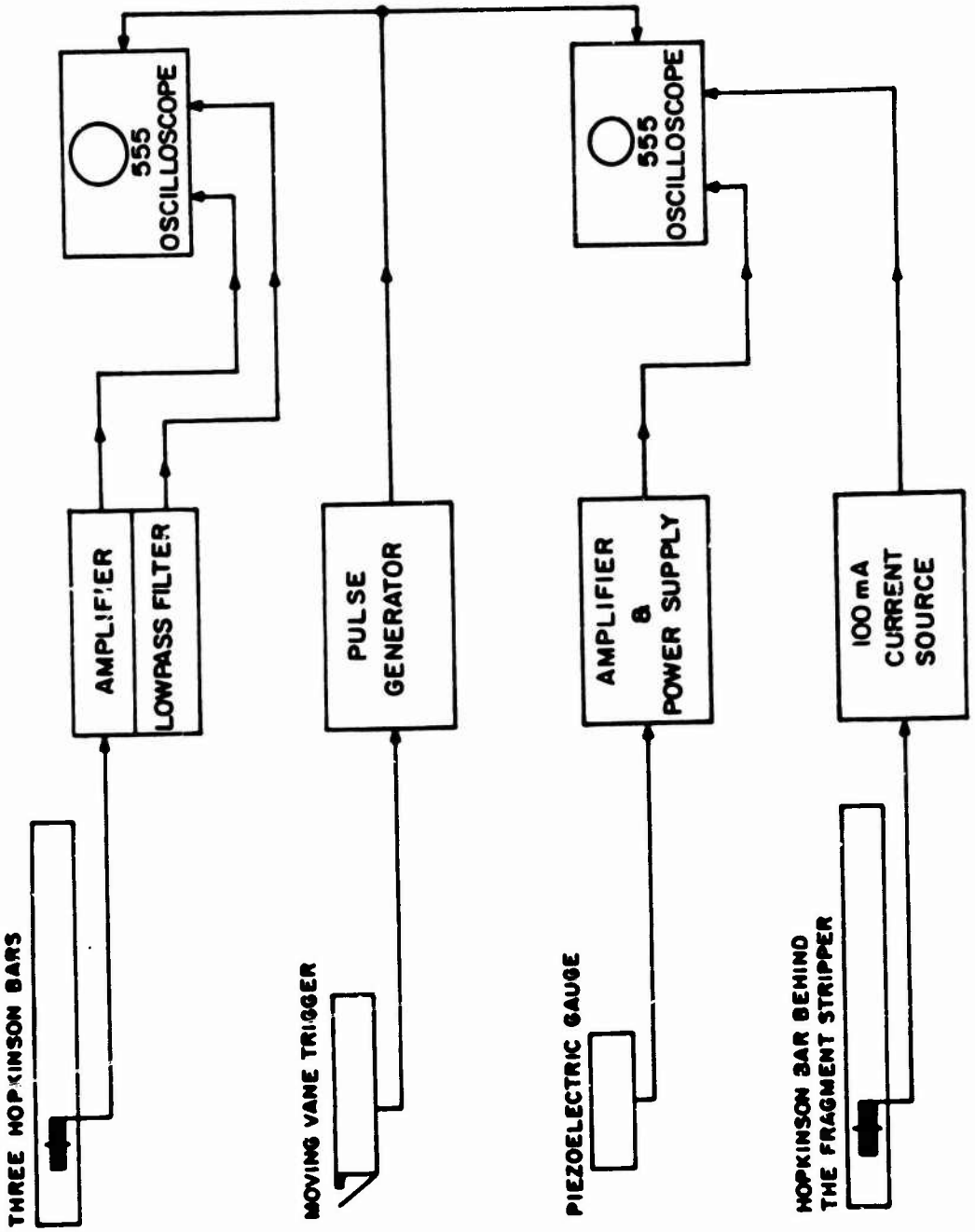

FIGURE 12. Block Diagram of Instrumentation System.

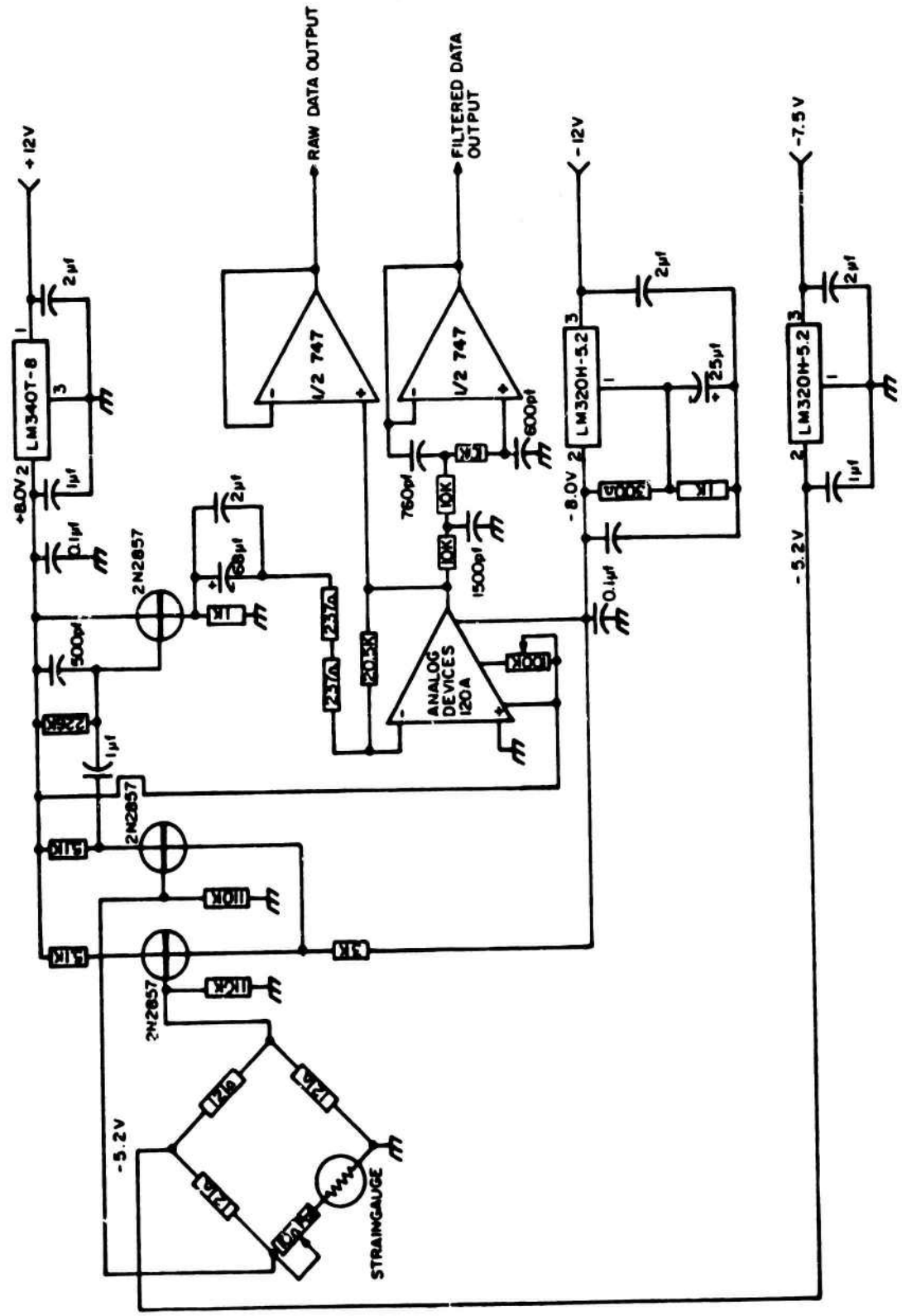

FIGURE 13. Strain Gauge Amplifier Circuit Diagram.

of the cylinders, using a 3/4-inch diameter, 3/4-inch long tetryl booster initiated by a #8 blasting cap. The cap and booster were held in place by a 1½-inch diameter wooden dowel. This dowel had cavities machined in it to house both the cap and the booster. The total assembly was attached to the top surface of a cylindrical explosive charge using very thin double sided adhesive tape.

An inexplicable phenomenon frequently manifested itself whenever a cylindrically shaped explosive charge was detonated. The output of the Hopkinson bars would show a short duration negative precursor prior to the initial rise of a typical airblast shock front. This precursor even appeared during some of the firings of the series of liquid surrounds. The piezoelectric pressure gauge never registered such a signal. This negative precursor does not appear to be an electromagnetic interference since its time of arrival is concurrent with that of the airblast shock front. Even though this phenomenon is not understood, it ceased to appear after the following modification had been affected. Whenever a cylindrically shaped explosive charge was to be detonated, a 1/16-inch-thick, 1 1/4-inch inside diameter and 2 1/2-inch-long steel tube was placed over the booster-cap assembly. This steel tube did not appear to have any effect whatsoever on the pressure-time data generated by the explosion. Therefore all of the high-density solid-surrounds were detonated with the steel tube modification over the booster-cap assembly.

Various container configurations were tried in the case of the three liquid surrounds. The different types of container configurations are shown in Fig. 14. The first type of liquid-charge container consisted of two glass tubes epoxied to a machined lucite base. This construction prevents the liquid from directly contacting the charge. This precaution was not necessary in the case of the three liquids employed in this test series since they are inert with respect to the pentolite explosive used. The pressure-time data resulting from the detonation of these charges were spiky. This suggested that the glass container, especially the double glass walls, was causing the problem due to the generation of microscopic fragments, see Fig. 15. As a result, the container design was changed. A single lucite tube, 1/8-inch thick and approximately 5½-inch outside diameter, was epoxied to a lucite base. The liquids were therefore, in direct contact with the explosive. Although the signals recorded were still of a spiky nature the characteristic shape of the resulting spikes superimposed on the data appeared to be of lower magnitude and a somewhat lower frequency, see Fig. 16. The entire liquid surround test series was fired with this charge/container configuration. Later in the program a final modification of a container for liquid surrounds was investigated. This consisted of a 1/16-inch-thick, 5 1/16-inch outside diameter cardboard box epoxied to the machined lucite base. After curing, the cardboard was impregnated with paraffin wax. The resulting pressure-time trace still showed some spiking, however, the spike frequency was considerably reduced, see Fig. 17. This final container design provided the most simple construction, with the lowest mass as well as

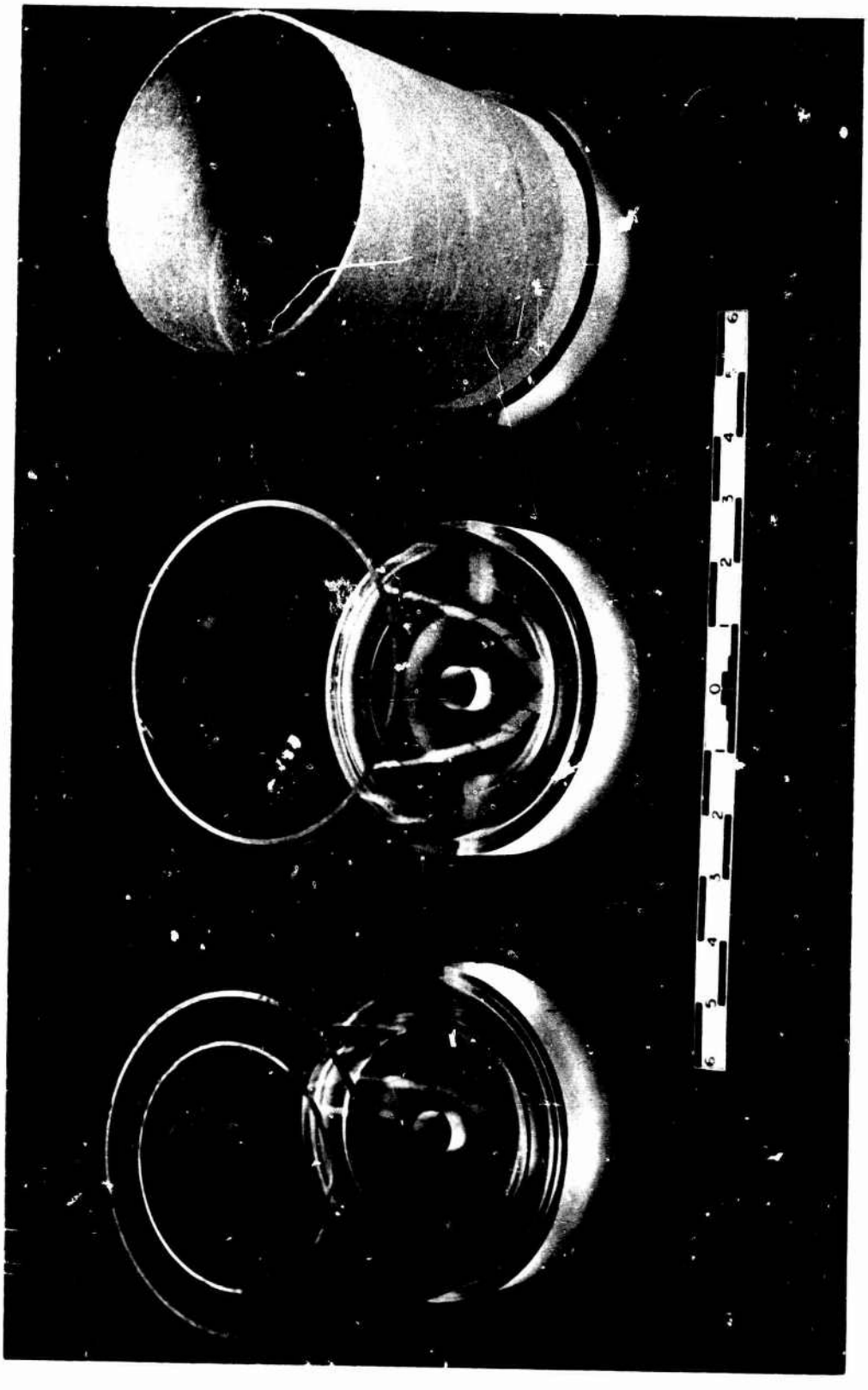

FIGURE 14. Different Types of Liquid Containers Used.

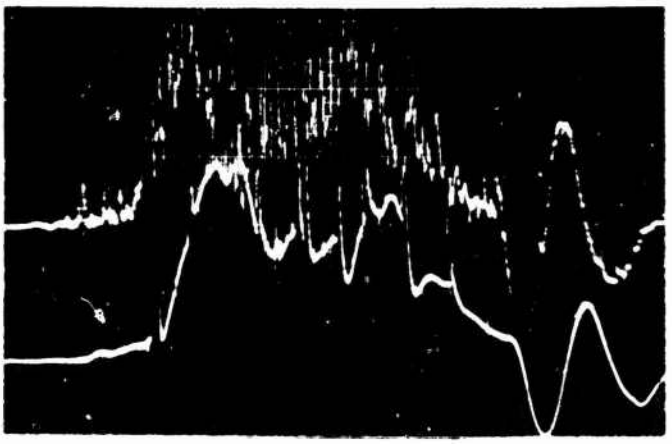

FIGURE 15. Pressure-Time Record from a Water/Glass Encased 672-Gram Pentolite Cylinder.

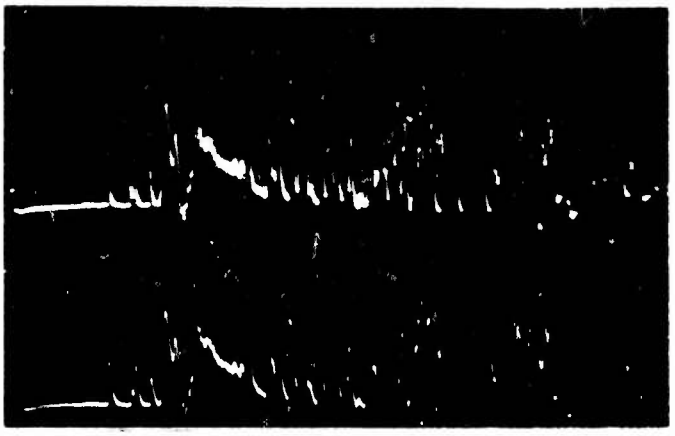

FIGURE 16. Pressure-Time Record from a 64-Series Water/Lucite Encased 582-Gram Pentolite Cylinder.

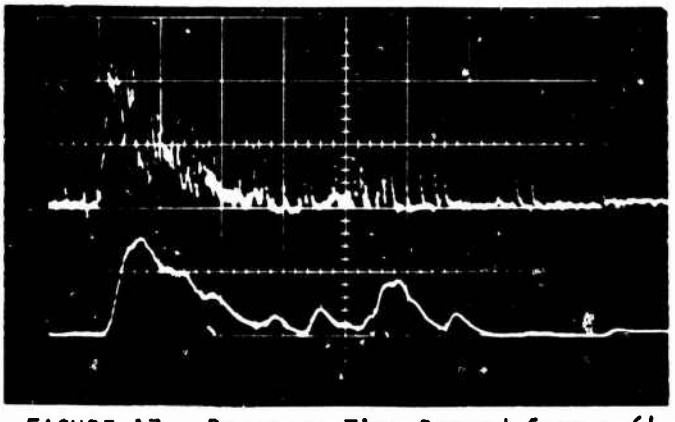

FIGURE 17. Pressure-Time Record from a 64-Series Water/Cardboard Encased 586-Gram Pentolite Cylinder.

lowest cost. The container/charge assembly is illustrated in Fig. 18. A glass encased explosive charge is shown in Fig. 19 resting on a triangular plywood platform. These platforms were always used to suspend the test charges whenever encased cylindrically shaped explosive charges were fired.

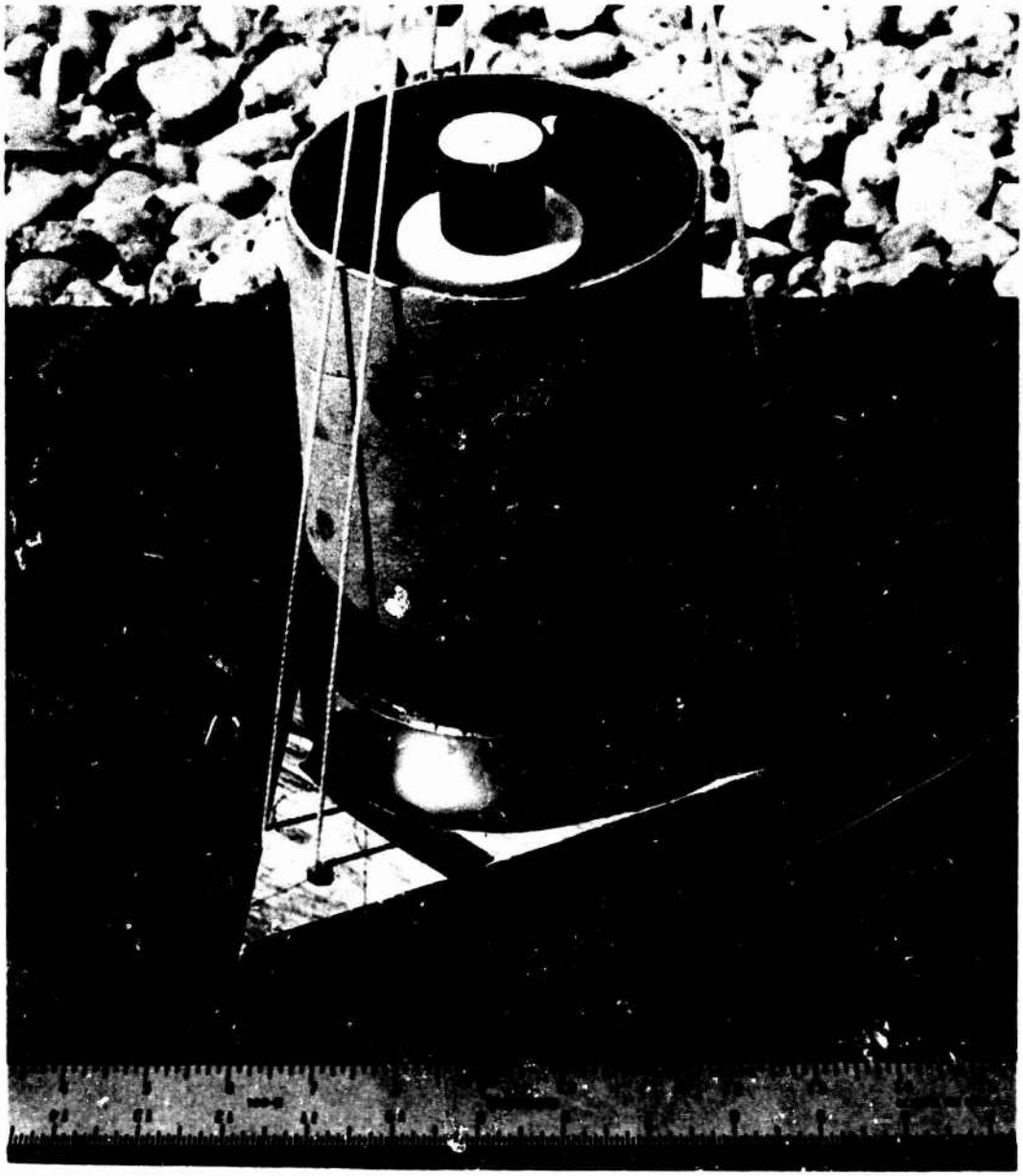

FIGURE 18. Final Configuration of an Explosive Charge and Liquid Encasement.

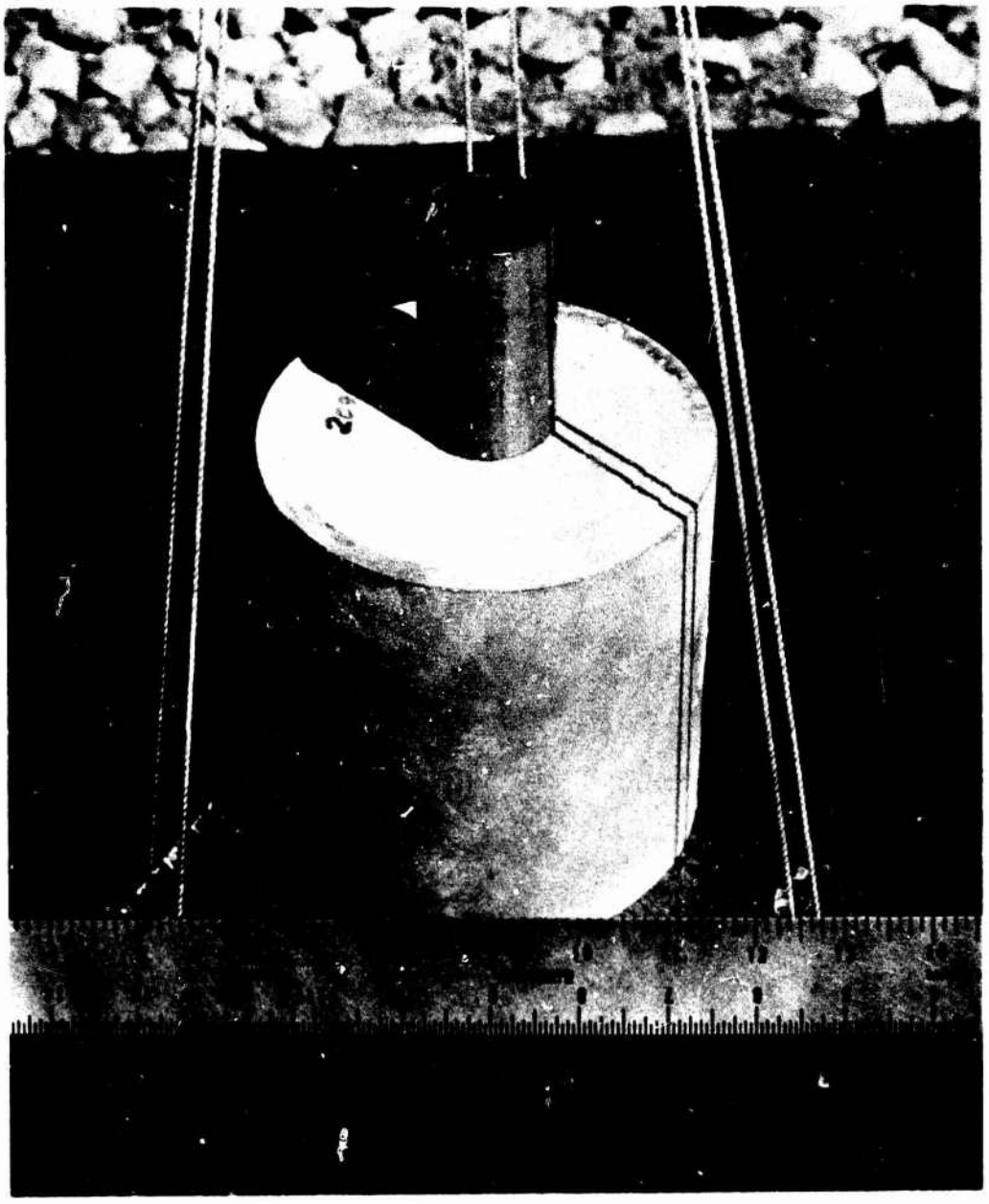

FIGURE 19. A 120-Series Glass Encased Pentolite Cylinder with Detonation End Modification of the Booster-Cap Assembly.

SPHERICAL TEST CHARGES

The Hopkinson pressure bars, used to determine the pressure-time data generated by fluidically encased explosive charges, were calibrated by firing a series of one-pound pentolite spheres. The resulting peak pressures were measured using a piezoelectric pressure transducer pre-calibrated by the manufacturer. The gauge type used was an ST-4, supplied by Susquehanna Instruments. The accumulated data were averaged to determine the calibration factors. The average peak pressure generated by six 480-gram pentolite spheres at a standoff distance of 3 feet was found to be 642 lb/in at an atmospheric pressure of 11.867 lb/in^2. When scaled to sea level this peak pressure becomes 795 lb/in^2. This figure correlates very closely with 780 lb/in^2 as published by the Ballistic Research Laboratories (BRL) in their memorandum report No. 1499 (Ref. 1). The data for this test series is presented in Table 1. The underlined values are not included in the average due to their obviously low values.

TABLE 1

Peak Pressures Generated by 480-Gram Pentolite Spheres at a 36-inch Standoff Distance Measured at an Atmospheric Pressure of 11.867 lb/in^2

Amplifier #1 Aluminum Bars (lb/in^2)	Amplifier #2 Aluminum/ Steel Bars (lb/in^2)	Amplifier #3 Aluminum Bars (lb/in^2)	Current Source Brass Bar (lb/in^2)	Piezoelectric Gauge #133 (lb/in^2)
677	647	629	587	645
642	613	594	733	768
434	669	704	665	627
399	599	-	587	595
642	616	642	665	627
607	702	-	616	589

The output voltage of each Hopkinson pressure bar system was also averaged for the six 480-gram test charges fired. In each case the average voltage was divided by 642 lb/in^2 resulting in a calibration factor, S (millivolts/lb/in^2), for each amplifier-bar combination. The results of

Ref. 1. Ballistic Research Laboratories. Measurements of Normally Reflected Shockwaves from Explosive Charges, by W. H. Jack, Jr., Aberdeen Proving Ground, Maryland, July 1963. (Memorandum Report No. 1499).

this calibration are shown in Table 2, for the Hopkinson pressure bars employed at the VADAM test facility. Also included in this table are the calibration factors determined for the tank facility. The difference in calibration factors for the aluminum bars is basically due to modifications that were made in the amplifier circuit when the move to the VADAM arena took place.

TABLE 2

Calibration Factors Determined for the Hopkinson Pressure Bars at an Atmospheric Pressure of 11.867 lb/in^2

	S#1 $\frac{mV}{lb/in^2}$	S#2 $\frac{mV}{lb/in^2}$	S#3 $\frac{mV}{ib/in2}$
Tank Arena			
Aluminum	0.59	0.56	
VADAM Arena			
Aluminum	0.29	0.25	0.26
Steel	0.10	0.09	0.09

A second series of 1-, 2- and 5-pound spherical pentolite charges were fired to serve as additional calibration for the Hopkinson bars. The peak pressure figures as well as the scale distance figures shown in Table 3 were altitude scaled to facilitate a comparison with the BRL data as published in BRL Report No. 1499 (Ref. 1). The test range altitude was assumed to be 6,000 ft. above sea level. As can be seen from the table, the correlation is excellent.

TABLE 3

Average Peak Pressures Measured During the Detonation of Spherical Pentolite Test Charges

Charge Weight (lb)	Scale Distance ($ft/lb^{1/3}$)	Peak Pressure (lb/in^2)	Altitude Scaled Scale Distance ($ft/lb^{1/3}$)	Alt. Scaled Peak Pressure (lb/in^2)	Approx. BRL Peak Pressure (lb/in^2)
1	3.00	595	2.79	742	763
2	2.38	1025	2.21	1279	1310
5	1.75	2200	1.63	2745	2693

ANALYTICAL CALIBRATION

The calibration factor, S, can also be calculated if Young's modulus is known for each Hopkinson bar material. It can be shown that S is given by:

$$S = \frac{\Delta\upsilon}{\Delta\sigma} \quad \frac{\text{Volts}}{\text{lb/in}^2} \qquad \text{(Eq. 1)}$$

$$S = \frac{A\, I_g\, k\, R_g \times 10^3}{E} \quad \frac{\text{millivolts}}{\text{lb/in}^2} \qquad \text{(Eq. 2)}$$

where

$\Delta\upsilon$ is the change in output voltage, mV

$\Delta\sigma$ is the change in applied pressure, lb/in^2

A is the system voltage gain, volts/volt

I_g is the strain gauge current, amperes

k is the gauge factor

R_g is the gauge resistance, ohms

E is Young's modulus, lb/in^2

The analytical calibration does not take into account the fact that the Hopkinson pressure bars were necessarily located behind the inserts forming the instrumentation ports. This requires that the shock front travel through a 1/2-inch-diameter orifice for approximately 1 3/8 inches prior to impacting the face of the bar. It was found that the spherical charge calibration values, determined using piezoelectric gauges in conjunction with Hopkinson bars, was lower than the analytically determined values. The net effect was that the experimentally determined calibration values were approximately 82.5 percent lower than those derived analytically. Therefore, in order to compare experimental calibration factors with those calculated, each calculated calibration factor must be multiplied by 0.825. The values used for the various parameters were:

$I_g = 21.4 \times 10^{-3}$ amperes

$k_{Al} = 2.09$

$k_{st} = 2.105$

$R_g = 121$ ohms

$E_{Al} = 10.6 \times 10^6$ lb/in^2

$E_{st} = 30 \times 10^6$ lb/in^2

The amplifier voltage gains are listed in Table 4.

TABLE 4

Amplifier Voltage Gains

Amplifier #1	Amplifier #2	Amplifier #3
730	690	530

Using the following equation, the corrected gain factors can be calculated, namely,

$$S = \frac{825\ A\ I_g\ k\ R_g}{E} \quad \frac{\text{millivolts}}{\text{lb/in}^2}$$

The gain factors are listed in Table 5 both for steel and aluminum Hopkinson bars.

TABLE 5

Analytical Calibration Factors for the Hopkinson Pressure Bars.

	S#1	S#2	S#3
	$\frac{\text{mV}}{\text{lb/in}^2}$	$\frac{\text{mV}}{\text{lb/in}^2}$	$\frac{\text{mV}}{\text{lb/in}^2}$
Aluminum	0.31	0.29	0.22
Steel	0.11	0.10	0.08

A general agreement between the calibrated factors determined both experimentally and analytically can be observed by comparing Table 2 and Table 5.

TEST RESULTS

SPHERICAL CHARGES

It was found that the impact end of the Hopkinson pressure bar could under no circumstance be coupled directly to the wall of the test facility when the wall was subjected to blast loading from test charges of the size fired during this program. Figure 20 shows two traces of the bar response under conditions of direct coupling, as obtained in the tank. Because of this, the impact ends of the Hopkinson bars were separated from the exits of the instrumentation port by distances of either 1/16-inch (as in the tank test facility) or 1/8-inch (as in the VADAM test facility). A typical bar response for the pressure-time output of a spherically shaped explosive charge is shown in Fig. 21.

PENTOLITE CYLINDER DATA

A phenomenon was encountered which produced a negative precursor in the signal response of a Hopkinson pressure bar when used to measure the pressure-time data generated during the detonation of a cylinder. This effect is shown in Fig. 22. Modification of the charge assembly by surrounding the detonator and booster with a thin walled metal tube cured the problem and all subsequent pressure traces resembled the one shown in Fig. 23 for the bare pentolite cylinders.

The average dimensions of the bare cylindrically shaped pentolite charges fired during this program are given in Table 6.

TABLE 6

Average Dimensions of Bare Pentolite Cylinders

Series	Length (mm)	Diameter (mm)	Length-to-Dia. Ratio	Mass (grams)
64	133	59	2.25	584
80	133	75	1.77	947
95	133	90	1.48	1366
110	133	105	1.27	1805
120	133	133	1.18	2111

The peak pressures produced by detonation of the pentolite cylinders having the above mentioned dimensions are presented in Table 7. The underlined values were not used in calculating the average values for each series. The reasons for disregarding these values was associated with the type of signal recorded. In some cases a serious negative

FIGURE 20. Hopkinson Bar Behavior Illustrating Direct Coupling Between the Bar and Instrumentation Port Following Detonation of a 2-Pound Pentolite Sphere.

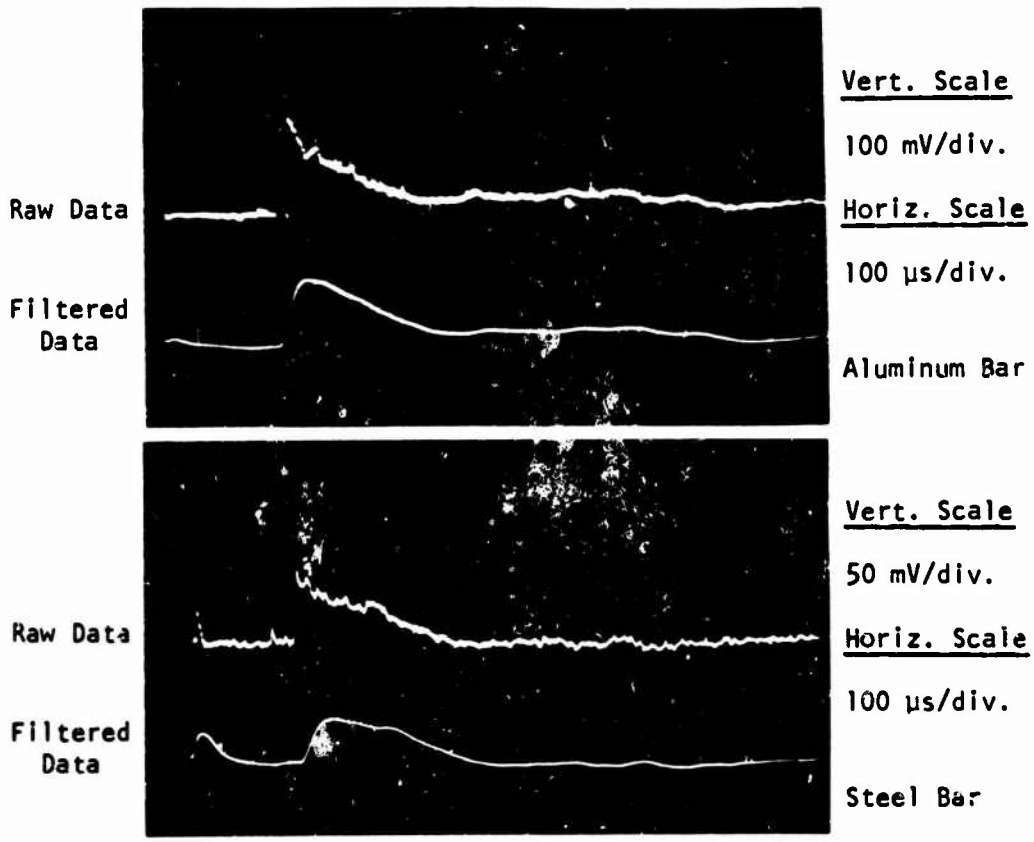

FIGURE 21. Hopkinson Pressure Bar Traces Obtained From the Detonation of a One-Pound Pentolite Sphere. Separation Distance Between Instrumentation Port Exit and Bar Impact Face was 1/16-Inch.

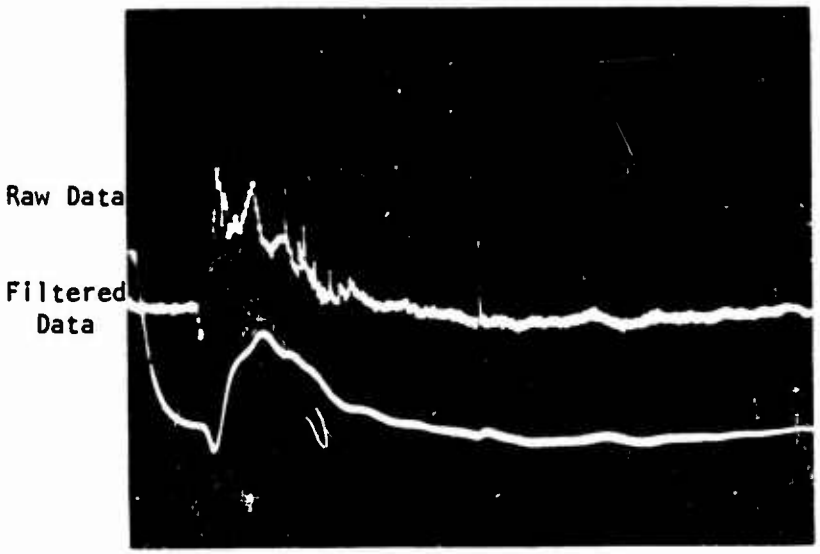

FIGURE 22. Pressure-time Trace of a 594-Gram Pentolite Cylinder Showing Negative Precursor.

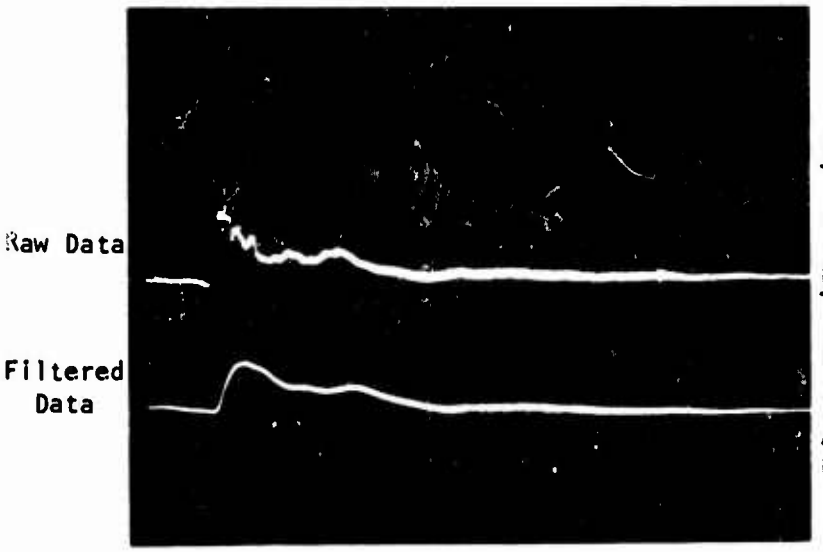

FIGURE 23. Pressure-time Trace of a 1,347-Gram Pentolite Cylinder Following Booster-Cap Assembly Modification.

TABLE 7

Peak Pressure Values Given by Pentolite Cylinders at an Atmospheric Pressure (P_r) of 11.867 lb/in^2.

Series	Shot No.	Amplifier #1 (lb/in^2)	Amplifier #2 (lb/in^2)	Amplifier #3 (lb/in^2)	Current Source and Yellow Brass Bar (lb/in^2)	Piezo Gauge (lb/in^2)	Avg. Reflected Peak Pressure (lb/in^2)	Standard Deviation
64	0320/1	1040	1653	1158	1476	658	1503	246
	0320/2	1737	1800	1612	1642	1411		
80	0306/5	-	1948	1996	1476	1844	1860	182
	0320/4	1131	1558	1511	1466	2010		
	0320/5	954	1863	1590	1173	2073		
95	0306/2	3566	[illegible]	2928	3387	2680	2694	417
	0306/3	-	3109	2770	3079	2667		
	0306/4	-	3221	3579	3079	2854		
	0323/4	-	-	3076	-	-		
	0324/2	2171	2865	3615	2893	2979		
	0408/1	2385	1874	2320	1584	1719		
110	0324/3	-	-	6043	2933	4146	2877	220
	0324/4	2080	5618	2806	2639	3125		
	0331/2	3211	2285	2518	2933	2854		
120	0331/3	1835	1798	-	2053	3000	3132	469
	0331/4	1606	3071	2464	2933	2823		
	0331/5	-	4288	3579	3460	3198		
	0403/3	2080	-	3273	2933	2563		

precursor problem existed, in others bad signals characterized by wild excursions and/or multiple peaks caused questionable interpretation of the data.

An overall comparison of peak pressure data recorded by different Hopkinson bars for the same shot or on a shot to shot basis can be made by observing Table 7. Included in this table are standard deviation values which show the data spread that might be expected when using this instrumentation and facility.

The areas under the recorded pressure-time curves produced from the filtered output of each amplifier were determined by means of a planimeter. These areas, multiplied by a corresponding scale factor give the filtered reflected impulse ($\overline{I}_r$) in lb/in^2 - milliseconds. The averaged filtered impulse values corresponding to the reflected peak pressures ($\hat{P}_r$) for the bare, cylindrically-shaped pentolite charges are given in Table 8.

TABLE 8

Average of Parameters Measured at an Atmospheric Pressure of 11.867 lb/in^2 for Bare Pentolite Cylinders

Series	Average Mass (lb)	Length-to-Diameter Ratio (L/D)	Reflected Peak Pressure ($\hat{P}_r$) (lb/in^2)	Filtered Reflected Impulse ($\overline{I}_r$) (lb/in^2 - msec)
64	1.29	2.25	1503	88.2
80	2.09	1.77	1860	116.1
95	3.02	1.48	2694	185.8
110	3.98	1.27	2877	242.0
120	4.66	1.18	3132	251.3

Sachs' scaling law (Ref. 2) states that dimensionless groups can be formed that involve pressure, time, impulse, and certain parameters for the ambient air and that these groups are unique functions of a dimensionless distance parameter. Specifically, the groups

$$\frac{p}{p_o}, \quad \frac{Ia_o}{E^{1/3} p_o^{2/3}}, \quad \frac{ta_o p_o^{1/3}}{E^{1/3}}$$

are stated to be unique functions of $(Rp_o^{1/3}/E^{1/3})$.

Ref. 2. Baker, Wilfred E., Explosions in Air, First Ed., Austin, Texas, Univ. of Texas Press 1973. Chap. 3, "Blast Scaling", pp 54-77.

Using the Sachs' scaling laws, as outlined by W. E. Baker in Ref. 2, the following relationships were employed to normalize the above data.

$$R = \frac{R_r (p_r)^{1/3}}{(E)^{1/3}} \qquad \text{(Eq. 3)}$$

$$\hat{P} = \frac{\hat{P}_r}{p_r} \qquad \text{(Eq. 4)}$$

$$T = \frac{T_r a_r (p_r)^{1/3}}{(E)^{1/3}} \qquad \text{(Eq. 5)}$$

$$\overline{T} = \frac{\overline{T}_r a_r}{(p_r)^{2/3}(E)^{1/3}} \qquad \text{(Eq. 6)}$$

where

R is the scaled distance

$\hat{P}$ is the reflected peak air blast overpressure, atmospheres

T is the duration of the reflected overpressure

$\overline{T}$ is the normally reflected positive impulse as determined through a 50 μsec rise time, low-pass filter

R_r is the standoff distance at range, inches

$\hat{P}_r$ is the reflected peak air blast overpressure as measured at the range, lb/in^2

T_r is the duration of the reflected overpressure as measured at the range, se-

p_r is the ambient atmospheric pressure at the range, lb/in^2

a_r is the acoustic velocity in air at 59^oF, in/sec

$\overline{T}_r$ is the normally reflected positive impulse, as determined through a 50 μsec rise time low-pass filter, and measured at the range, $lb\text{-}sec/in^2$

E is the energy of the explosive, in-lb

The following numerical values were used for the constants in these equations:

$$p_r = 11.867 \text{ lb/in}^2$$

$$E = 20.5 \times 10^6 \text{ in-lb/lb}$$

$$R_r = 36.0 \text{ in}$$

$$a_r = 13{,}397 \text{ in/sec}$$

Table 9 is a summary of the normalized data for the series of bare pentolite cylinders.

TABLE 9

Averaged Normalized Blast Parameters for Pentolite Cylinders

Series	Length to Diameter Ratio (L/D)	Scaled Distance (R) $\frac{R_r(p_r)^{1/3}}{(E)^{1/3}}$	Peak Reflected Overpressure(P) $\frac{\hat{P}_r}{P_r}$	Filtered Normally Reflected Positive Impulse (I) $\frac{I_r a_r (p_r)^{1/3}}{(E)^{1/3}}$
64	2.25	0.276	126.7	0.763
80	1.77	0.235	156.7	0.855
95	1.48	0.208	227.0	1.210
110	1.27	0.189	242.4	1.437
120	1.18	0.180	263.9	1.416

All the bare pentolite cylinder blast parameters are graphically presented in Fig. 24 through Fig. 26.

ENCASED CHARGES

Fifteen fluidically encased pentolite charges were fired at the tank test site. In each case the liquids were contained in a lucite cylinder having a wall thickness of approximately 1/8 inch. A small series of four liquid encased charges were detonated at the VADAM test facility. However, in this case the liquid container was manufactured from a paraffin impregnated cardboard tube having a wall thickness of

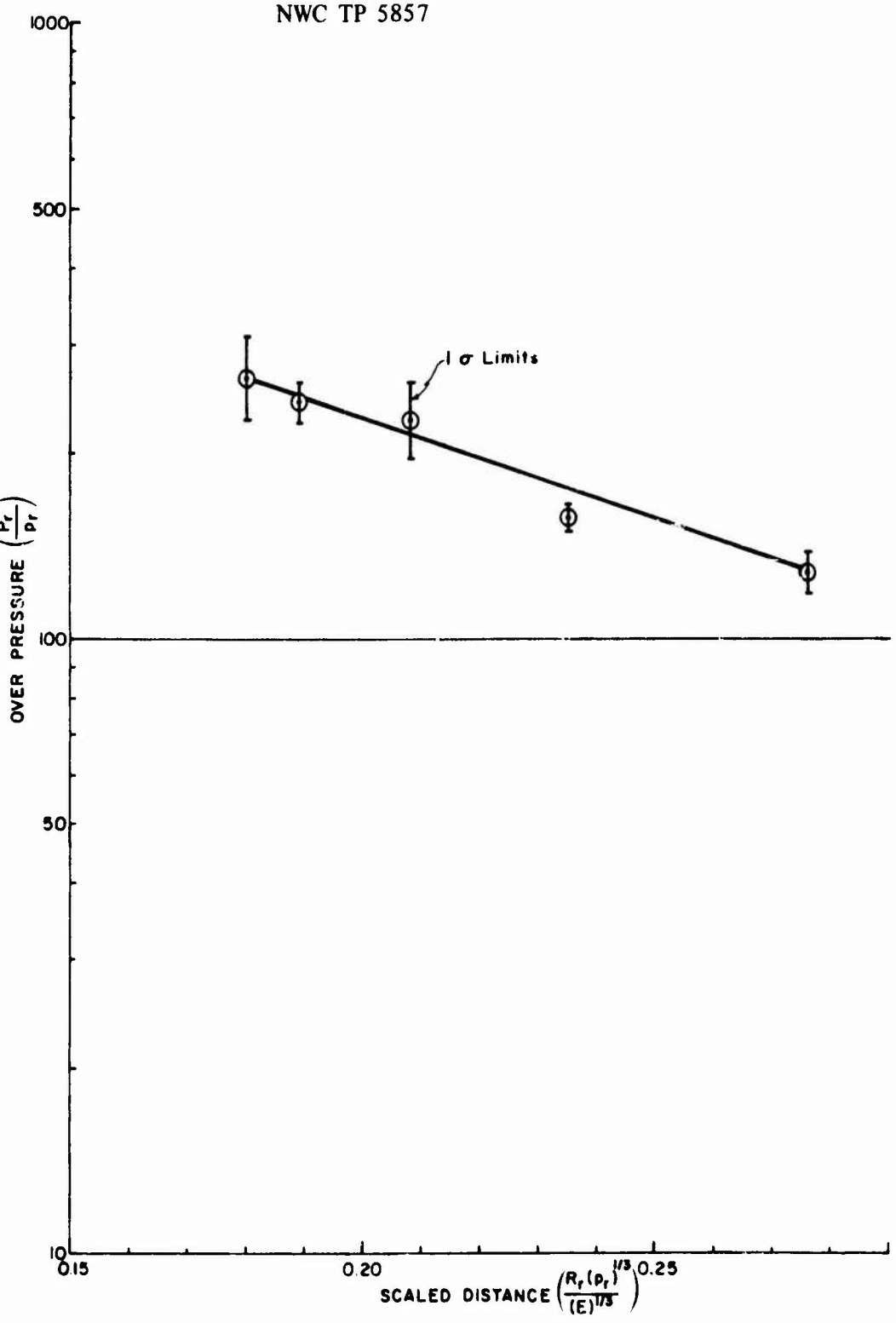

FIGURE 24. Peak Overpressure versus Scaled Distance for Bare Pentolite Cylinders (Normalized Data).

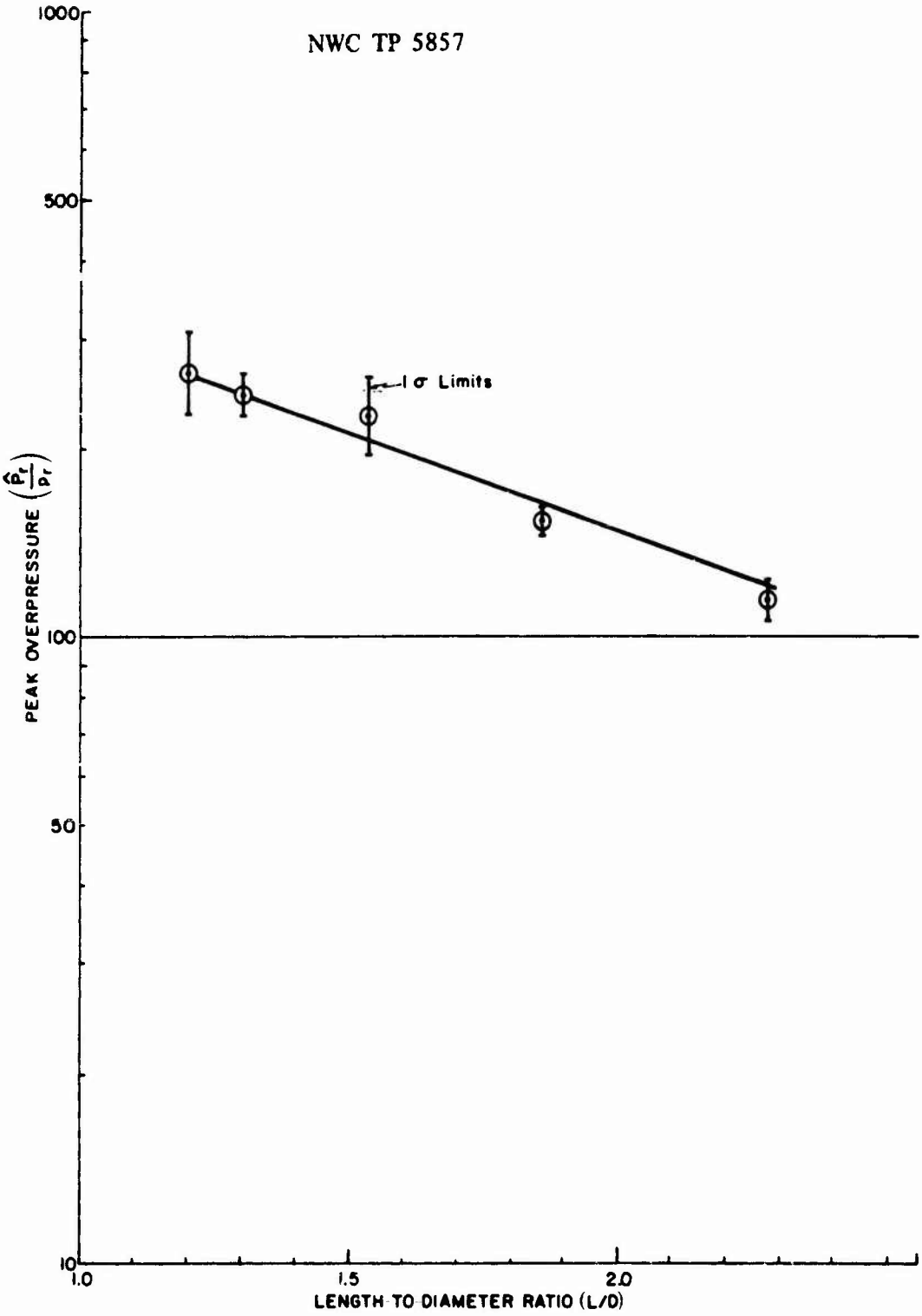

FIGURE 25. Peak Overpressure versus Length-to-Diameter Ratio for Bare Pentolite Cylinders (Normalized Data).

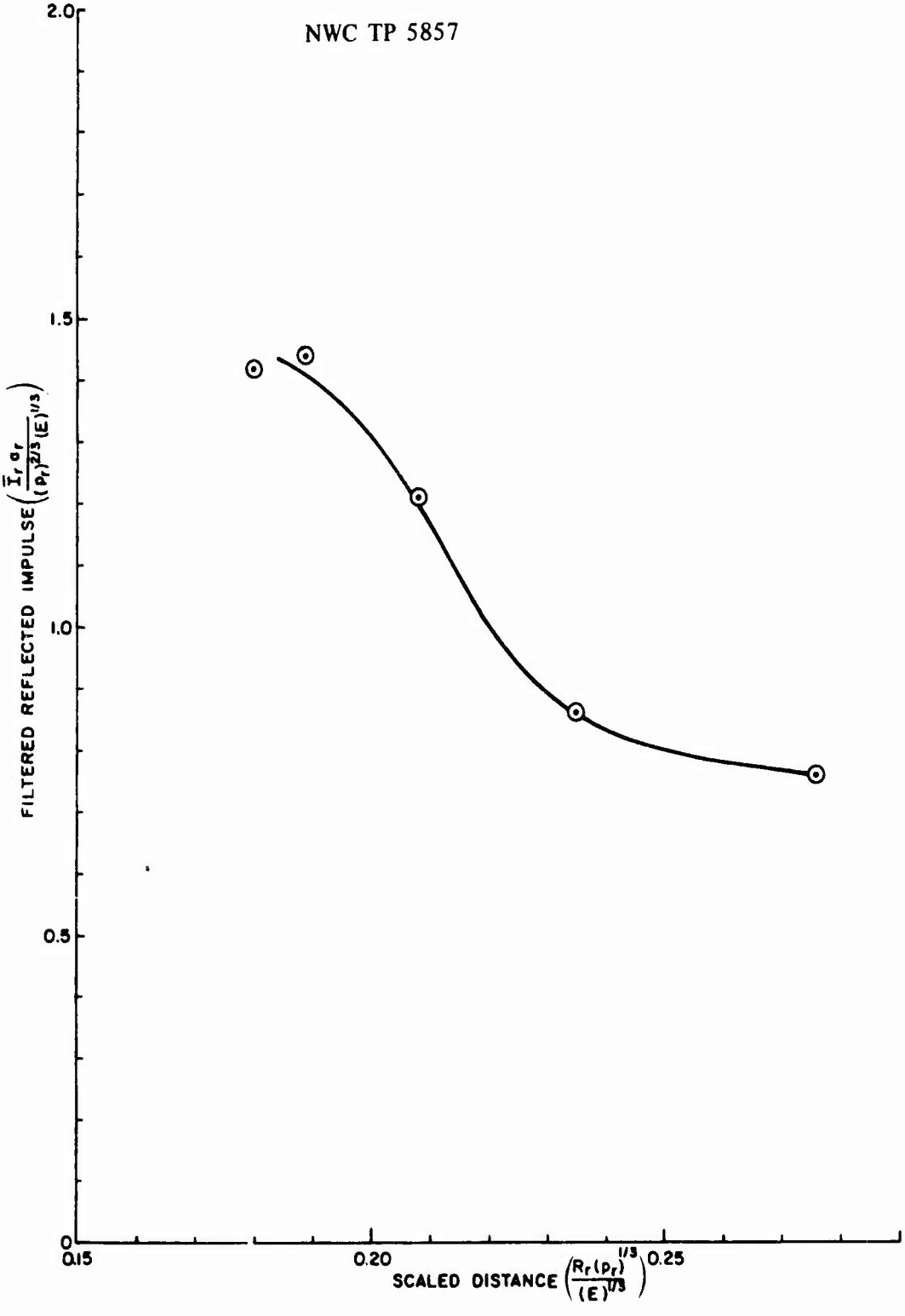

FIGURE 26. Average Filtered Reflected Impulse versus Scaled Distance for Bare Pentolite Cylinders (Normalized Data).

TABLE 10

Fluidically Encased Charge Dimensions

Series	Type of Encasement	Charge Length (mm)	Charge Diameter (mm)	Length-to-Diameter Ratio (L/D)	Charge Mass (grams)	Surround Mass* (grams)	Charge-to-Mass Ratio (C/M)
64	Water/Lucite	133	59	2.25	582	1350	0.43
	Ethylene Glycol/Lucite	133	59	2.25	570	1511	0.38
	Glycerol/Lucite	133	59	2.25	568	1661	0.34
80	Water/Lucite	133	75	1.77	944	1140	0.83
	Ethylene Glycol/Lucite	133	75	1.77	958	1229	0.78
	Glycerol/Lucite	133	75	1.77	953	1363	0.70
95	Water/Lucite	133	90	1.48	1385	866	1.60
	Ethylene Glycol/Lucite	133	90	1.48	1368	979	1.40
	Glycerol/Lucite	133	90	1.48	1351	1064	1.27
110	Water/Lucite	133	105	1.27	1869	561	3.33
	Ethylene Glycol/Lucite	133	105	1.27	1907	620	3.08
	Glycerol/Lucite	133	105	1.27	1868	648	2.88
120	Water/Lucite	133	113	1.18	2143	388	5.52
	Ethylene Glycol/Lucite	133	113	1.18	2173	392	5.54
	Glycerol/Lucite	133	113	1.18	2187	432	5.06
64	Solder	127	60	2.12	592	11350	0.05
	Leaded Glass	127	60	2.12	590	6971	0.09
	Glass	126	60	2.10	550	3571	0.15
	Water/Cardboard	133	59	2.25	588	1350	0.44

TABLE 10 (Continued)

Series	Type of Encasement	Charge Length (mm)	Diameter (mm)	Length-to-Diameter Ratio (L/D)	Charge Mass (grams)	Surround Mass* (grams)	Charge-to-Mass Ratio (C/M)
80	Solder	127	75	1.69	953	9472	0.10
	Leaded Glass	120	73	1.64	814	5673	0.14
	Glass	126	73	1.73	899	3000	0.30
	Water/Cardboard	133	75	1.77	960	1126	0.85
95	Solder	127	90	1.41	1230	7232	0.18
	Leaded Glass	125	95	1.32	1428	4224	0.34
	Glass	128	95	1.35	1425	2100	0.68
110	Solder	127	105	1.21	1819	4607	0.40
	Leaded Glass	124	105	1.18	1732	3028	0.57
	Glass	126	105	1.20	1777	1832	0.97
120	Solder	127	115	1.10	2103	2867	0.73
	Leaded Glass	126	115	1.10	2147	2051	1.05
	Glass	125	114	1.10	2095	1085	1.93

*Exclusive of lucite or cardboard

1/16 inch. In addition, a series of fourteen fluidically encased explosive charges were fired at the VADAM test arena. These high density surrounds were manufactured from solder and glass. Table 10 is a summary of the pertinent charge and surround dimensions as well as the mass of the surround materials. The density values for the surround materials mentioned in Table 10 are given in Table 11. The density values for the liquids are published values whereas those for the three solid materials were calculated from the dimensions of the surrounds.

TABLE 11

Encasement Material Densities

Material Type	Density (g/cm^3)
Water	1.00
Ethylene Glycol	1.11
Glycerol	1.26
Glass	2.68
Leaded Glass	5.37
Solder	9.04

All the blast parameters for fluidically encased explosive charges are unscaled. The quoted values were measured at an atmospheric pressure of 11.867 lb/in^2. The following parameters need to be defined:

P_r is the peak pressure as given by the response of the 50 μsec rise time low-pass filter. This is not the maximum excursion of the spikes shown in the raw data. It is, therefore, called the "filtered reflected peak pressure, lb/in^2".

I_r is the area under the filtered pressure time curve. It is called the "filtered reflected positive impulse, lb/in^2 - msec".

The measured near-field blast parameters for the fluidically encased pentolite cylinders are given in Table 12 and Table 13. Referring to Table 12, the wide variation in peak pressure and positive impulse existent for a number of the surround charge combinations can be observed. For example, in the 64-Series, glycol/lucite, leaded glass, glass and water/cardboard exhibited variations in the data ranging by factors of 2.9, 6.8, 10.1 and 11.3 for the filtered peak pressure values and by factors of 1.7, 8.0, 8.4 and 12.4 for the filtered impulse values respectively. Data for the other charge series show similar variations. It is felt that the primary cause for the wide variation in data is relatable to the size of the impacting particles, when these particles impact, and the total time over which the particles impact the face of the bar. For example, a uniformly expanding fine

TABLE 12

Blast Parameters for Fluidically Encased Pentolite Cylinders as Measured at an Atmospheric Pressure of 11.867 lb/in^2 and at a 36.0-inch Standoff Distance.

Series	Type of Encasement	Charge-to-Mass Ratio (C/M)	Filtered Reflected Peak Pressure ($\bar{P}_r$) (lb/in^2)	Filtered Reflected Positive-Impulse ($\bar{i}_r$) (lb/in^2 - msec)	Hopkinson Pressure Bar Material
64	Water/Lucite	0.43	1563	322	Brass
			1855	267	Aluminum
	Glycol/Lucite	0.38	2769	353	Brass
			971	208	Aluminum
	Glycerol/Lucite	0.34	2427	358	Aluminum
80	Water/Lucite	0.83	2631	631	Aluminum
	Glycol/Lucite	0.78	1140	277	Aluminum
			1340	288	Aluminum
			1422	266	Brass
	Glycerol/Lucite	0.70	2283	326	Aluminum
			1546	298	Brass
95	Water/Lucite	1.60	1861	425	Aluminum
			1855	445	Brass
	Glycol/Lucite	1.40	1813	517	Aluminum
			1484	366	Brass
	Glycerol/Lucite	1.27	1737	325	Aluminum
			1608	305	Brass
110	Water/Lucite	3.33	2072	434	Aluminum
			2730	425	Aluminum
			2534	374	Brass
	Glycol/Lucite	3.08	2085	389	Aluminum
			2102	421	Brass
	Glycerol/Lucite	2.88	2134	441	Aluminum
			2287	399	Brass
120	Water/Lucite	5.52	1986	379	Aluminum
			2936	429	Brass
	Glycol/Lucite	5.54	1861	417	Aluminum
			2936	489	Brass
	Glycerol/Lucite	5.06	2590	450	Aluminum
			2730	442	Brass
64	Solder	0.05	9416	2355	Steel
	Leaded Glass	0.09	8487	2909	Steel
			4963	1726	Steel
			33810	13767	Steel
	Glass	0.015	5475	1557	Steel
			1985	690	Steel
			13979	5801	Steel
	Water/Cardboard	0.44	3286	1083	Steel
			3997	1003	Steel
			1688	360	Steel
			1324	468	Steel
			14907	4481	Steel

TABLE 12 (Continued)

Series	Type of Encasement	Charge-to-Mass Ratio (C/M)	Filtered Reflected Peak Pressure ($\bar{P}_r$) (lb/in^2)	Filtered Reflected Positive-Impulse ($\bar{T}_r$) (lb/in^2 - msec)	Hopkinson Pressure Bar Material
80	Solder	0.10	15223	-	Aluminum
			19571	4258	Aluminum
			12189	-	Aluminum
			15237	1986	Aluminum
			27800	-	Steel
	Leaded Glass	0.14	14236	3721	Steel
			6618	1973	Steel
			47949	13248	Steel
	Glass	0.30	9582	2506	Steel
			3805	1578	Steel
			47949	15118	Steel
	Water/Cardboard	0.85	2738	949	Steel
			2628	623	Steel
			1191	385	Steel
			3508	399	Steel
			10143	2251	Steel
			7069	1061	Steel
95	Solder	0.18	19847	5012	Aluminum
			15672	2729	Aluminum
			65511	15092	Steel
	Leaded Glass	0.35	This data was lost (when tank test facility cracked)		
	Glass	0.68	9582	3227	Steel
			7445	1923	Steel
			33810	15672	Steel
110	Solder	0.40	24161	4078	Aluminum
			53604	18544	Steel
	Leaded Glass	0.57	18889	3227	Steel
			11581	4192	Steel
			33195	9827	Steel
	Glass	0.97	3805	1638	Steel
			11343	4641	Steel
120	Solder	0.73	13140	2278	Steel
			4963	2624	Steel
			15368	3810	Steel
	Leaded Glass	1.05	7528	2088	Steel
			2647	2613	Steel
			12294	3723	Steel
	Glass	1.93	2190	425	Steel
			2316	404	Steel
			3842	398	Steel

TABLE 13

Averaged Filtered Blast Parameters for Fluidically Encased Pentolite Cylinders as Measured at an Atmospheric Pressure of 11.867 lb/in^2 and at a 36.0-inch Standoff Distance.

Series	Type of Encasement	Charge-to-Mass Ratio (C/M)	Filtered Reflected Peak Pressure ($\overline{P}_r$) (lb/in^2)	Filtered Reflected Positive Impulse ($\overline{I}_r$) (lb/in^2 - msec)
64	Water/Lucite	0.43	1709	300
	Glycol/Lucite	0.38	1870	281
	Glycerol/Lucite	0.34	2427	358
80	Water/Lucite	0.83	2631	631
	Glycol/Lucite	0.78	1301	277
	Glycerol/Lucite	0.70	1915	312
95	Water/Lucite	1.60	1858	435
	Glycol/Lucite	1.40	1649	442
	Glycerol/Lucite	1.27	1673	315
110	Water/Lucite	3.33	2445	441
	Glycol/Lucite	3.08	2094	405
	Glycerol/Lucite	2.88	2211	420
120	Water/Lucite	5.52	2461	404
	Glycol/Lucite	5.54	2399	453
	Glycerol/Lucite	5.06	2660	446
64	Solder	0.05	9416	2355
	Leaded Glass	0.09	15753	6134
	Glass	0.15	9146	2683
	Water/Cardboard	0.44	5040	1479
80	Solder	0.10	18004	3122
	Leaded Glass	0.14	22934	6314
	Glass	0.30	20445	6401
	Water/Cardboard	0.85	4546	945
95	Solder	0.18	33677	7611
	Glass	0.68	16946	6941
110	Solder	0.40	38883	11311
	Leaded Glass	0.57	21222	5749
	Glass	0.97	7574	3140
120	Solder	0.73	11157	2904
	Leaded Glass	1.05	7490	2808
	Glass	1.93	2783	409

particulate cloud would be far more likely to produce more consistent results than an expanding mass of particulate matter containing a number of relatively large fragments. These larger fragments can impact the bar after, before, or during the impact of the smaller particles in the expanding mass and could cause the degree of variation observed in the data. An example of a pressure-time history recorded for a particulate mass felt to contain both small and large particles can be observed in Fig. 39. The data reported in Table 12 are presented graphically in Figs. 27 through 32. In order to compare the data in Table 12, the values for each surround was arithmetically averaged. These averaged values are given in Table 13 and are presented graphically in Fig. 33 and Fig. 34.

For leaded glass, Series 95, data points are missing due to the fact that this test was fired in the tank test facility. This test, followed by a 110-series solder test, led to the rupture of the tank. The tank failure, however, did not cause the loss of data. The data were lost due to the fact that all the strain gauge leads were spalled off from the Hopkinson pressure bars. The difficulty with the loss of this data point is that it would probably have produced a maximum in the filtered reflected peak pressure as well as a maximum filtered reflected positive impulse for the leaded glass test series. The graphs shown in Fig. 33 through 35 for the leaded glass series were drawn to conform to a shape similar to the solder and glass series.

The graph shown in Fig. 35 was plotted to illustrate the enhancement achieved by the use of fluidic surrounds. The length-to-diameter ratios are all kept constant at the values obtained for the bare cylindrically shaped charges. These values do vary as shown in Table 10; however, the error incurred is not very great and does not effect the obvious enhancement illustrated by the curves. Typical pressure-time traces, as measured by Hopkinson pressure bars, during the detonation of fluidically encased Pentolite cylinders, are shown in Fig. 36 through 40.

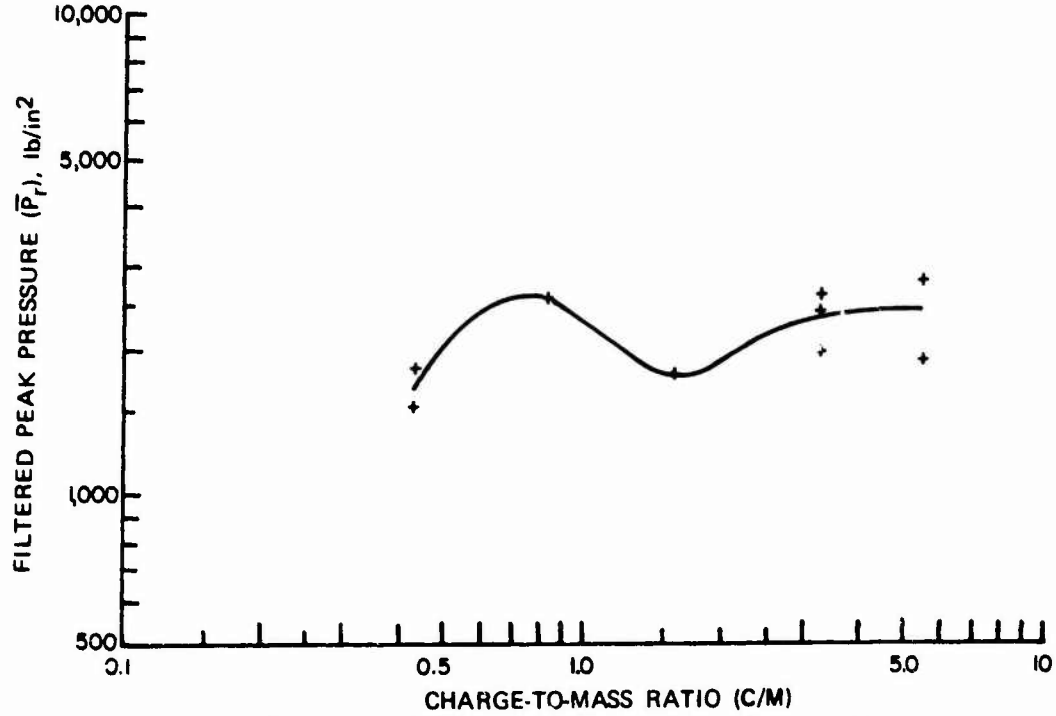

FIGURE 27. Filtered Reflected Peak Pressure Versus Charge-to-Mass Ratio for Water/Lucite Surround.

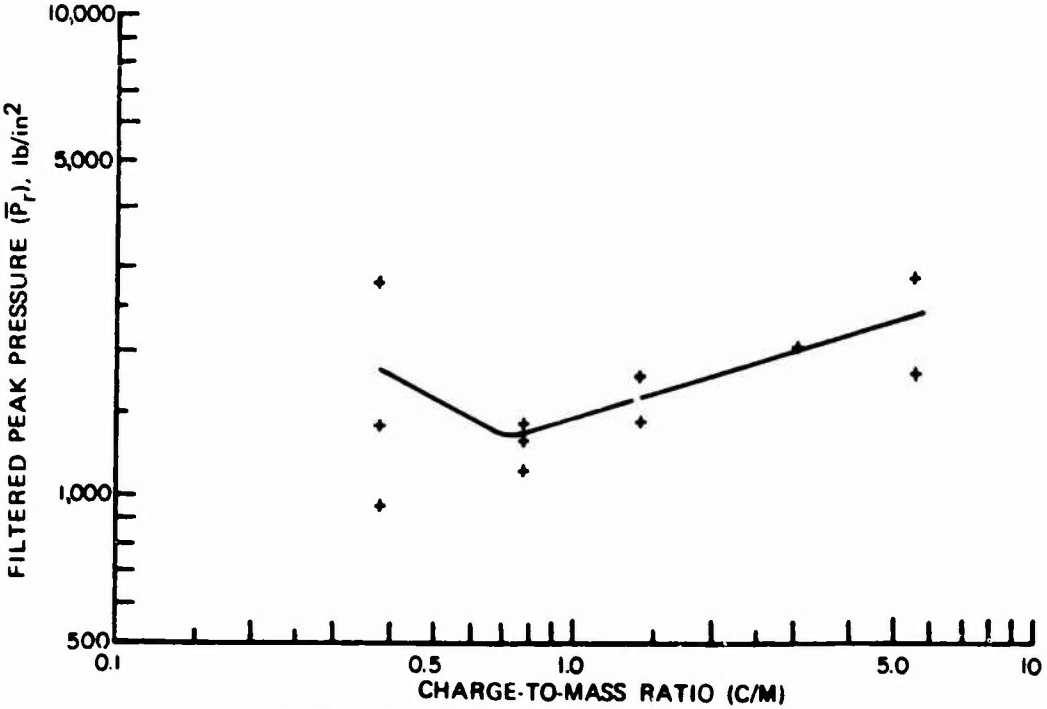

FIGURE 28. Filtered Reflected Peak Pressure Versus Charge-to-Mass Ratio for Glycol/Lucite Surround.

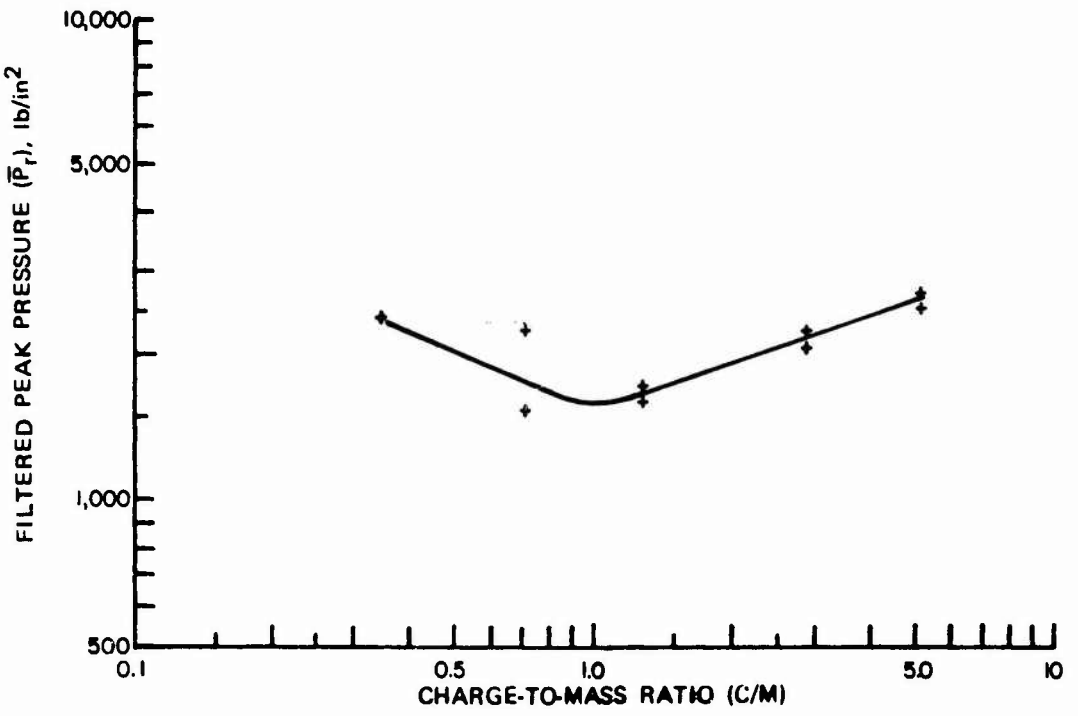

FIGURE 29. Filtered Reflected Peak Pressure Versus Charge-to-Mass Ratio for Glycerol/Lucite Surround.

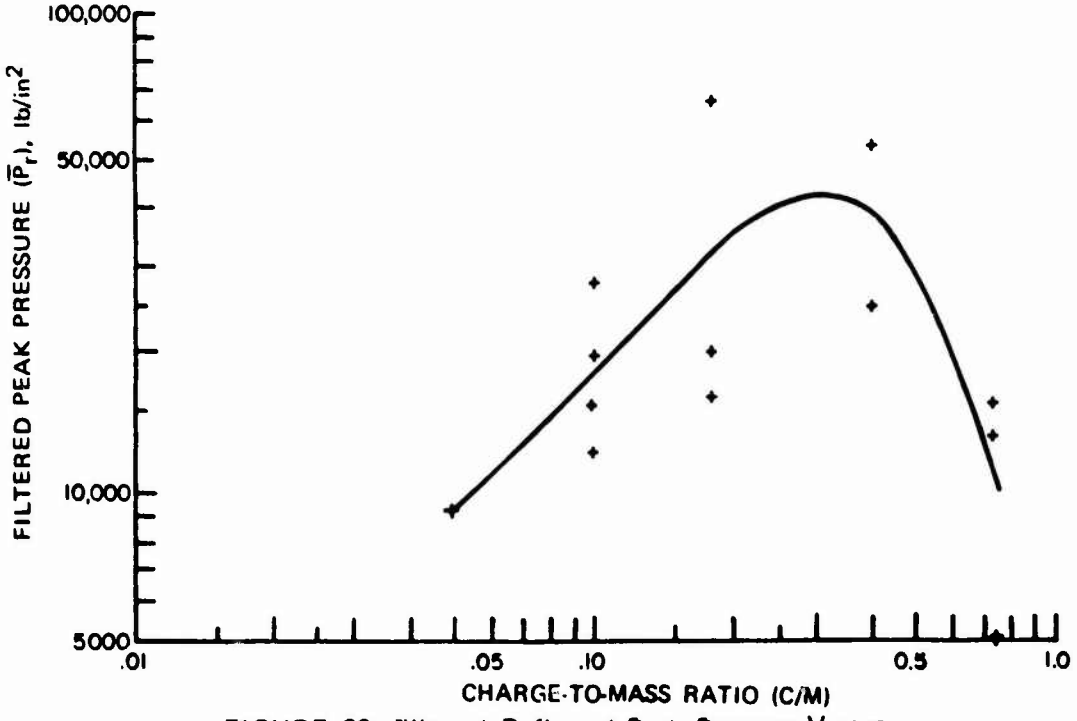

FIGURE 30. Filtered Reflected Peak Pressure Versus Charge-to-Mass Ratio for Solder Surround.

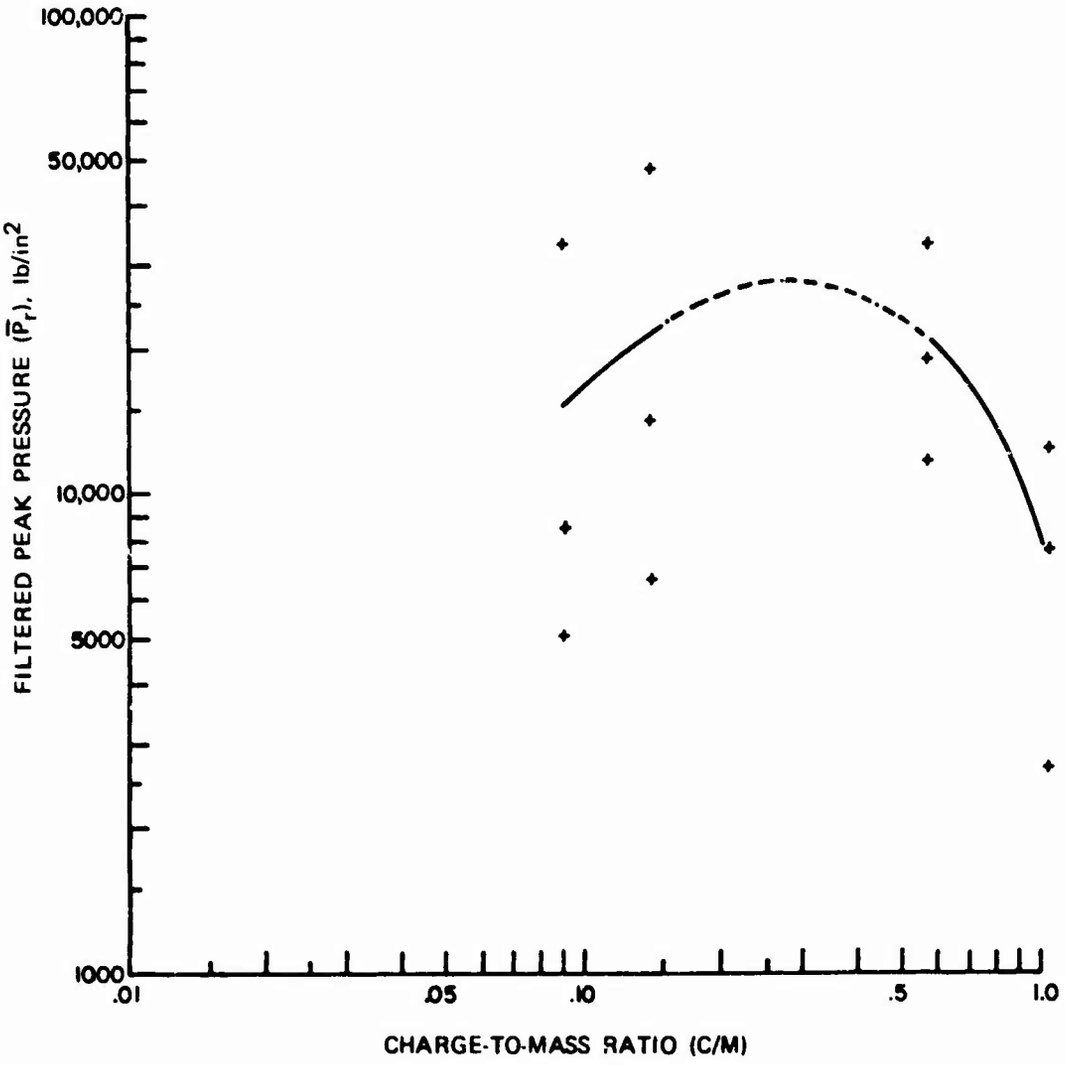

FIGURE 31. Filtered Reflected Peak Pressure Versus Charge-to-Mass Ratio for Leaded Glass Surround.

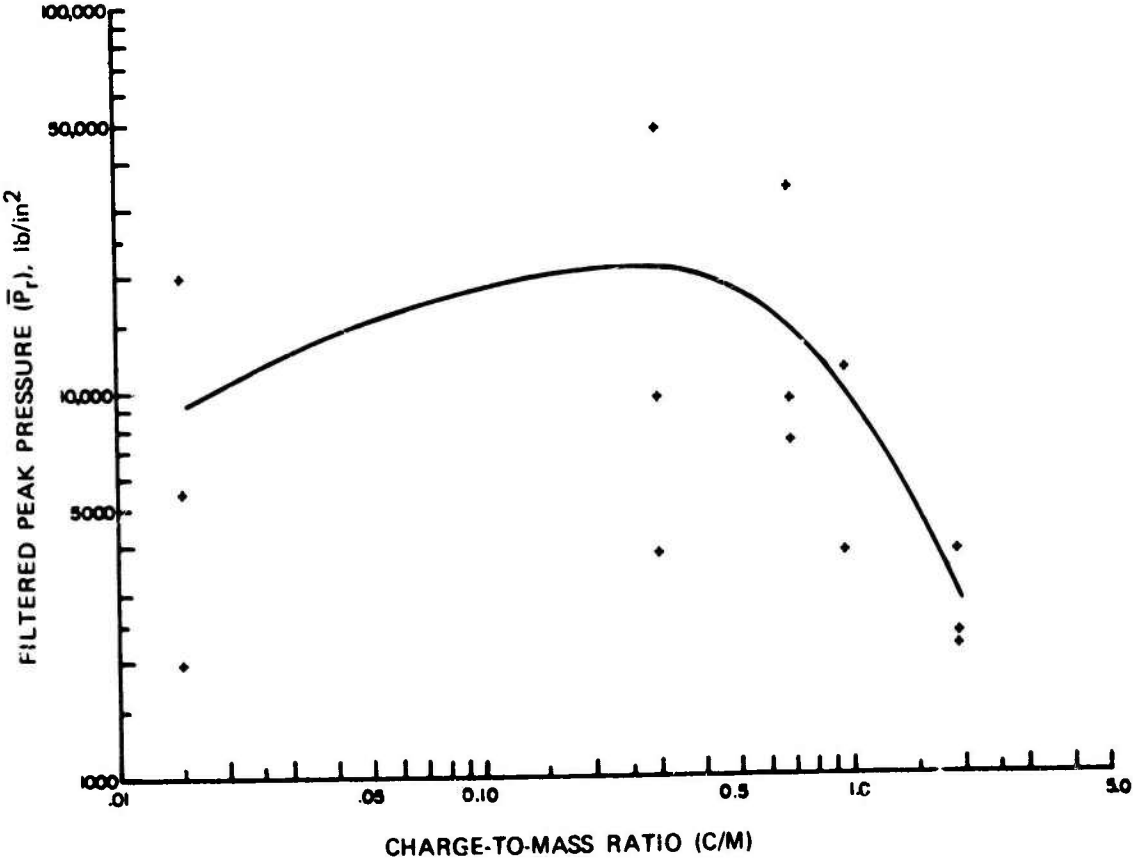

FIGURE 32. Filtered Reflected Peak Pressure Versus Charge-to-Mass Ratio for Glass Surround.

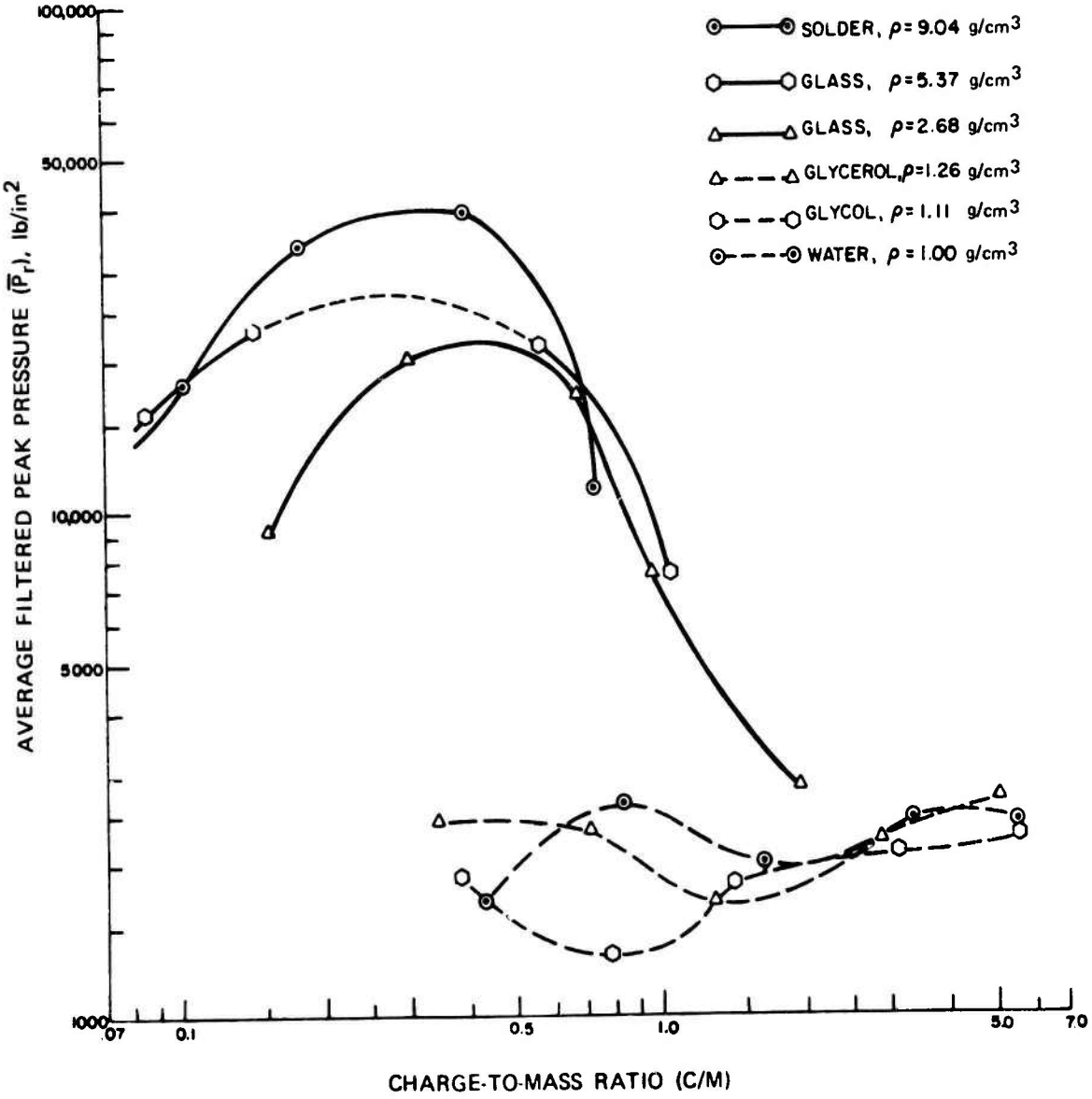

FIGURE 33. Average Filtered Peak Pressure Versus Charge-to-Mass Ratio (Atmospheric Pressure (P_r) of 11.867 lb/in^2).

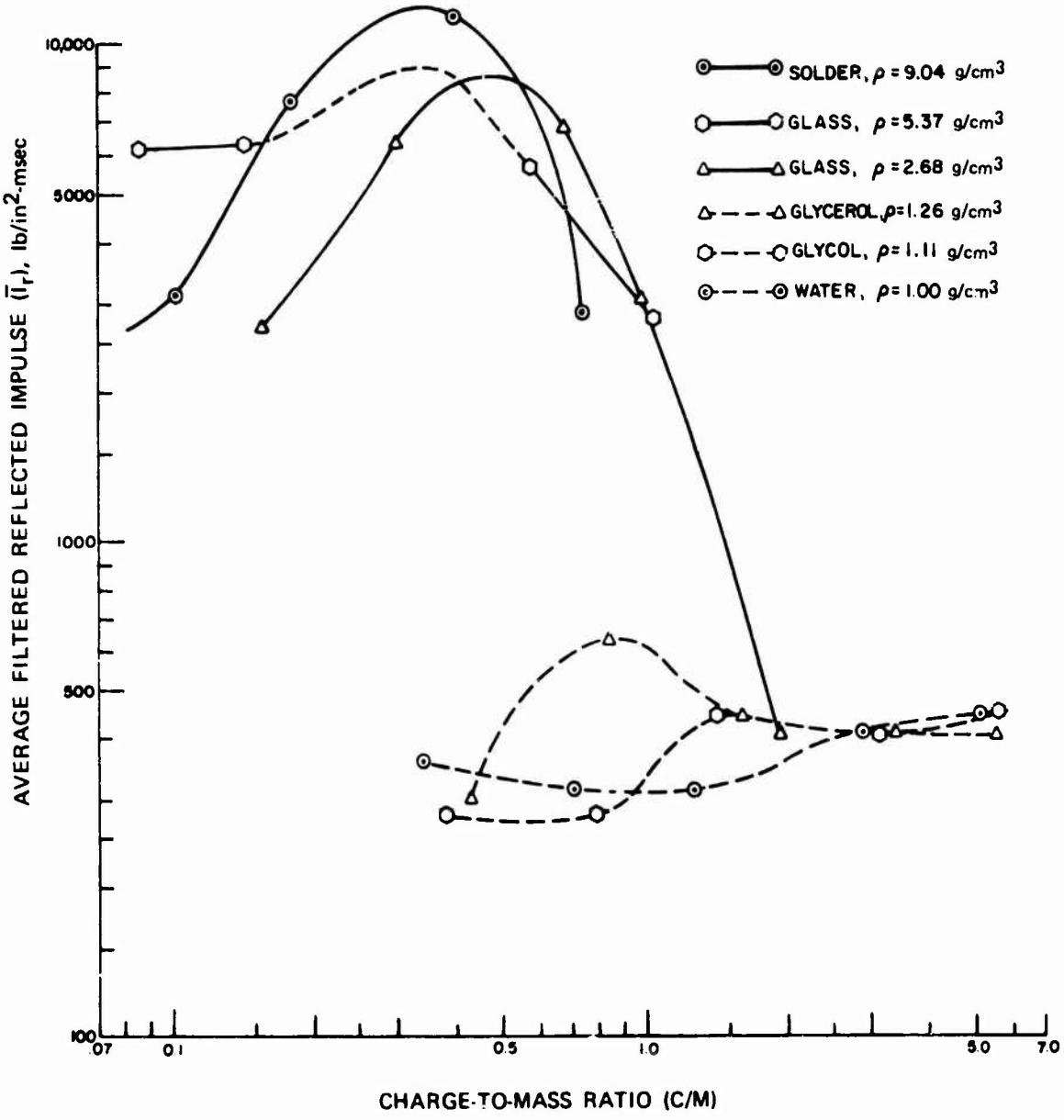

FIGURE 34. Average Filtered Reflected Impulse Versus Charge-to-Mass Ratio (Atmospheric Pressure (P_r) of 11.867 lb/in^2).

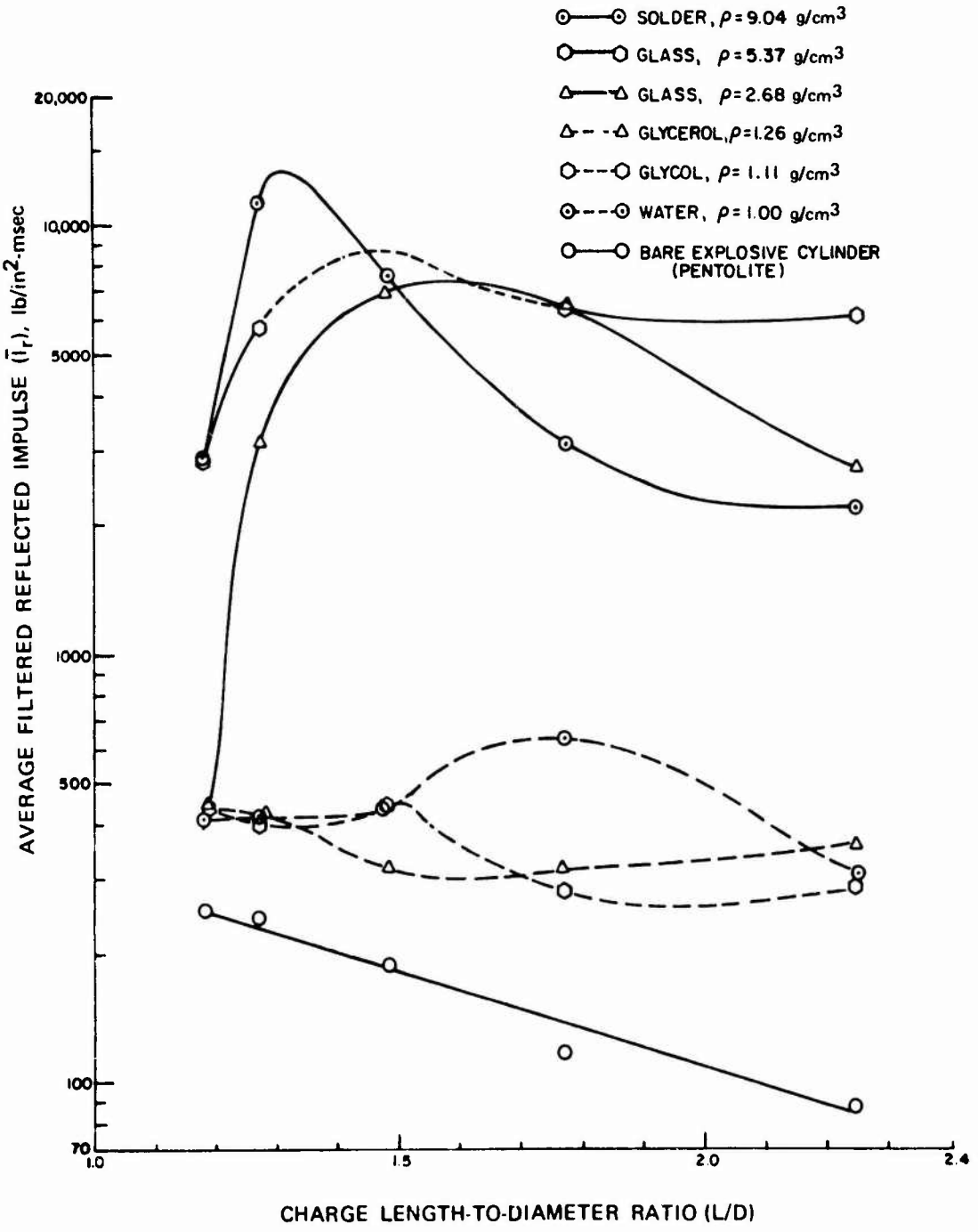

FIGURE 35. Average Filtered Reflected Impulse Versus Charge Length-to-Diameter Ratio (Atmospheric Pressure (P_r) of 11.867 lb/in^2).

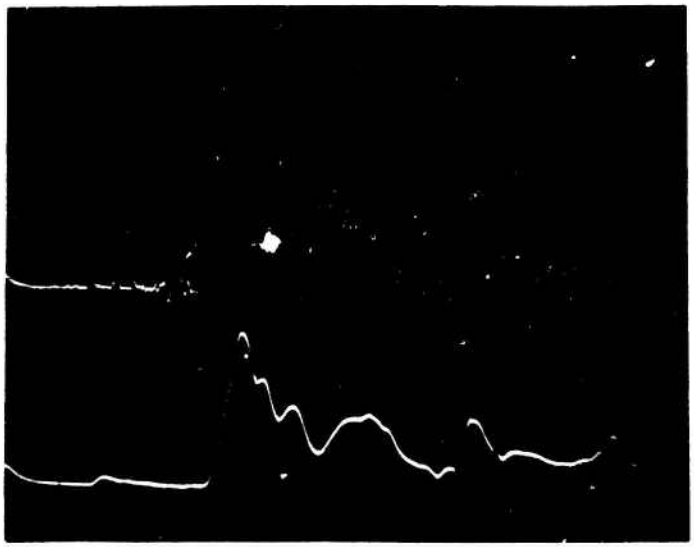

64-Series Water/Lucite
C/M = 0.43

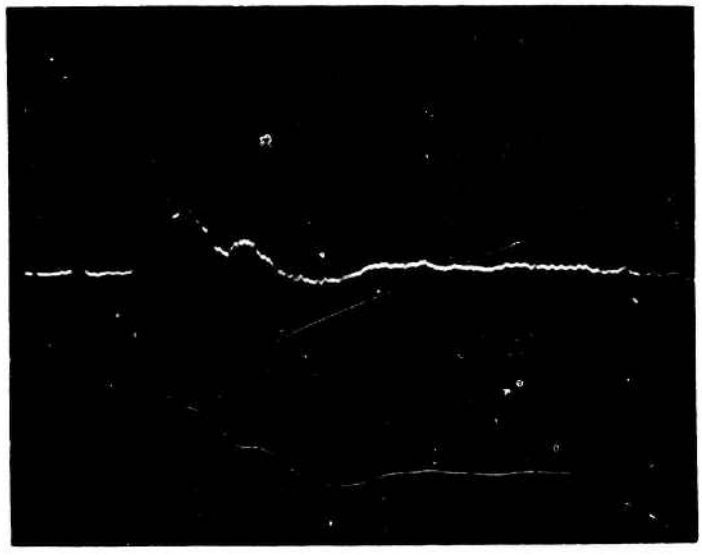

110-Series Water/Lucite
C/M = 3.33

FIGURE 36. Pressure-time Data from Water/Lucite Encased Pentolite Cylinders.

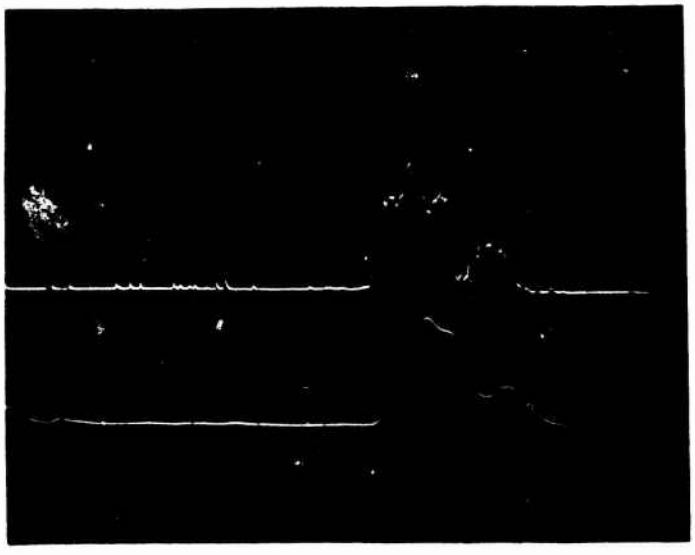

80-Series Solder
C/M = 0.10

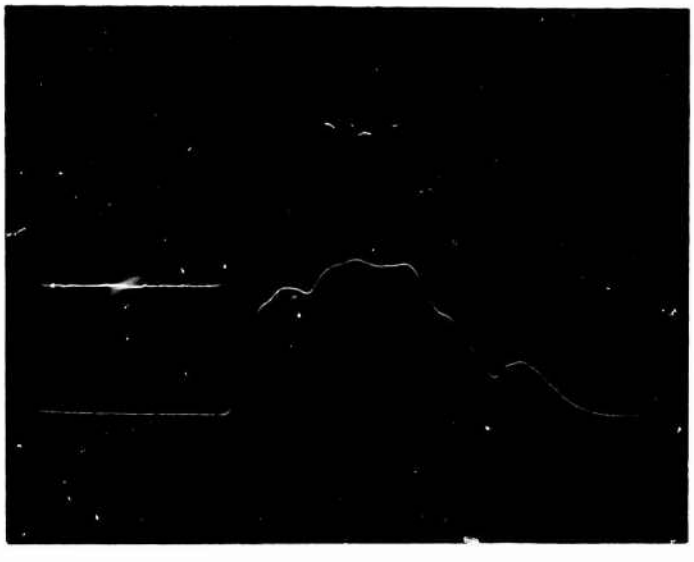

110-Series Solder
C/M = 0.40

FIGURE 37. Pressure-time Data Generated by Solder Encased Pentolite Cylinders.

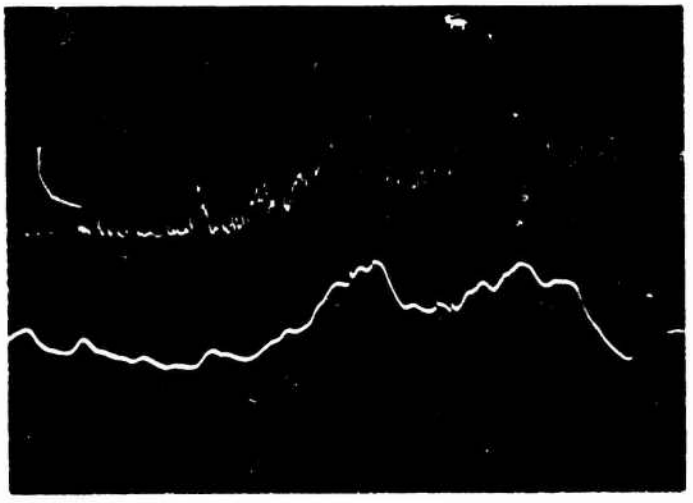

64-Series Leaded Glass
C/M = 0.09

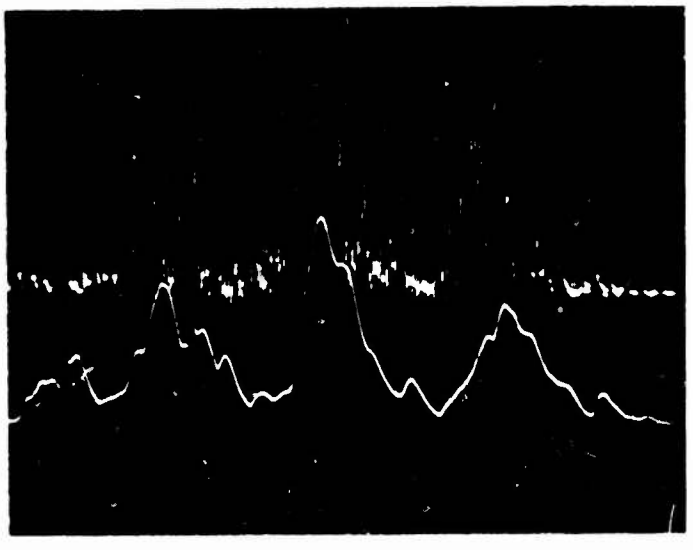

110-Series Leaded Glass
C/M = 0.57

FIGURE 38. Pressure-time Data Generated by Leaded Glass Encased Pentolite Cylinders.

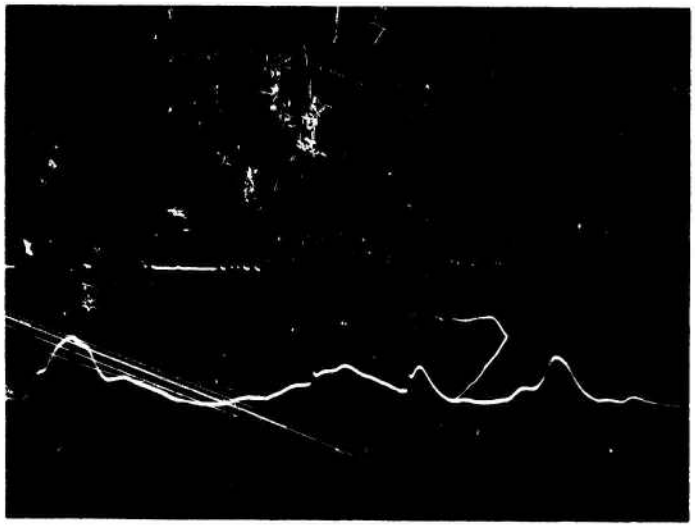

64-Series Glass
C/M = 0.15

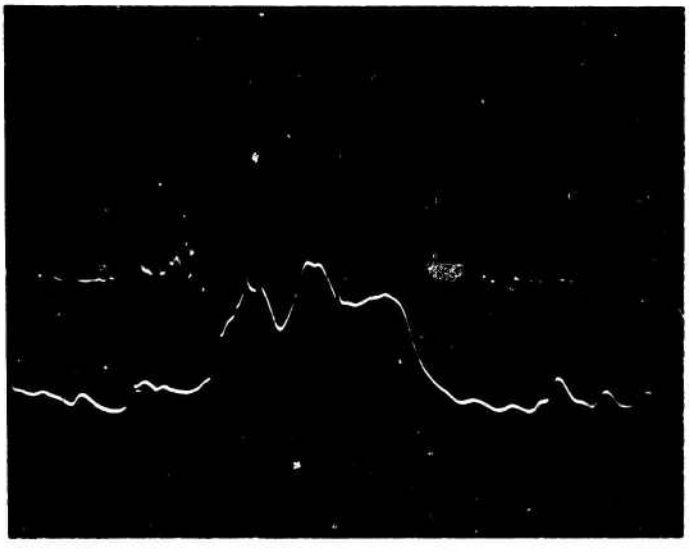

80-Series Glass
C/M = 0.30

FIGURE 39. Pressure-time Data Generated by Glass Encased Pentolite Cylinders.

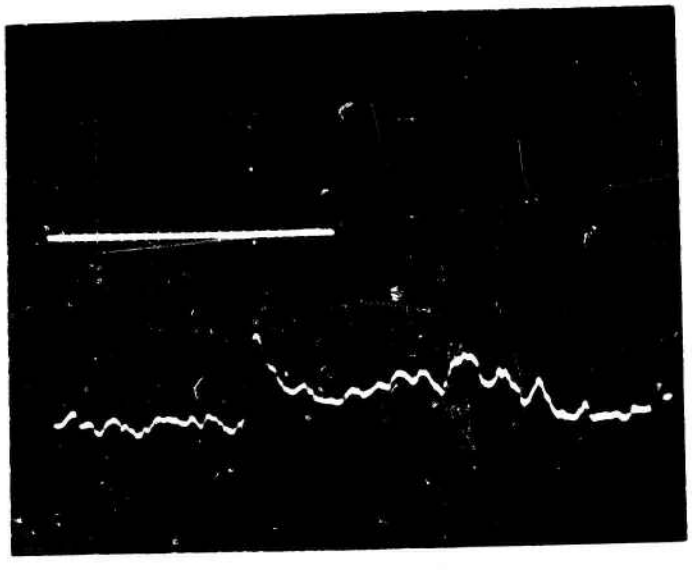

Lower Trace

Vert. Scale

977 $\frac{lb/in^2}{div.}$

Horiz. Scale

100 μs/div

Yellow Brass
Hopkinson Bar

110-Series Solder
C/M = 0.40

FIGURE 40. Pressure-time Data Recorded by a Yellow Brass Hopkinson Bar Situated Behind a Fragment Stripper for a Solder Encased Pentolite Cylinder.

CONCLUSIONS

A tremendous enhancement in blast performance is realized through the use of fluidic surrounds. The enhancement obtained in both peak pressure and positive impulse is phenomenal, especially for the higher density surrounds, i.e., glass, leaded glass, and solder. Maximum peak pressures for these surrounds ranged from approximately 20,000 to 40,000 lb/in^2, while maximum impulse values ranged from approximately 7,000 to 11,000 lb/in^2-msec. Bare cylinder data for the same charge series produced peak pressures ranging from 1,500 to 3,100 lb/in^2, and maximum impulse values ranging from approximately 90 to 250 lb/in^2-msec. Comparison of the values for the optimum surrounds to values obtained for bare pentolite cylinders shows an increase by roughly a multiple of 10 for peak pressure and a multiple of 50 for positive impulse due to charge encasement.

While the enhancement realized for the liquid surrounds was not nearly as phenomenal as that for the solid surrounds, a significant increase in blast performance was observed. The principal increase was in positive impulse which was approximately 2 to 5 times higher than the bare charge data. Peak pressures for the liquid surrounds tended to show a general decrease when compared to the 95, 110 and 120 series bare-charge data, and a general increase when compared to the 64- and 80-series bare-charge data.

The optimum charge to mass ratio appears to decrease as the surround density goes up, at least for the three high density surrounds, as shown in Fig. 34. The maximum reflected impulse seems to increase with the increasing density of the encasement material.

There appear to be three blast wave components associated with the fluidically encased explosives charges: an air blast shock front, high velocity particulate matter, and a slower moving vaporized cloud (especially at high surround densities). The respective times of arrival at the impact ends of the Hopkinson pressure bars changes with the surround density as well as the charge-to-mass ratio.

The peak pressure registered on the yellow brass Hopkinson pressure bar mounted behind the fragment stripper was markedly lower than that obtained from a bare pentolite cylinder of comparable dimensions. This would indicate that there is a degradation of air blast due to the surround material, and that the enhancement observed is due to a momentum transfer mechanism (vaporized cloud as well as particulate matter).

A degradation of rise time appeared to occur whenever the vaporized cloud was the predominant damage producing agent. This can be observed in Figs. 37 through 39.

In future work of this nature, it would be useful to place the Hopkinson bars at different standoff distances so that the pressure-distance profile of the observed blast enchancement could be determined. The effect would be better understood if a method could be devised to measure the three blast components separately but concurrently. Having a sensitive Hopkinson pressure bar system mounted behind a fragment stripper would be the logical initial step.

RECOMMENDATIONS

It is felt that the number of surround materials should be reduced in favor of more tests of the same density surround materials at different charge-to-mass ratios. In the case of liquids, water should be used throughout to first establish an impulse versus charge-to-mass ratio curve with an increased level of confidence in the data. The spread of the data obtained to date does not provide sufficient confidence in the enhancement effect obtained with liquids.

The problem of the negative precursor could probably be solved by center point initiation of the test cylinders instead of a single end point initiation.

Future tests should incorporate various target configurations and target materials to determine the enhanced damage potential from encased charges at the same time that the blast profile measurements are being obtained.

APPENDIX A

PNEUMATIC LAUNCHER

The pneumatic launcher shown in Fig. A-1 was used in the first attempt to calibrate the Hopkinson pressure bars. This launcher fires projectiles having a 1/2-inch diameter and lengths of 1/2-inch, 1 1/2-inch, 3 inches and 6 inches. The system used to determine the projectile velocity consisted of two light beams, spaced 8 inches apart, situated at the muzzle end of the pneumatic launch tube. The interval between the interruption of the two beams, by the projectile, provided a measure of the average projectile velocity. Projectiles made from steel, aluminum and yellow brass were fired at predetermined velocities to simulate the approximate impulse from an explosive test charge. Since the projectiles and Hopkinson bars were manufactured from the same metallic alloy in each case, the calibration factor for each system was calculated using the following equation:

$$S = \frac{\Delta\upsilon}{72\ \rho\ C\ V_p}\ \frac{\text{millivolts}}{\text{lb/in}^2}$$

$\Delta\upsilon$ is the change in output voltage, mV

ρ is the density of the metallic bar, lb-sec^2/in^4

C is the acoustic velocity in the bar, ft/sec

V_p is the projectile velocity, ft/sec

Results obtained from the pneumatic launcher did not provide a satisfactory calibration for the Hopkinson pressure bars. A typical oscilloscope trace is shown in Fig. A-2. While the traces look correct the calculated calibration factors did not always correspond to the calibration factors determined from piezoelectric gauge measurements obtained during the detonation of bare spherical test charges. The reason for this appeared to be an inaccurate measurement of projectile velocity over the 8-inch separation distance between detectors as a result of friction and/or skipping or sticking of the projectile.

Table A-1 illustrates the inconsistency of this method for calibrating the Hopkinson pressure bars. For this reason the calibration factors determined by the pneumatic launcher technique were not used for computations during the course of this program.

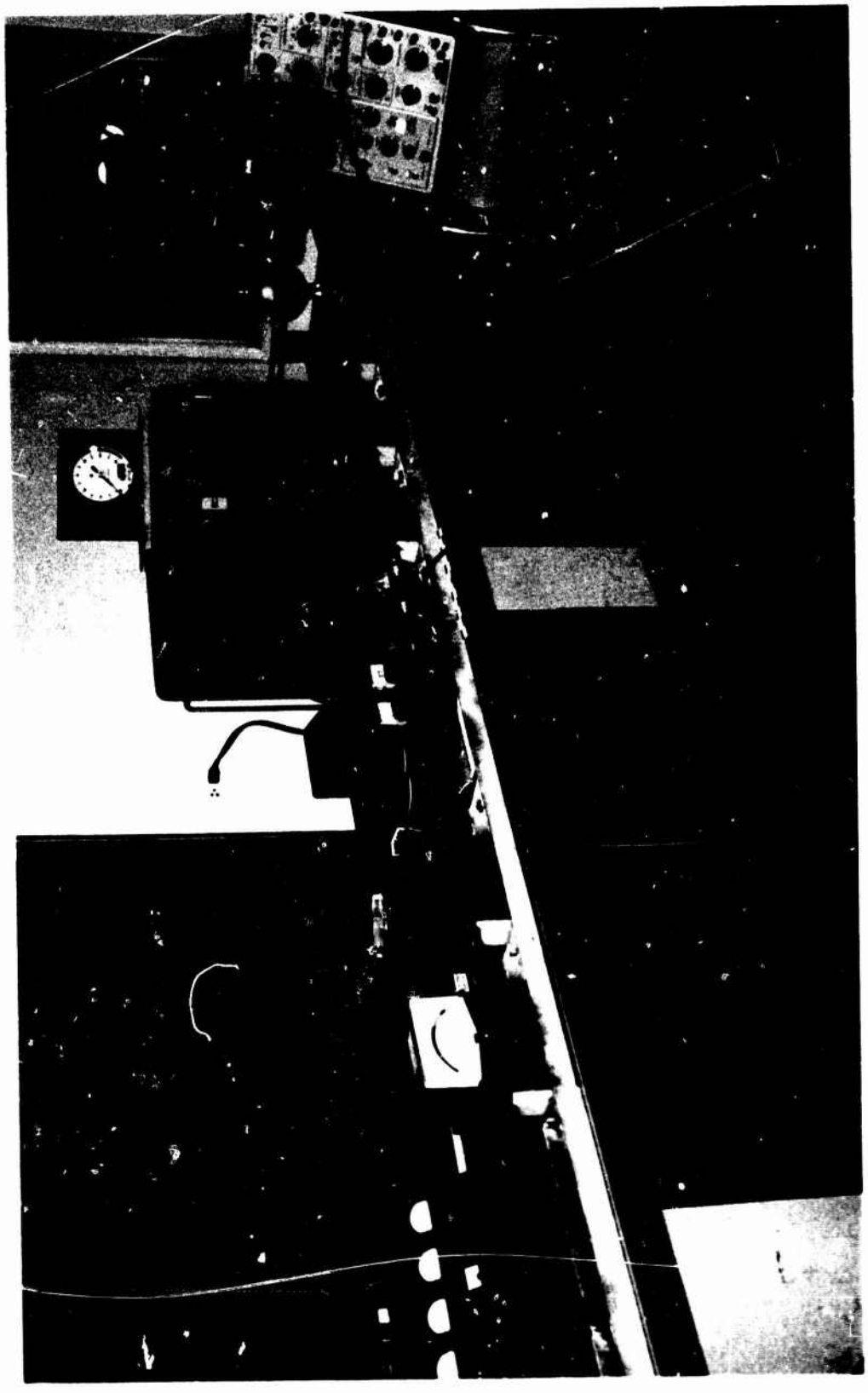

FIGURE A-1. Pneumatic Launcher.

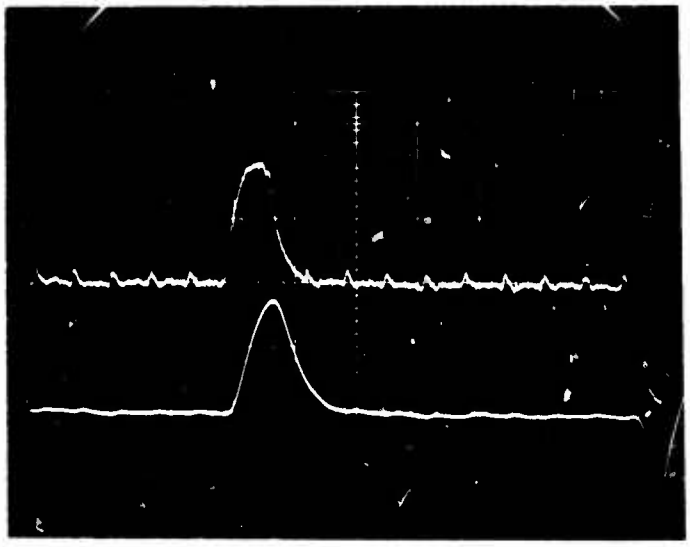

FIGURE A-2. Calibration Trace Using Pneumatic Launcher; Projectile Velocity = 3.89 ft/sec, Projectile Length = 6.0-inch.

TABLE A-1

Calibration Factors, S, Obtained by Using Different Calibration Methods on Aluminum Bars

Amplifier Number	Spherical Charge Calibration ($mV/lb/in^2$)	Analytical Calibration ($mV/lb/in^2$)	Launcher Calibration ($mV/lb/in^2$)
1	0.29	0.31	0.31
2	0.25	0.29	0.35

APPENDIX B

RAW DATA

Included in this appendix are the unfiltered and filtered raw pressure-time data obtained from one shot of each test series for both the bare pentolite and the encased pentolite cylinders. Review of these data provides a better understanding of the type of signals recorded as well as the difficulties encountered in interpretation of some of the data.

In each figure (for the first three sets of records) the top data trace is the unfiltered (or raw data) signal and the bottom trace is the filtered signal as recorded through a 50 μsec rise time low-pass filter. The fourth set of traces recorded are from a piezoelectric gauge (normally top) and a brass bar current source (bottom). The sweep rate for each trace is 100 μsec per cm unless otherwise noted. The amplifier arrangement is normally 1, 2, 3 and 4 reading upper left, upper right, lower left and lower right, respectively.

Aluminum Bar, 690 lb/in^2/div

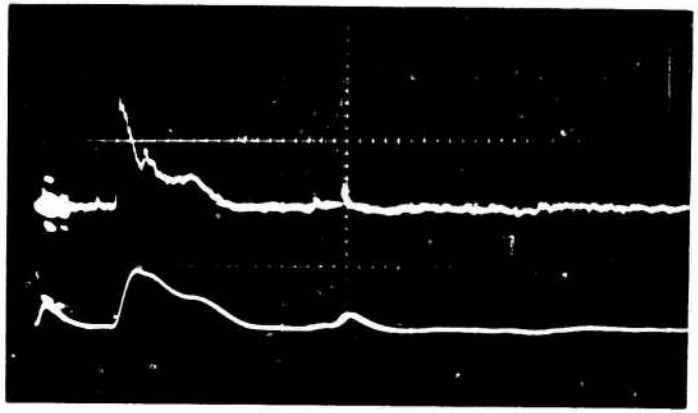

Steel Bar, 1111 lb/in^2/div

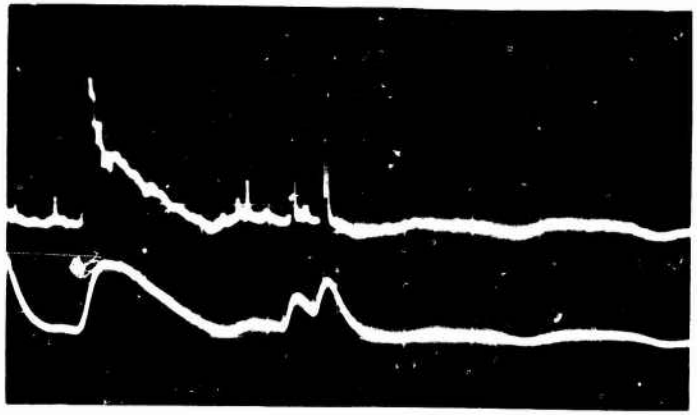

Aluminum Bar, 769 lb/in^2/div

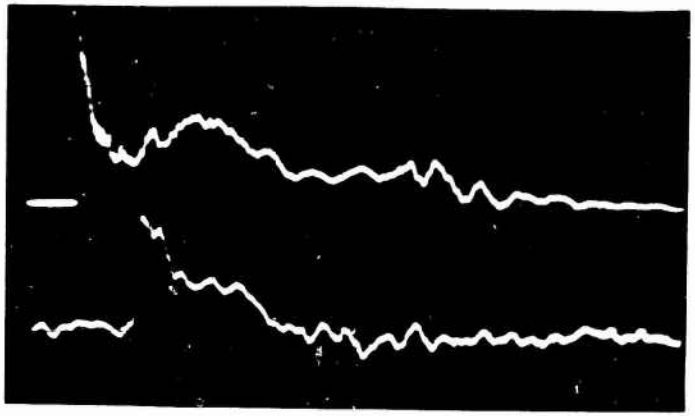

Piezoelectric Gauge, 521 lb/in^2/div (top)
Fragment Stripper In
Current Source, 905 lb/in^2/div (bottom)

FIGURE B-1. Pressure-Time Data from a 64-Series, 573-Gram, Pentolite Cylinder. Cylinder Dimensions, 2¼-inch OD by 5-inches Long. Sweep Rate 100 µsec/div.

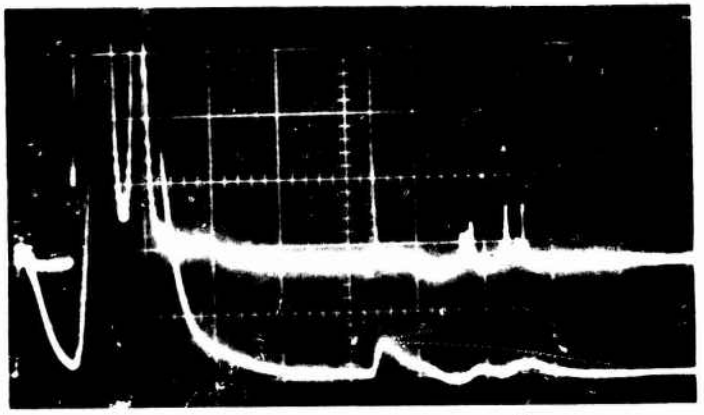

Aluminum Bar, 1724 lb/in^2/div

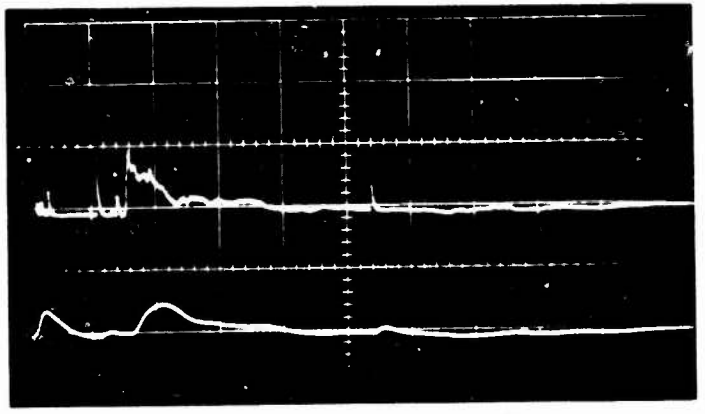

Aluminum Bar, 2000 lb/in^2/div

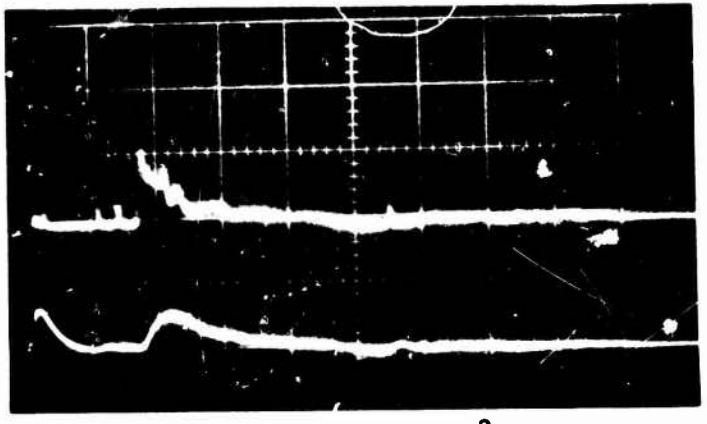

Aluminum Bar, 1923 lb/in^2/div

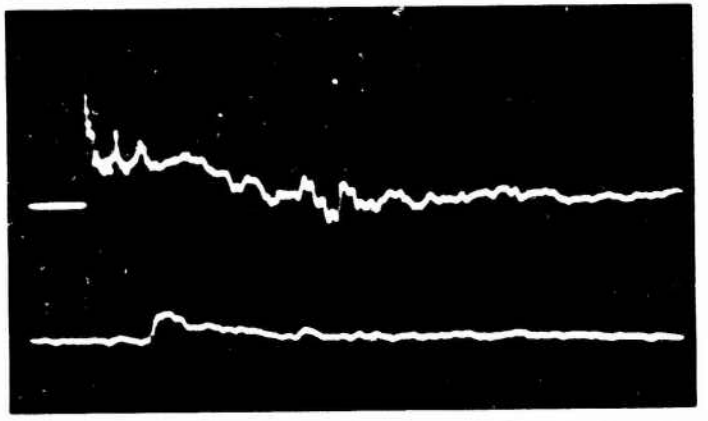

Piezoelectric Gauge, 1042 lb/in^2/div (top)
Fragment Stripper In
Current Source, 3690 lb/in^2/div (bottom)

FIGURE B-2. Pressure-Time Data from an 80-Series, 945-Gram, Pentolite Cylinder. Cylinder Dimensions, 3-inch OD by 5-inches Long. Sweep Rate 100 µsec/div.

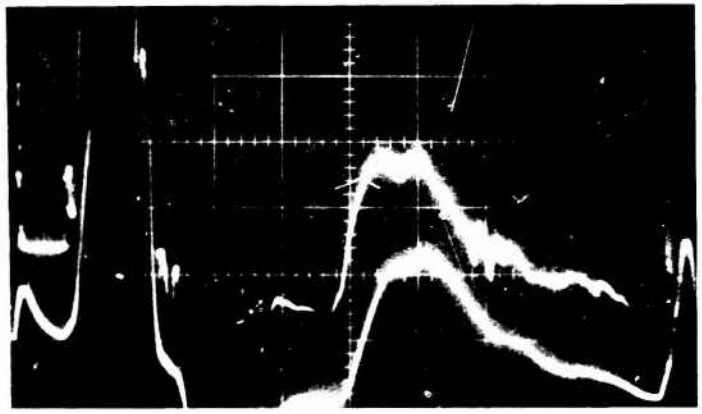

Aluminum Bar, 3448 lb/in^2/div

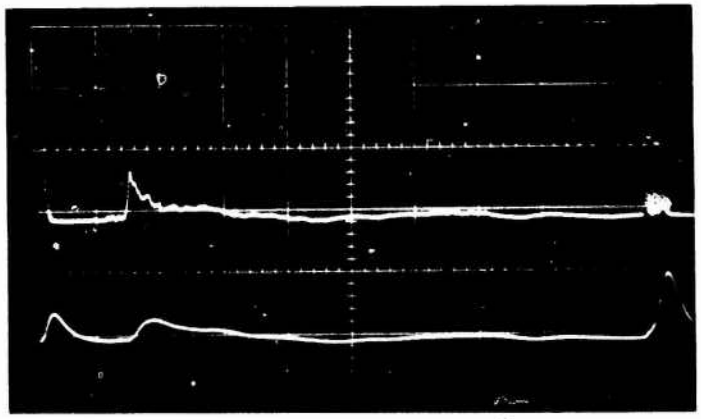

Aluminum Bar, 4000 lb/in^2/div

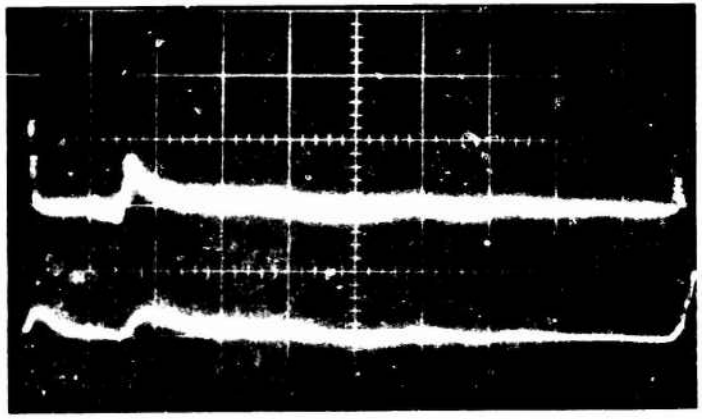

Aluminum Bar, 3846 lb/in^2/div

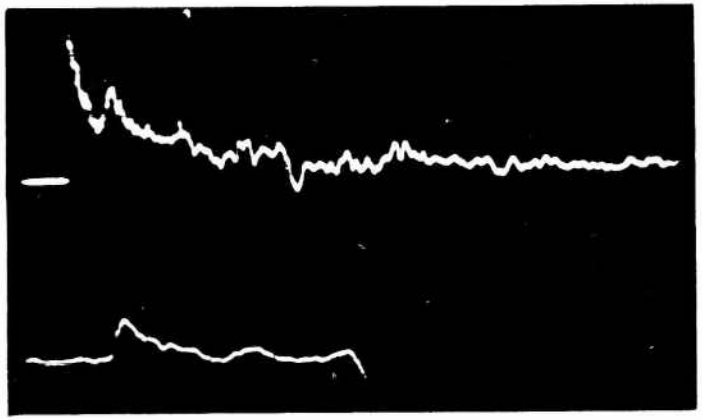

Piezoelectric Gauge, 1042 lb/in^2/div (top)
Current Source, 5210 lb/in^2/div (bottom)

FIGURE B-3. Pressure-Time Data from a 95-Series, 1370-Gram, Pentolite Cylinder. Cylinder Dimensions, 3½-inch OD by 5-inches Long. Sweep Rate 100 µsec/div.

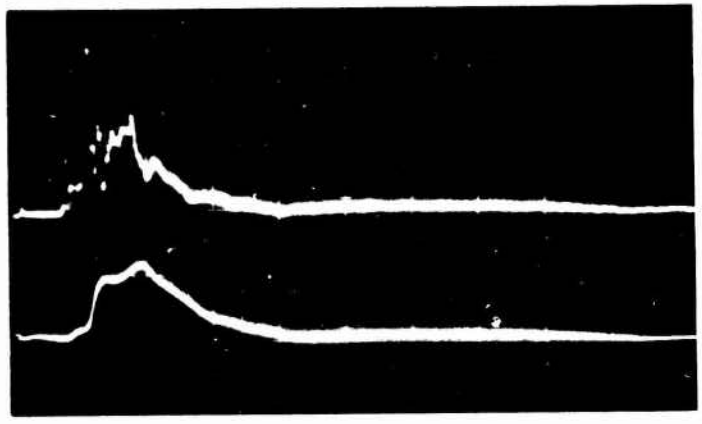

Aluminum Bar, 1724 lb/in^2/div

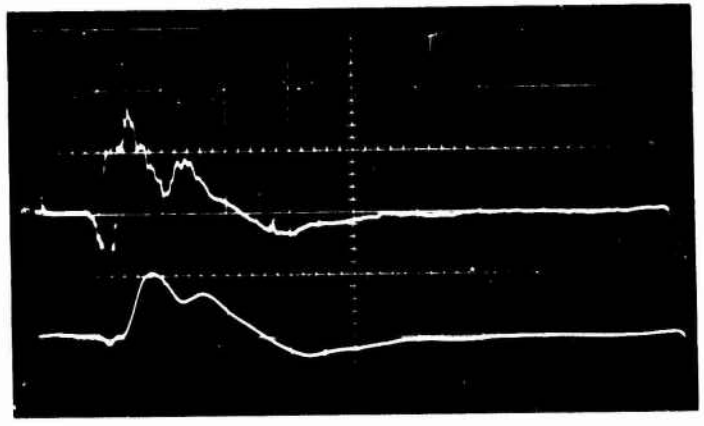

Aluminum Bar, 2000 lb/in^2/div

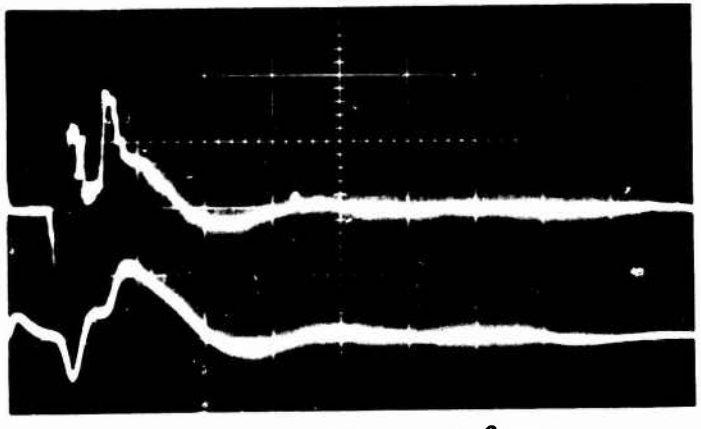

Aluminum Bar, 1923 lb/in^2/div

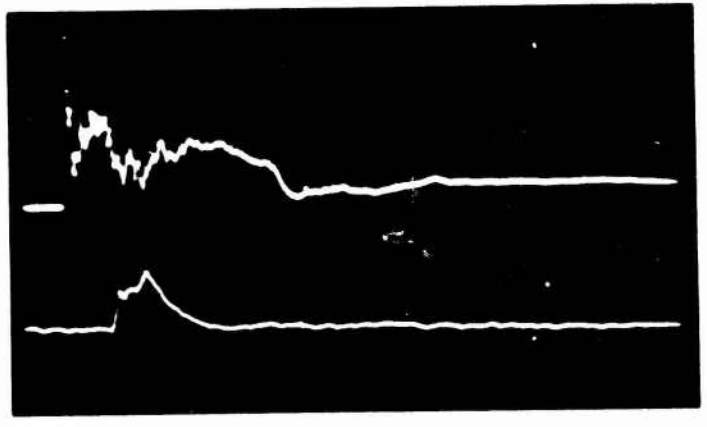

Piezoelectric Gauge, 1042 lb/in^2/div (top)
Fragment Stripper In
Current Source, 4545 lb/in2/div (bottom)

FIGURE B-4. Pressure-Time Data from a 110-Series, 1838-Gram, Pentolite Cylinder. Cylinder Dimensions, 4-inch OD by 5-inches Long. Sweep Rate 100 µsec/div.

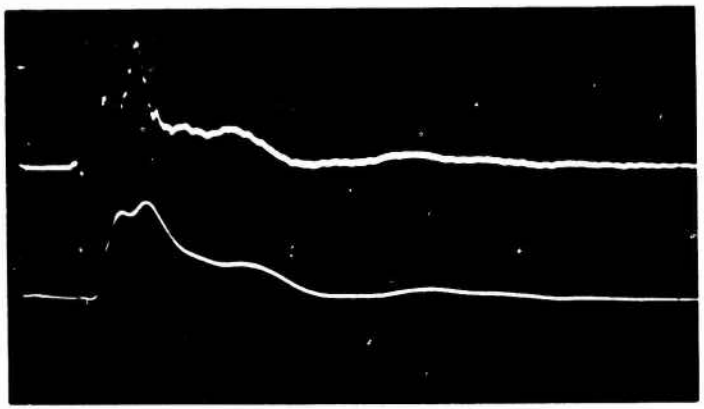

Aluminum Bar, 1724 lb/in^2/div

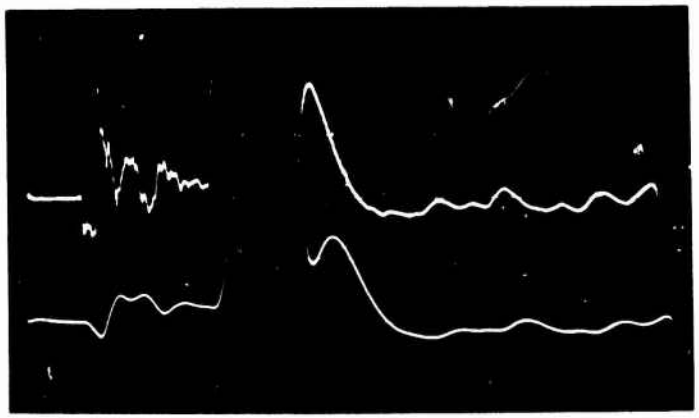

Aluminum Bar, 2000 lb/in^2/div

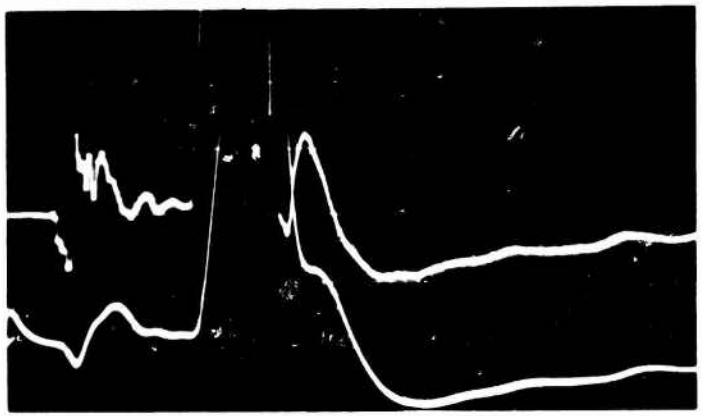

Aluminum Bar, 1923 lb/in^2/div

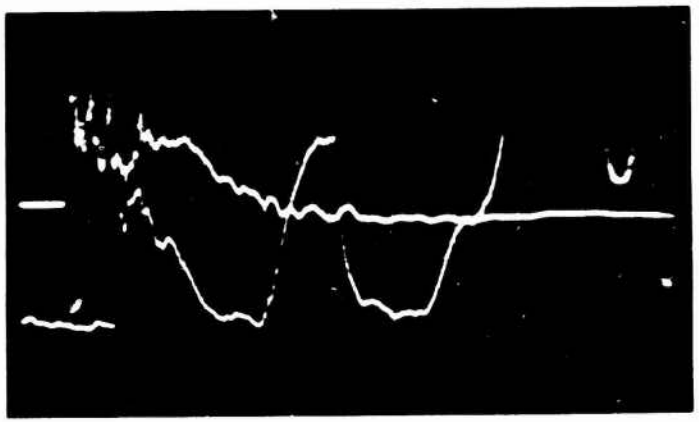

Piezoelectric Gauge, 1042 lb/in^2/div (top)
Current Source, 1810 lb/in^2/div (bottom)

FIGURE B-5. Pressure-Time Data from a 120-Series, 2112-Gram, Pentolite Cylinder. Cylinder Dimensions, 4½-inch OD by 5-inches Long. Sweep Rate 100 µsec/div.

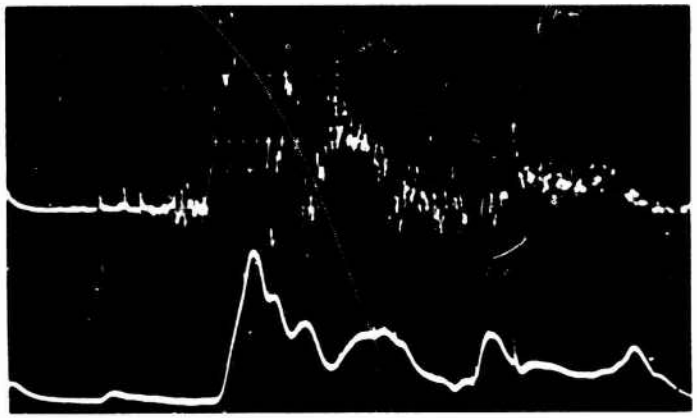

Brass Bar, 707 lb/in^2/div

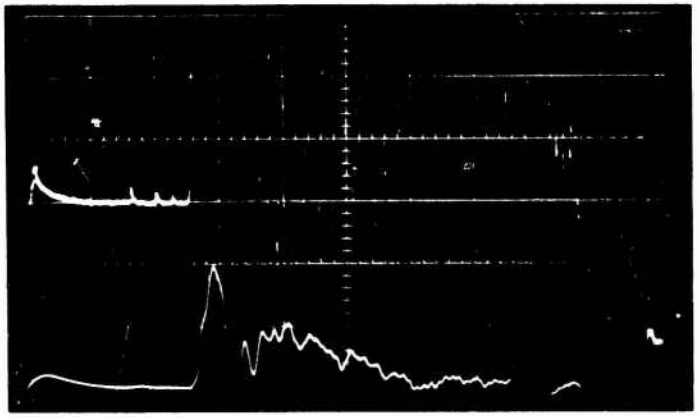

Aluminum Bar, 840 lb/in^2/div

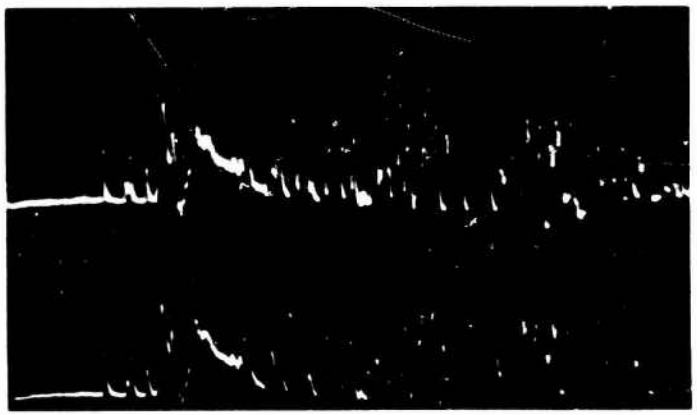

Aluminum Bar, 891 lb/in^2/div

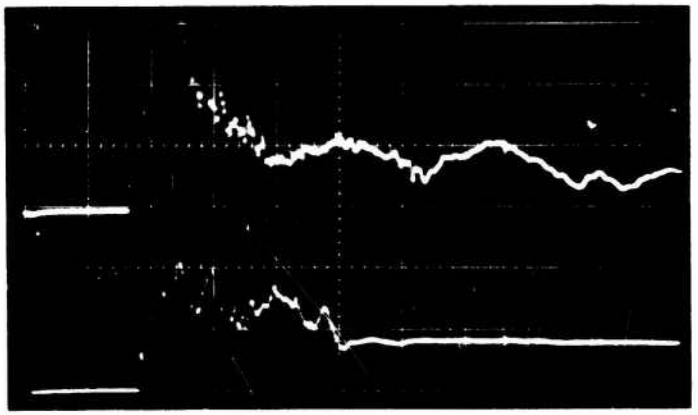

Piezoelectric Gauge #1, 1060 lb/in^2/div (top)
Piezoelectric Gauge #2, 1090 lb/in^2/div (bottom)

FIGURE B-6. Pressure-Time Data from a 64-Series, Water/Lucite Surround. Charge to Mass Ratio 0.43. Sweep Rate 100 μsec/div.

Aluminum Bar

1782 lb/in^2/div

Fragment sheared
off portion of bar

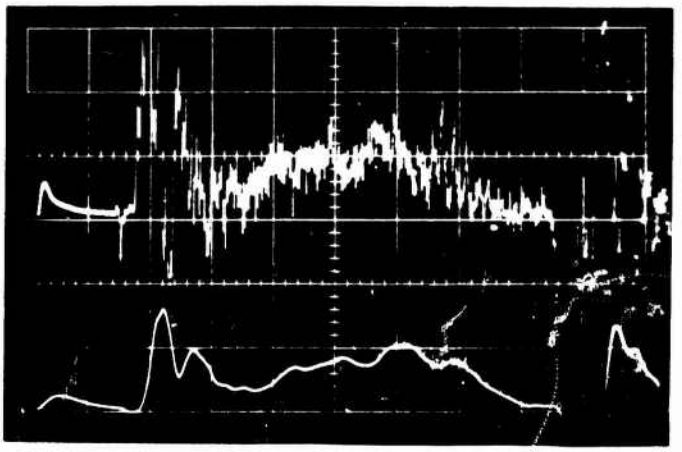

Aluminum Bar

1681 lb/in^2/div

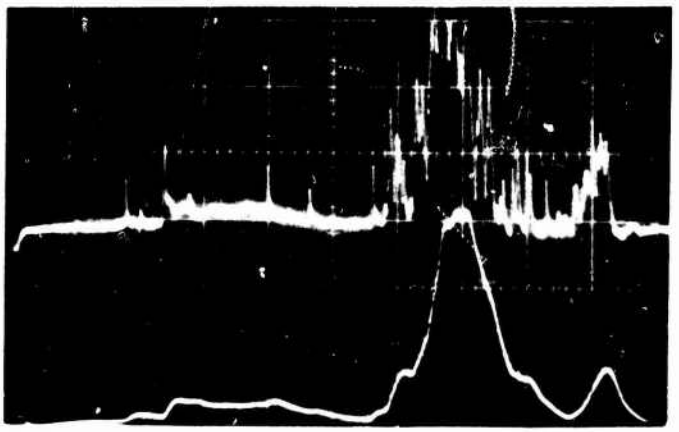

Brass Bar

2114 lb/in^2/div

FIGURE B-7. Pressure-Time Data from an80-Series, Water/Lucite Surround. Charge to Mass Ratio 0.83. Sweep Rate 100 µsec/div.

Aluminum Bar

1782 lb/in^2/div

Nylon Insert Broke

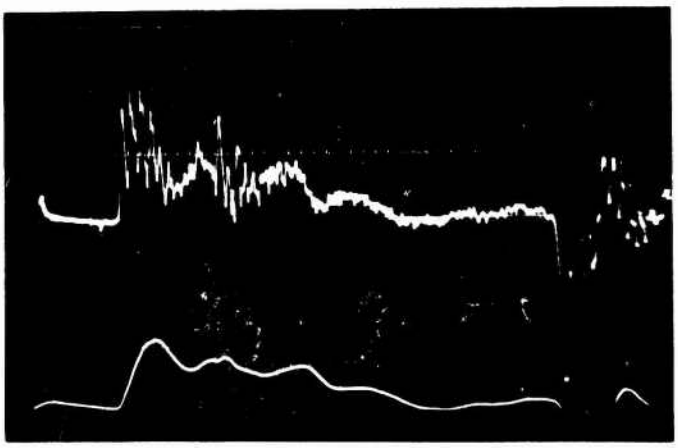

Aluminum Bar

1681 lb/in^2/div

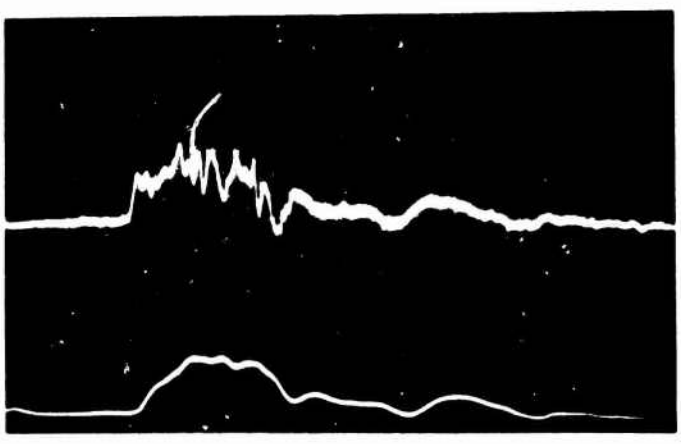

Brass Bar

2114 lb/in^2/div

FIGURE B-8. Pressure-Time Data from a 95-Series, Water/Lucite Surround. Charge to Mass Ratio 1.60. Sweep Rate 100 µsec/div.

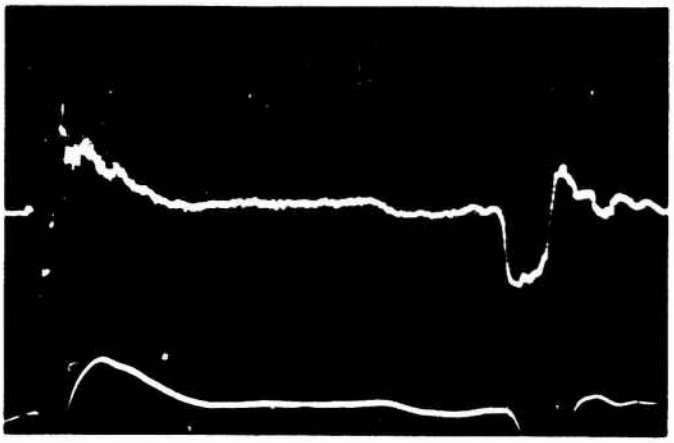

Aluminum Bar

1782 lb/in^2/div

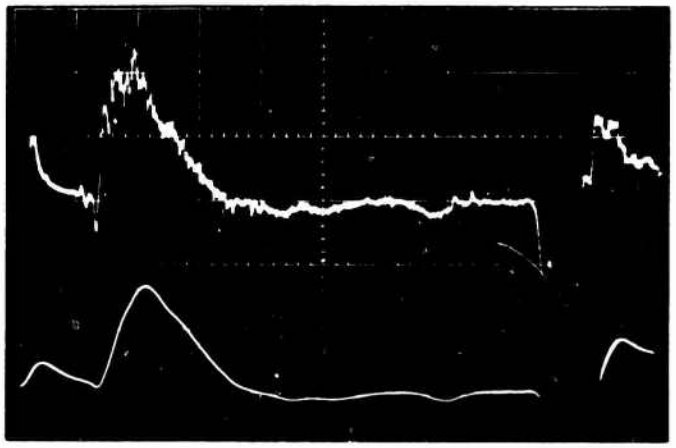

Aluminum Bar

1681 lb/in^2/div

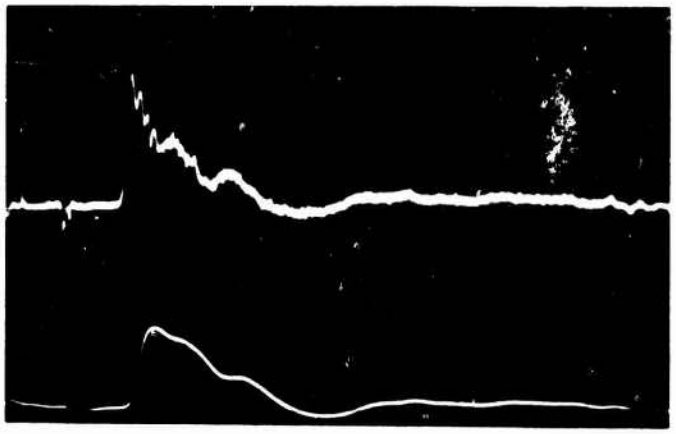

Brass Bar

2114 lb/in^2/div

FIGURE B-9. Pressure-Time Data from a 110-Series, Water/Lucite Surround. Charge to Mass Ratio 3.33. Sweep Rate 100 μsec/div.

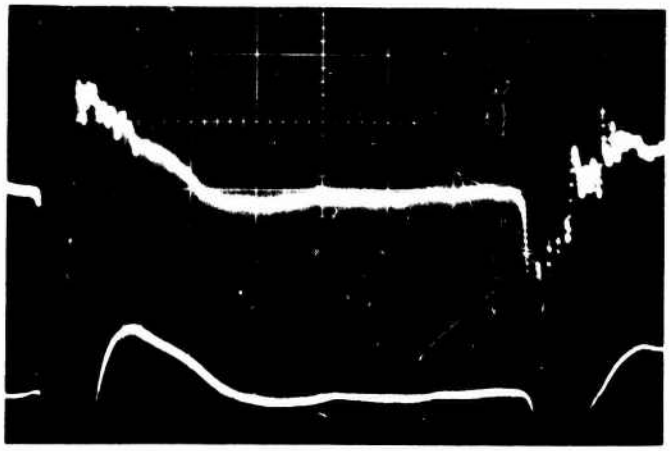

Aluminum Bar

1782 lb/in^2/div

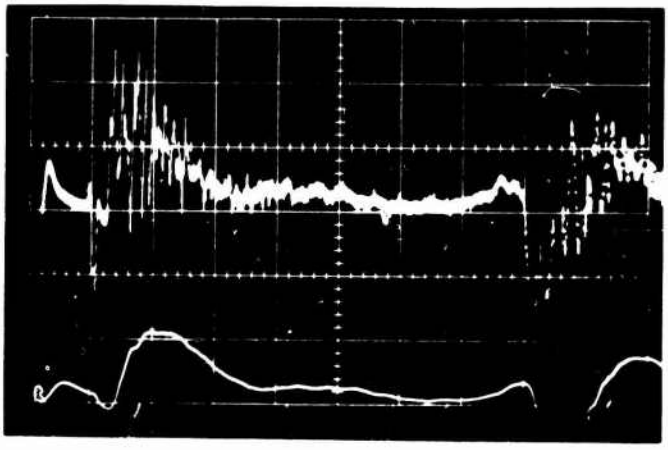

Aluminum Bar

1681 lb/in^2/div

Brass Bar

2114 lb/in^2/div

FIGURE B-10. Pressure-Time data from a 120-Series, Water/Lucite Surround. Charge to Mass Ratio 5.52. Sweep Rate 100 µsec/div.

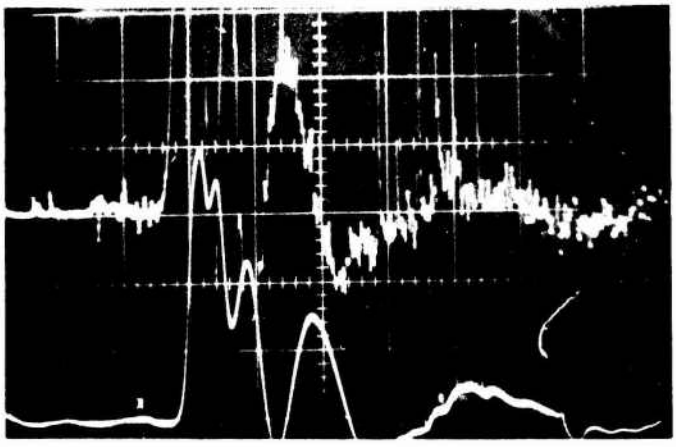

Brass Bar

707 lb/in^2/div

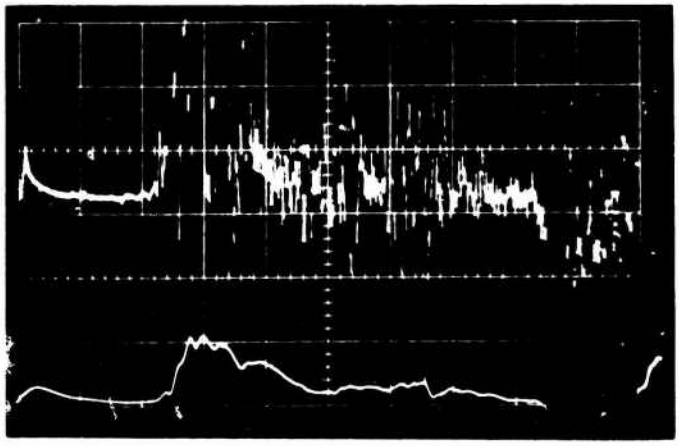

Aluminum Bar

840 lb/in^2/div

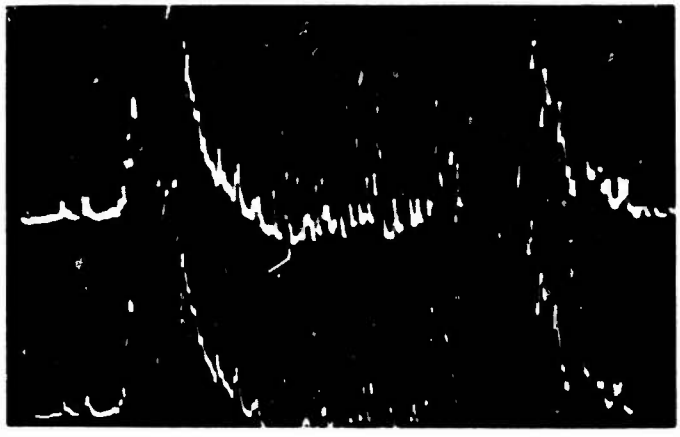

Aluminum Bar

891 lb/in^2/div

FIGURE B-11. Pressure-Time Data from a 64-Series, Ethylene Glycol/Lucite Surround. Charge-to-Mass Ratio 0.38. Sweep Rate 100 μsec/div.

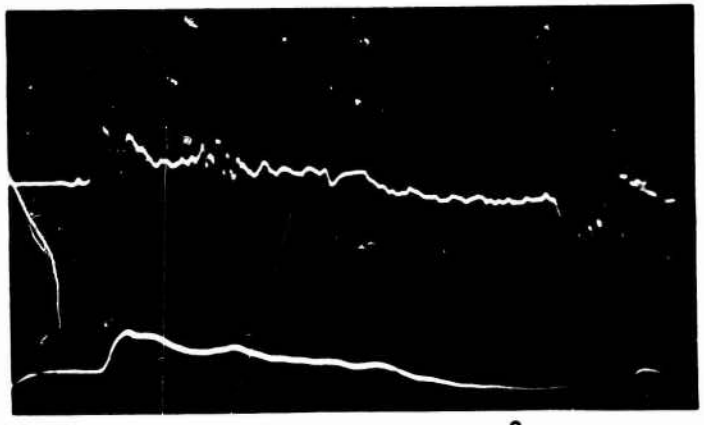

Aluminum Bar, 1782 lb/in^2/div

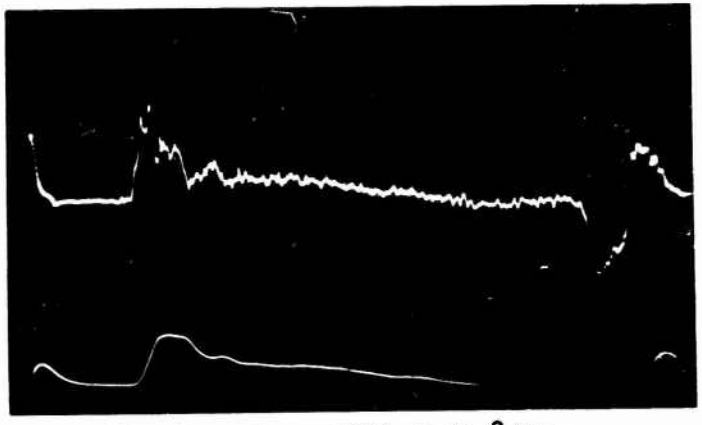

Aluminum Bar, 1681 lb/in^2/div

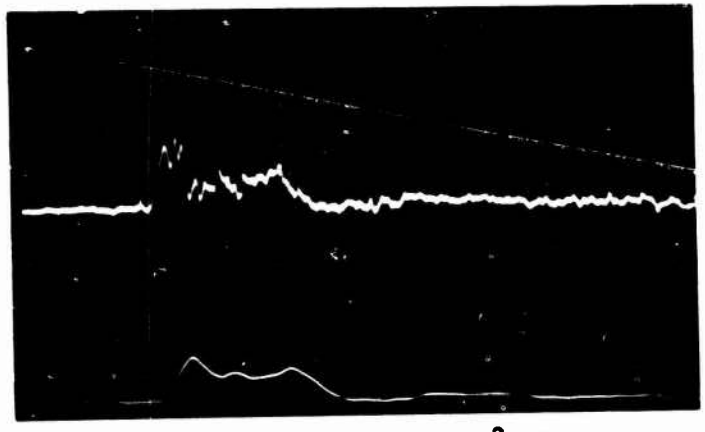

Brass Bar, 2114 lb/in^2/div

Piezoelectric Gauge, 2740 lb/in^2/div

FIGURE B-12. Pressure-Time Data from a 80-Series, Ethylene Glycol/Lucite Surround. Charge-to-Mass Ratio 0.78. Sweep Rate 100 µsec/div.

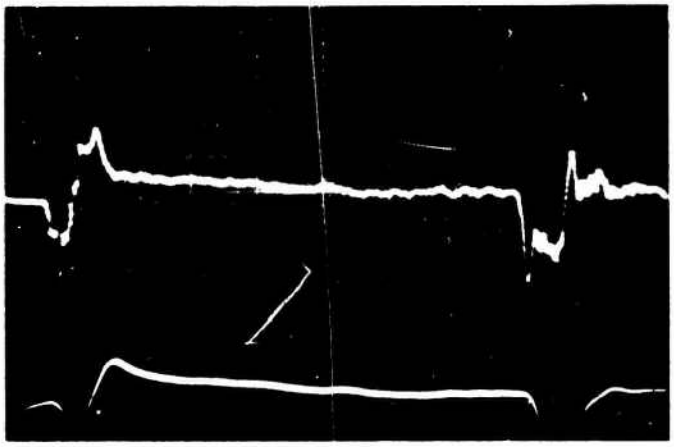

Aluminum Bar

1782 lb/in^2/div

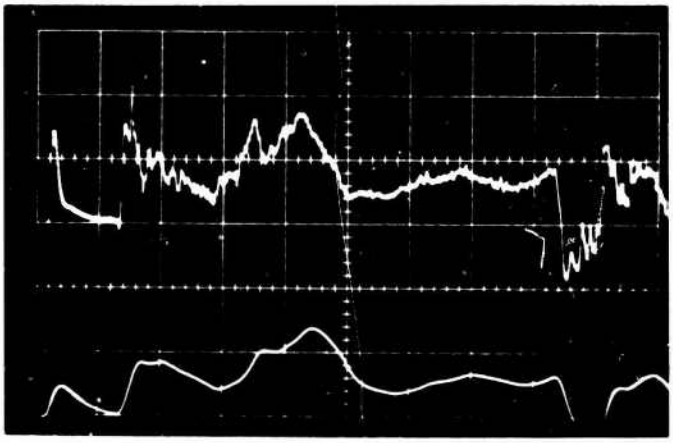

Aluminum Bar

1681 lb/in^2/div

insert broke

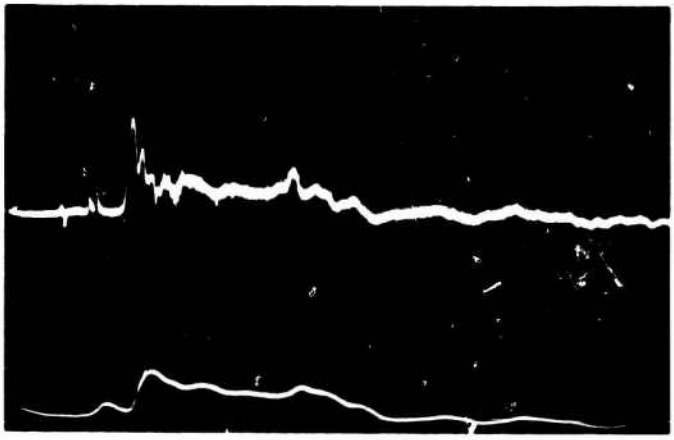

Brass Bar

2114 lb/in^2/div

insert broke

FIGURE B-13. Pressure-Time Data from a 95-Series, Ethylene Glycol Surround. Charge-to-Mass Ratio 1.40. Sweep Rate 100 μsec/div.

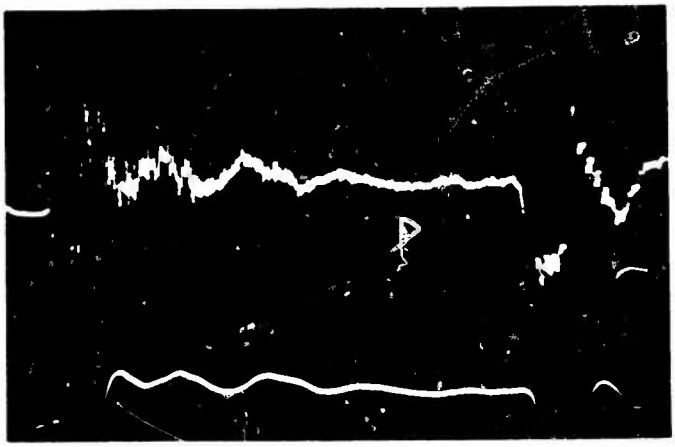

Aluminum Bar

1782 lb/in^2/div

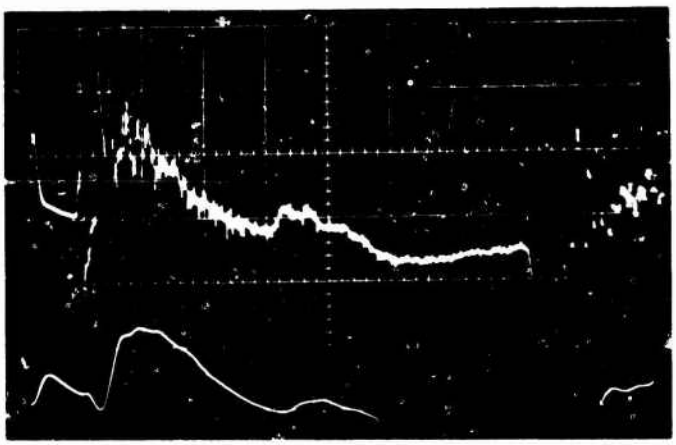

Aluminum Bar

1681 lb/in^2/div

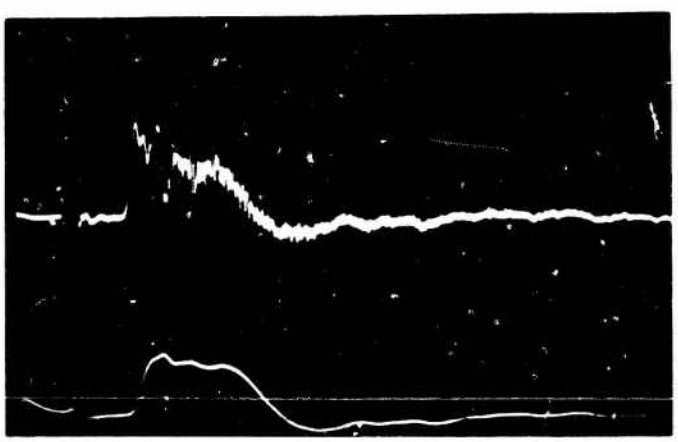

Brass Bar

2114 lb/in^2/div

FIGURE B-14. Pressure-Time Data from a 110-Series, Ethylene Glycol Surround. Charge-to-Mass Ratio 3.08. Sweep Rate 100 µsec/cm.

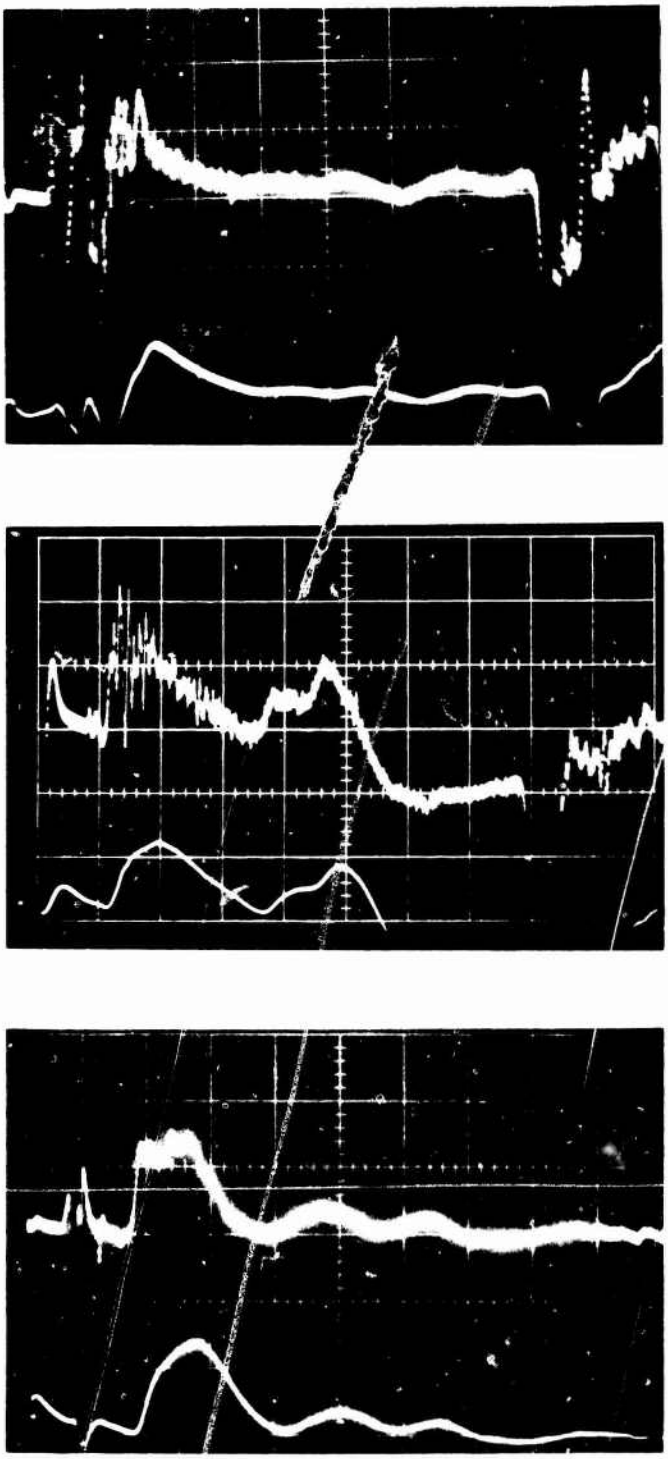

Aluminum Bar

1782 lb/in^2/div

Aluminum Bar

1681 lb/in^2/div

Brass Bar

2114 lb/in^2/div

FIGURE B-15. Pressure-Time Data from a 120-Series, Ethylene Glycol Surround. Charge-to-Mass Ratio 5.54. Sweep Rate 100 μsec/div.

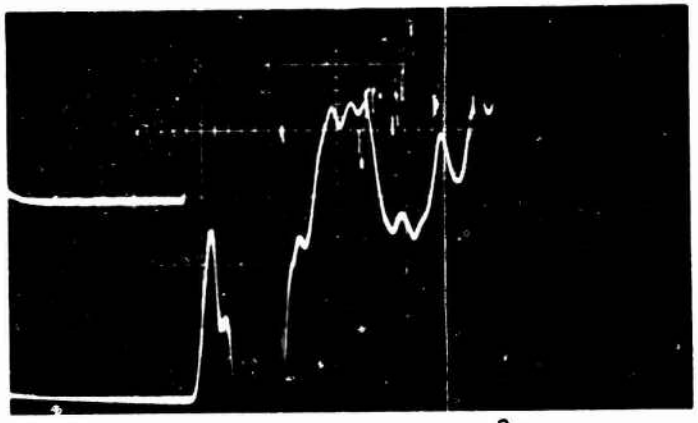

Brass Bar, 1414 lb/in^2/div

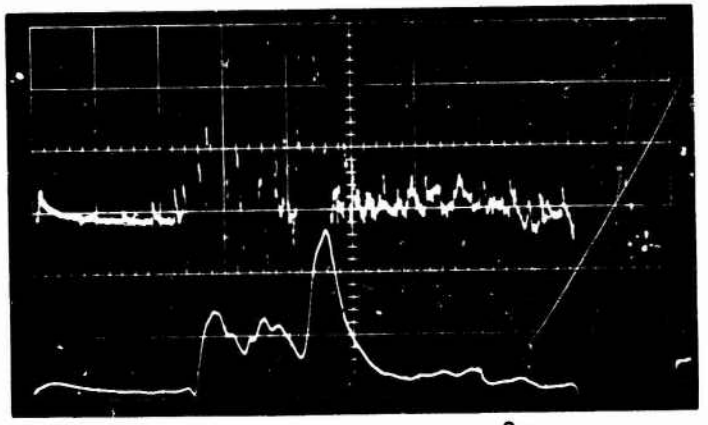

Aluminum Bar, 1681 lb/in^2/div

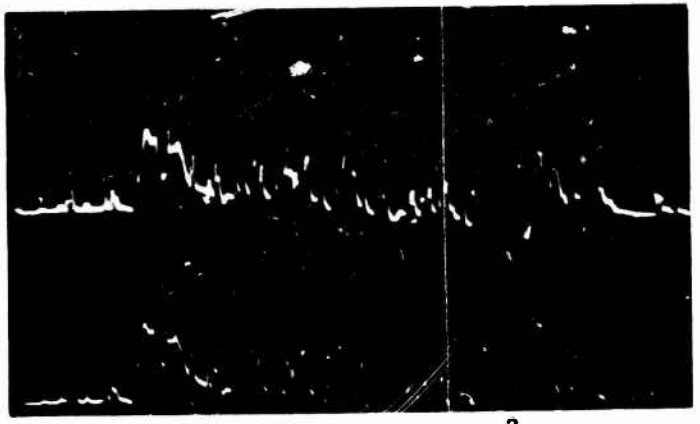

Aluminum Bar, 1782 lb/in^2/div

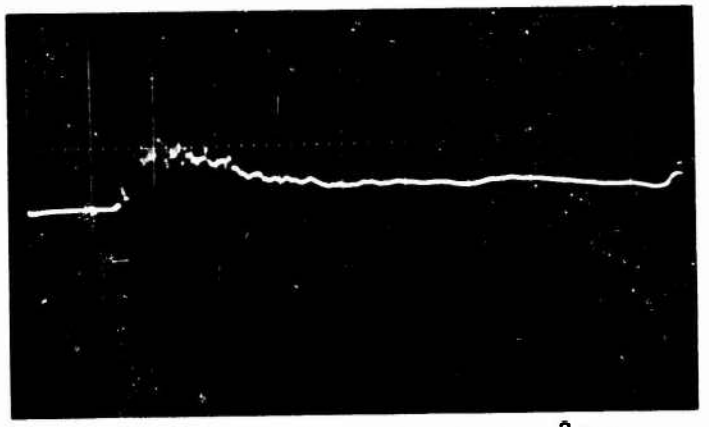

Piezoelectric Gauge, 2740 lb/in^2/div

FIGURE B-16. Pressure-Time Data from a 64-Series, Glycerol/Lucite Surround. Charge-to-Mass Ratio 0.34. Sweep Rate 100 μsec/cm.

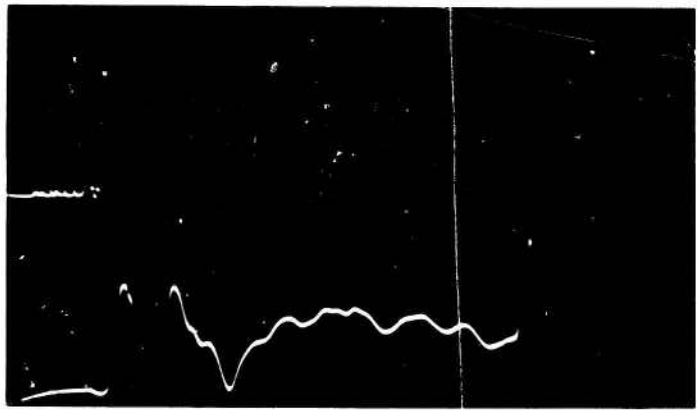

Aluminum Bar, 1782 lb/in^2/div

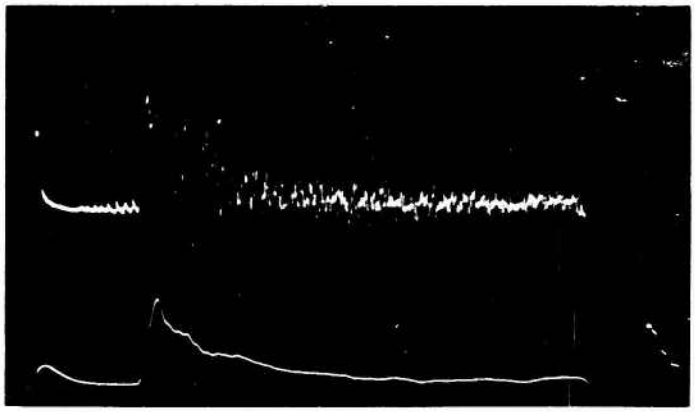

Aluminum Bar, 1681 lb/in^2/div

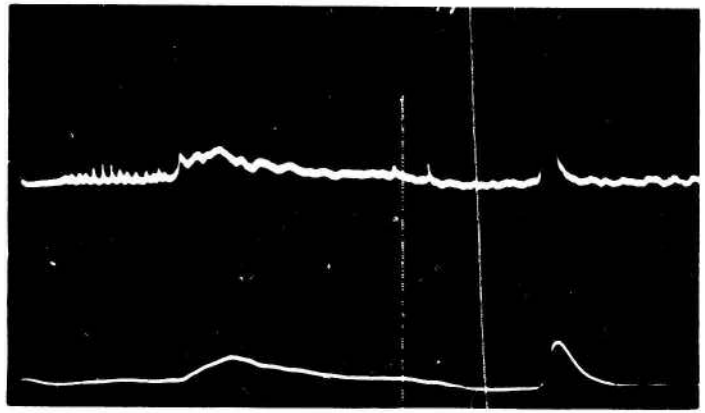

Brass Bar, 2114 lb/in^2/div

Piezoelectric Gauge, 2740 lb/in^2/div

FIGURE B-17. Pressure-Time Data from a 80-Series, Glycerol/Lucite Surround. Charge-to-Mass Ratio 0.70. Sweep Rate 100 µsec/cm.

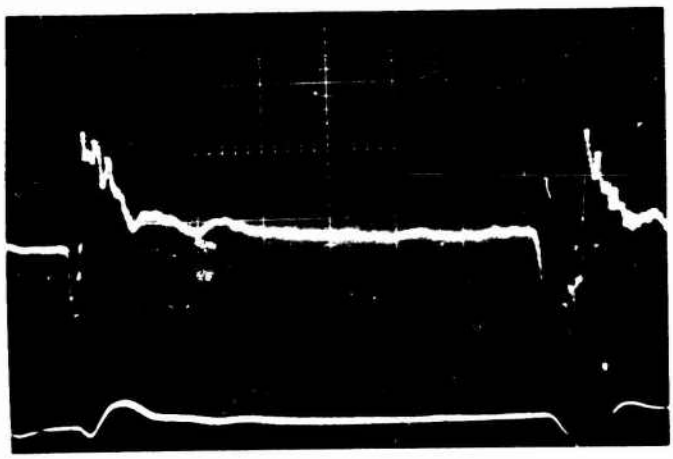

Aluminum Bar

1782 lb/in^2/div

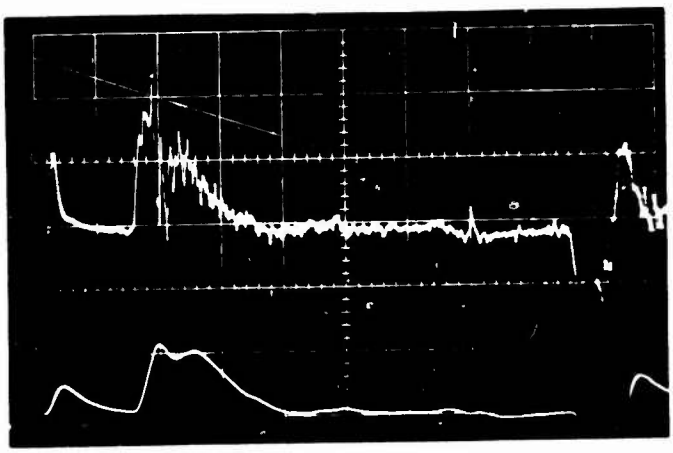

Aluminum Bar

1681 lb/in^2/div

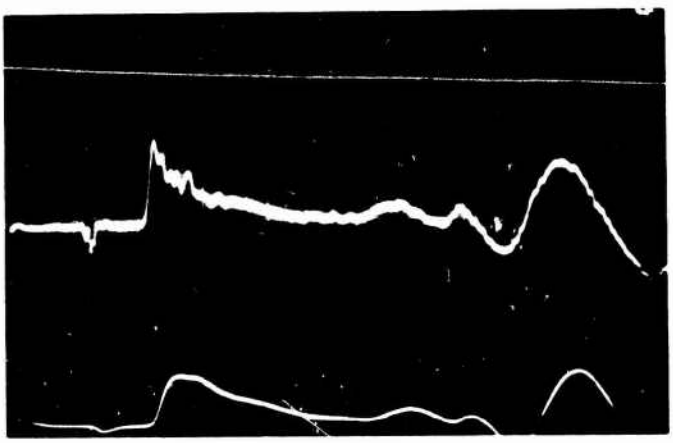

Brass Bar

2114 lb/in^2/div

FIGURE B-18. Pressure-Time Data from a 95-Series, Glycerol/Lucite Surround. Charge-to-Mass Ratio 1.27. Sweep Rate 100 μsec/div.

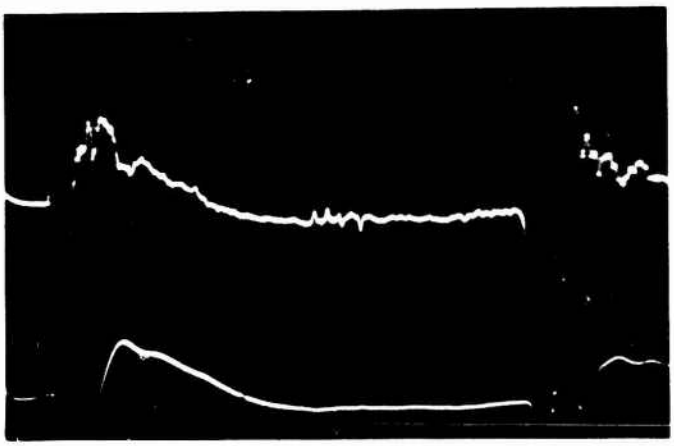

Aluminum Bar

1782 lb/in^2/div

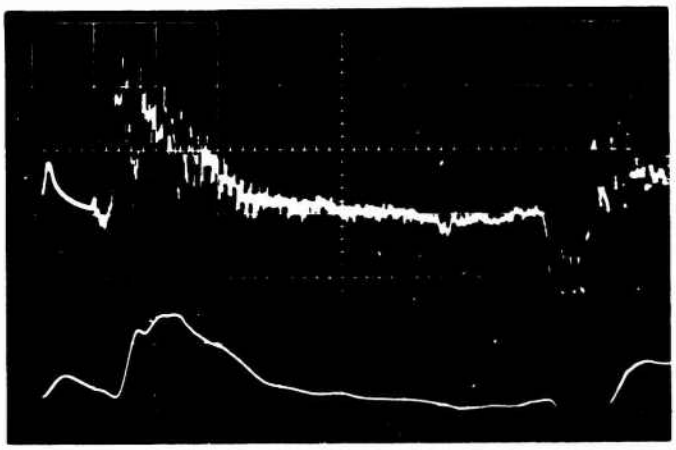

Aluminum Bar

1681 lb/in^2/div

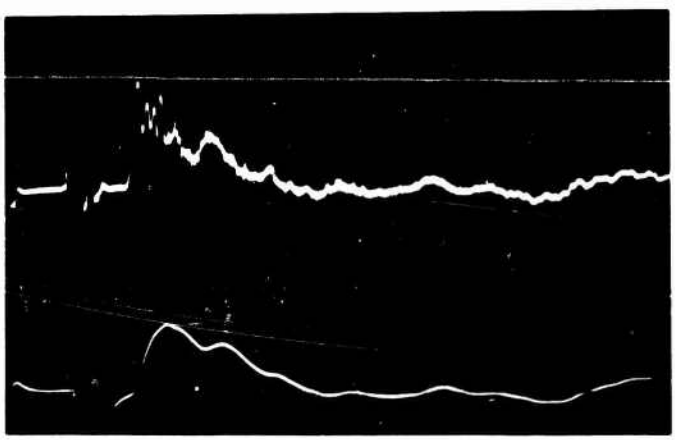

Brass Bar

2114 lb/in^2/div

FIGURE B-19. Pressure-Time Data from a 110-Series, Glycerol/Lucite Surround. Charge-to-Mass Ratio 2.88. Sweep Rate 100 μsec/div.

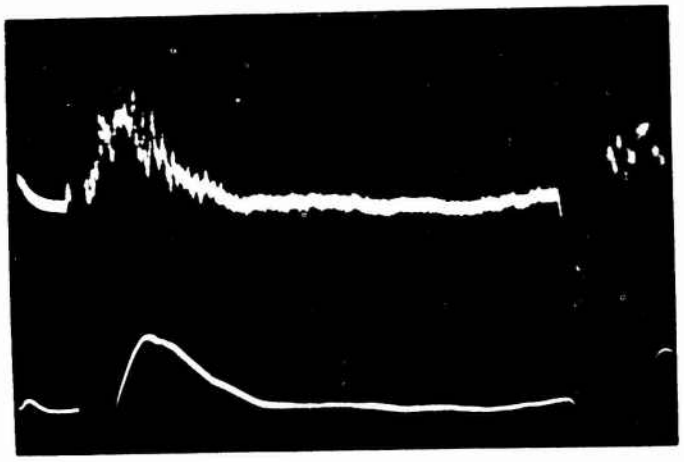

Aluminum Bar

1782 lb/in^2/div

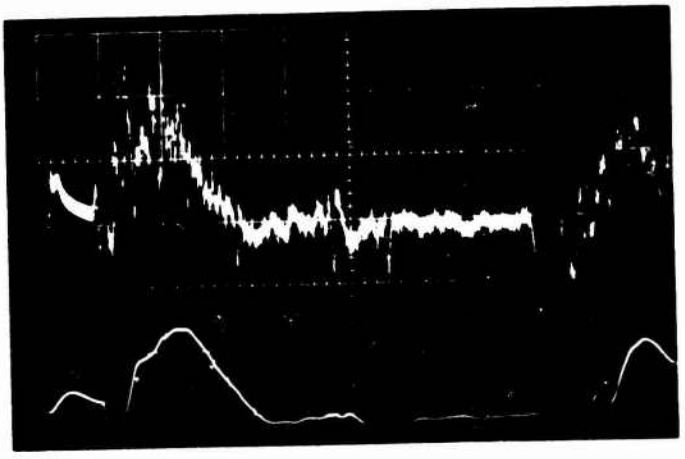

Aluminum Bar

1681 lb/in^2/div

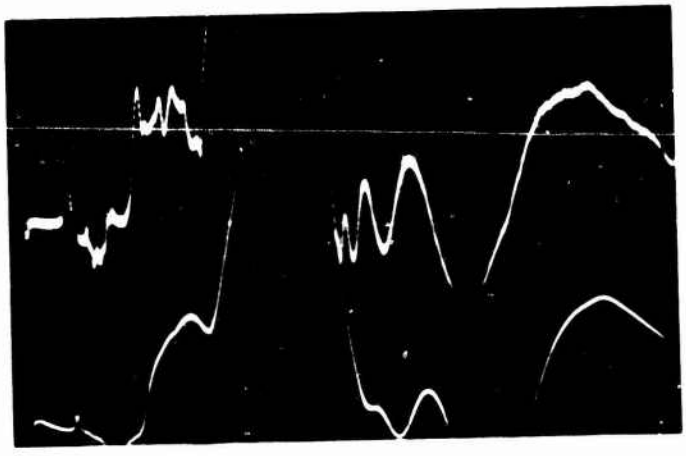

Brass Bar

2114 lb/in^2/div

FIGURE B-20. Pressure-Time Data from a 120-Series Glycerol/Lucite Surround. Charge-to-Mass Ratio 5.06. Sweep Rate 100 µsec/div.

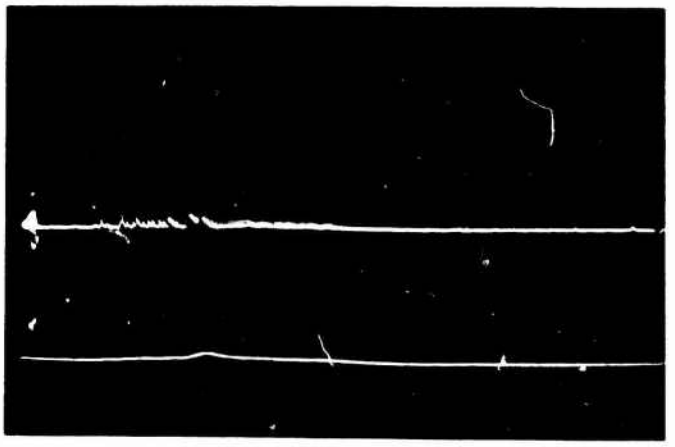

Steel Bar

20,000 lb/in^2/div

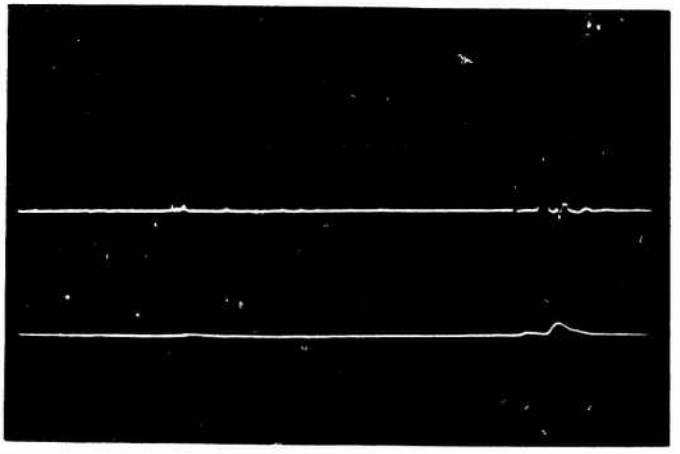

Steel Bar

22,222 lb/in^2/div

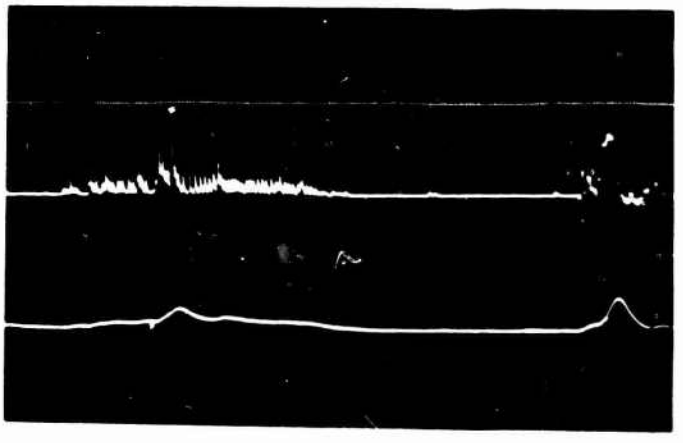

Steel Bar

22,222 lb/in^2/div

FIGURE B-21. Pressure-Time Data from a 64-Series Solder Surround. Charge-to-Mass Ratio 0.05. Sweep Rate 100 µsec/div.

Aluminum Bar

6896 lb/in^2/div

Steel Bar

22,222 lb/in^2/div

Aluminum Bar

7692 lb/in^2/div

FIGURE B-22. Pressure-Time Data from a 80-Series Solder Surround. Charge-to-Mass Ratio 0.10. Sweep Rate 100 µsec/div.

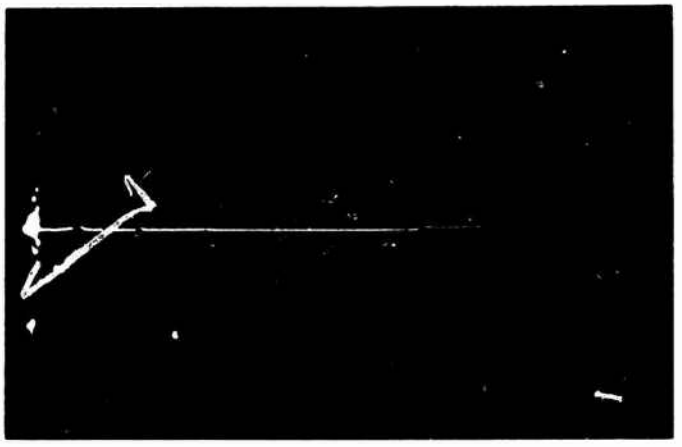

Aluminum Bar

6896 lb/in^2/div

Steel Bar

22,222 lb/in^2/div

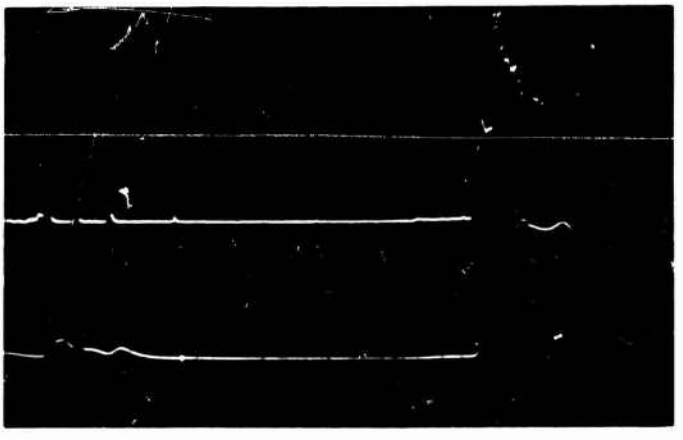

Aluminum Bar

7692 lb/in^2/div

FIGURE B-23. Pressure-Time Data from a 95-Series Solder Surround. Charge-to-Mass Ratio 0.18. Sweep Rate 100 µsec/div.

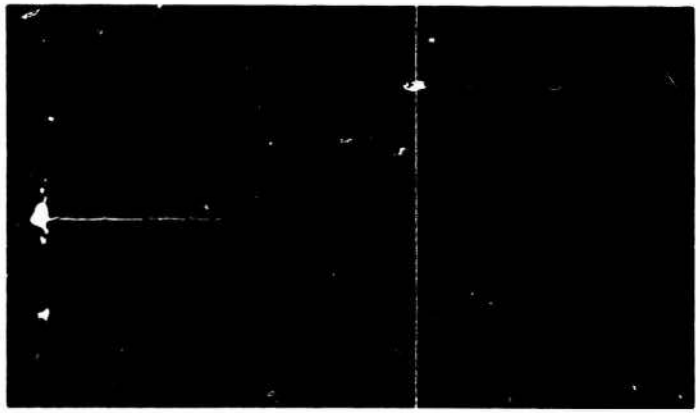

Aluminum Bar, 6896 lb/in^2/div

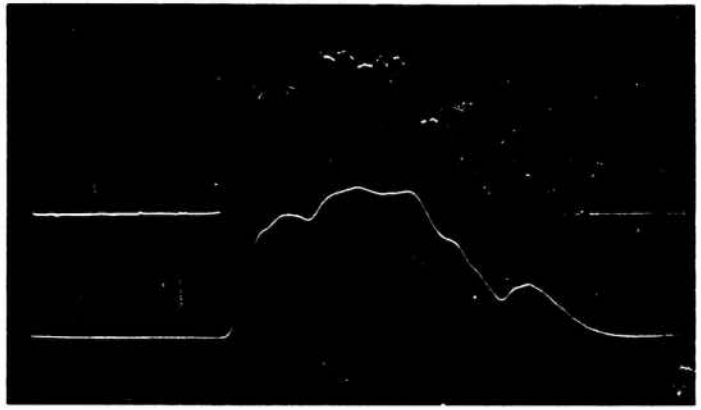

Steel Bar, 22,222 lb/in^2/div

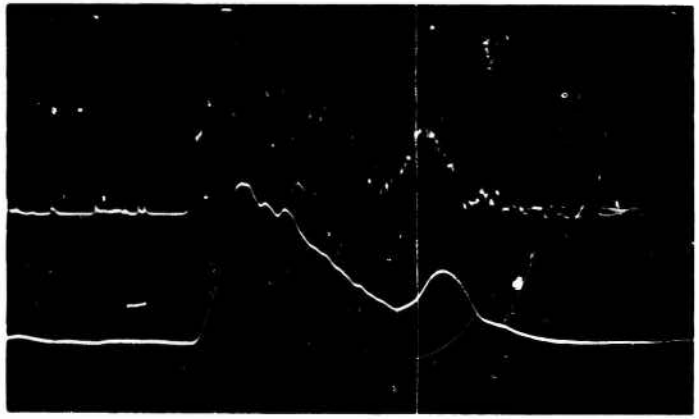

Aluminum Bar, 7692 lb/in^2/div

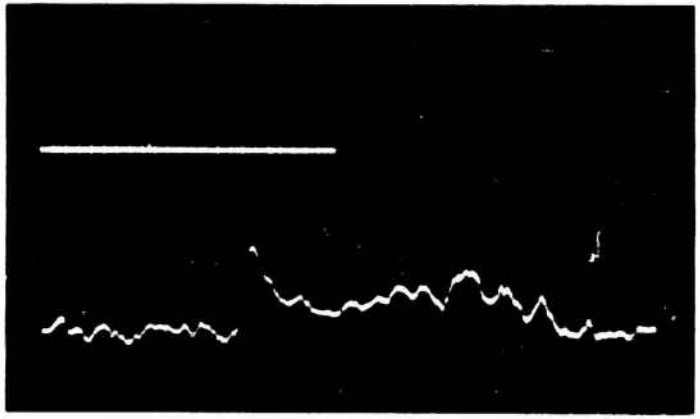

Brass Bar, 977 lb/in^2/div
Fragment Stripper In

FIGURE B-24. Pressure-Time Data from a 110-Series Solder Surround. Charge-to-Mass Ratio 0.40. Sweep Rate 100 μsec/div.

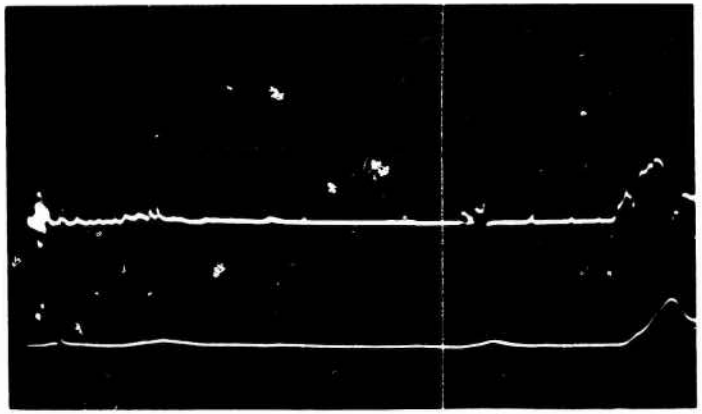

Steel Bar, 20,000 lb/in^2/div

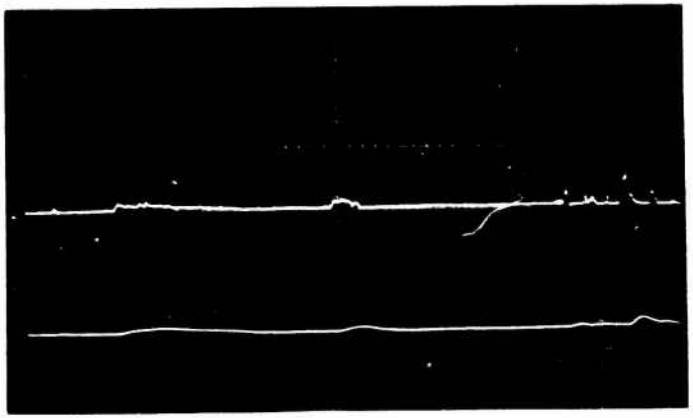

Steel Bar, 22,222 lb/in^2/div

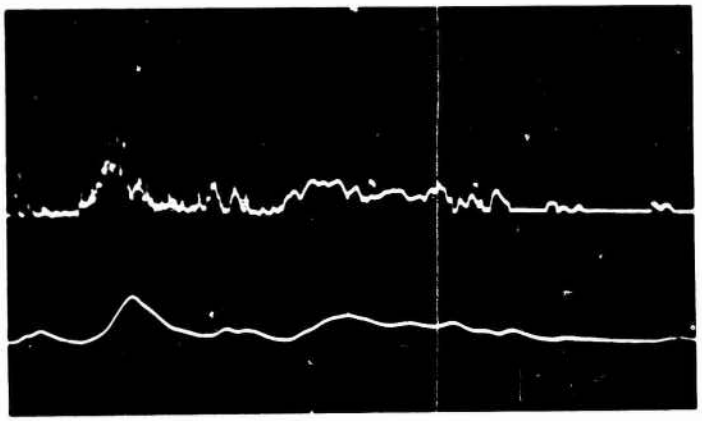

Steel Bar, 22,222 lb/in^2/div

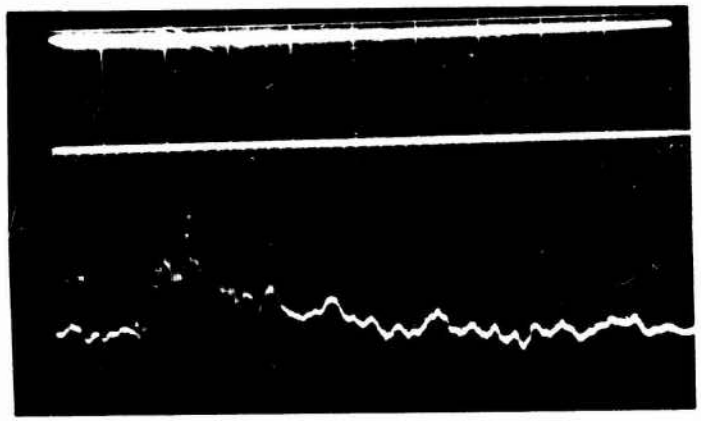

Current Source, Brass Bar, 905 lb/in^2/div
Frag. Stripper In, Sweep Rate 200 µsec/div

FIGURE B-25. Pressure-Time Data from a 120-Series Solder Surround. Charge-to-Mass Ratio 0.73. Sweep Rate 100 µsec/div.

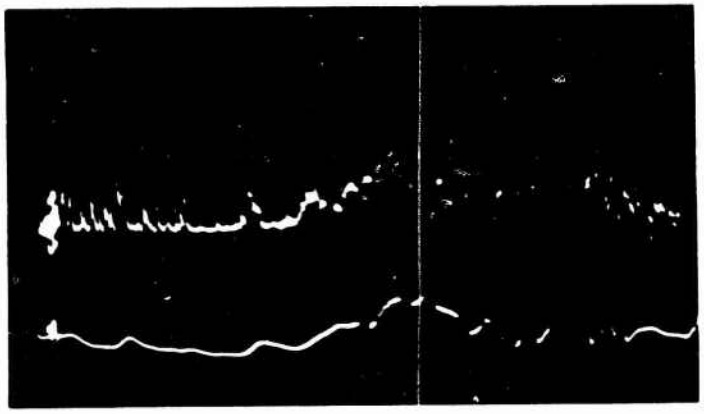

Steel Bar, 10,000 lb/in^2/div

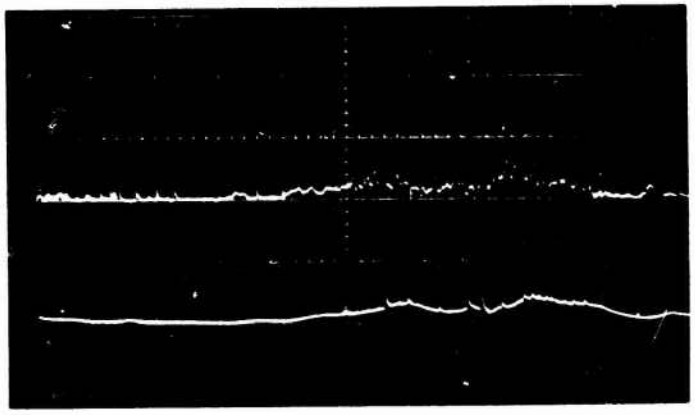

Steel Bar, 11,111 lb/in^2/div

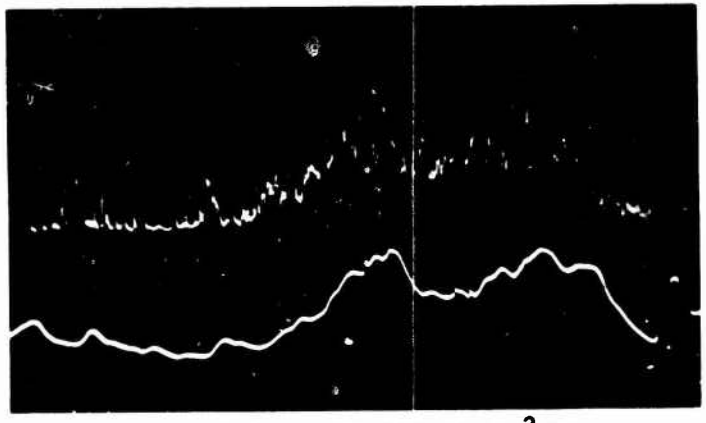

Steel Bar, 22,222 lb/in^2/div

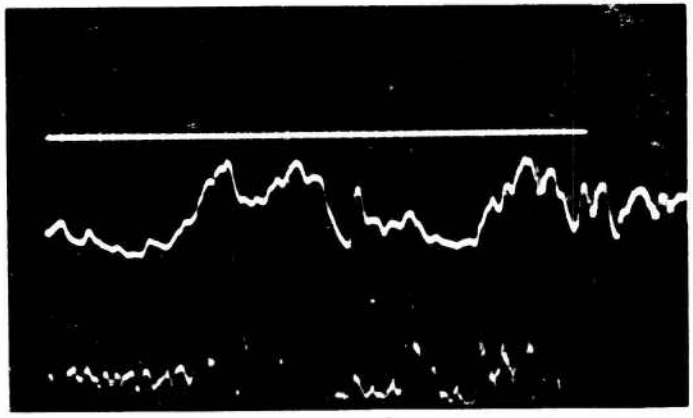

Steel Bar, 22,222 lb/in^2/div (top)
Current Source, 905 lb/in^2/div (bottom)
Frag. Stripper In, Sweep Rate 200 µsec/div

FIGURE B-26. Pressure-Time Data from a 64-Series Leaded Glass Surround. Charge-to-Mass Ratio 0.09. Sweep Rate 100 µsec/div.

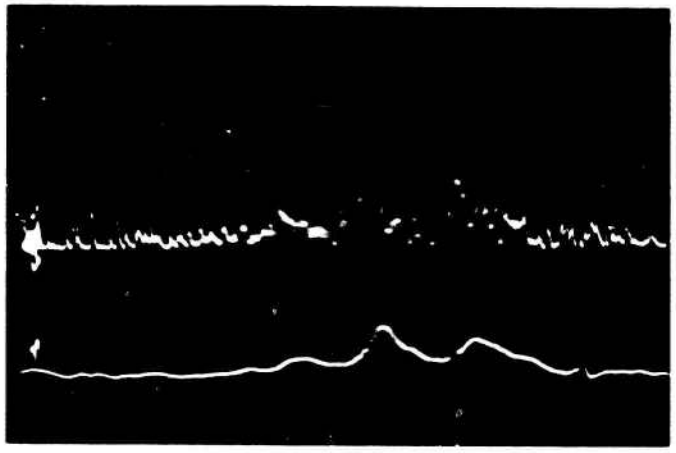

Steel Bar

20,000 lb/in^2/div

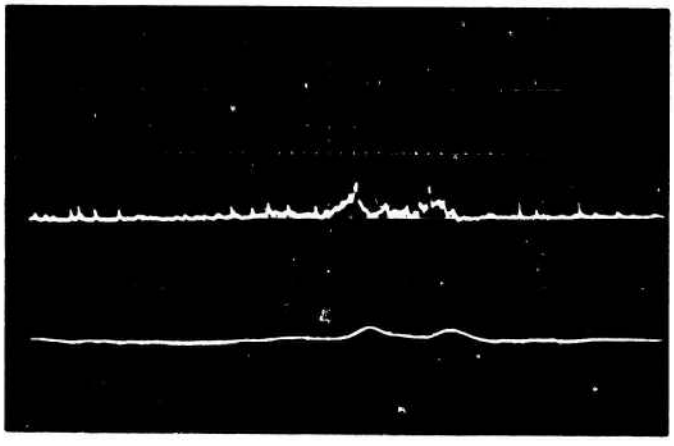

Steel Bar

22,222 lb/in^2/div

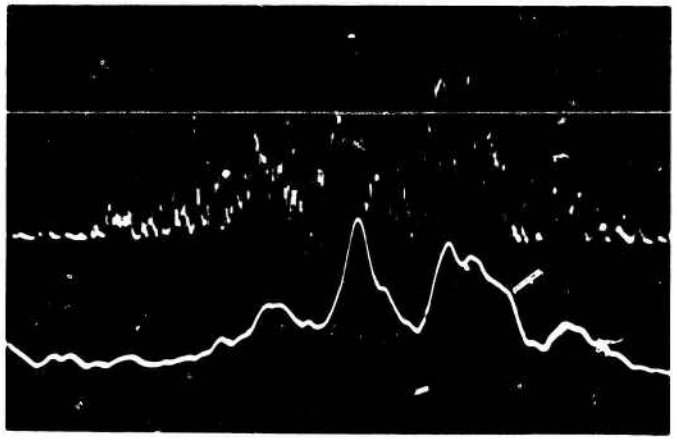

Steel Bar

22,222 lb/in^2/div

FIGURE B-27. Pressure-Time Data from a 80-Series Leaded Glass Surround. Charge-To-Mass Ratio 0.14. Sweep Rate 100 μsec/div.

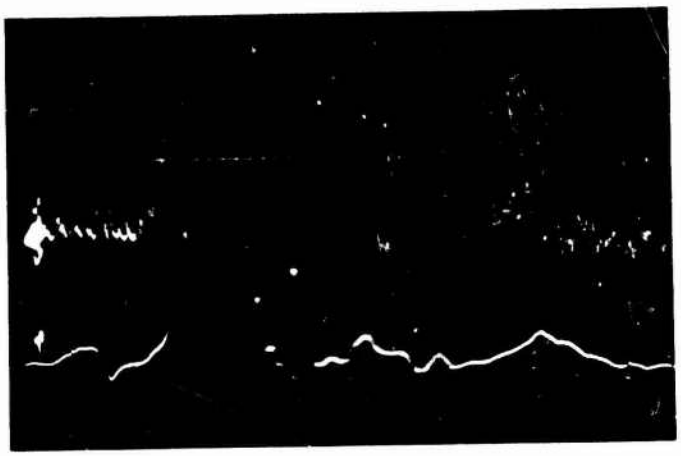

Steel Bar

10,000 lb/in^2/div

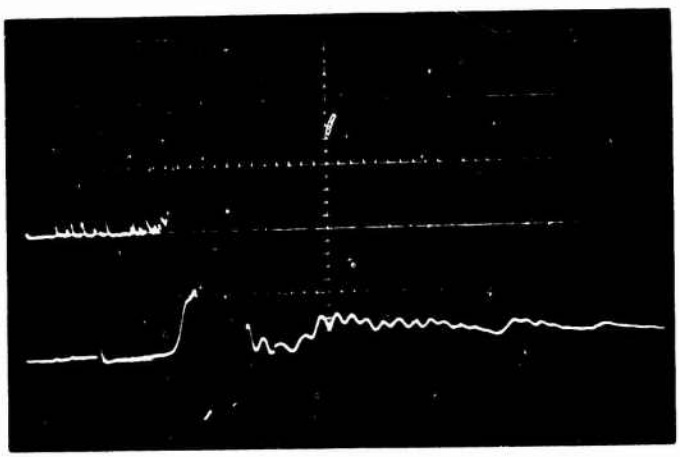

Steel Bar

11,111 lb/in^2/div

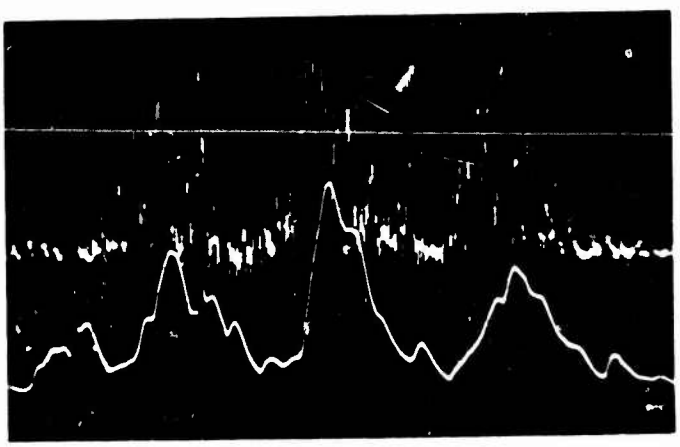

Steel Bar

11,111 lb/in^2/div

FIGURE B-28. Pressure-Time Data from a 110-Series Leaded Glass Surround. Charge-to-Mass Ratio 0.57. Sweep Rate 100 μsec/div.

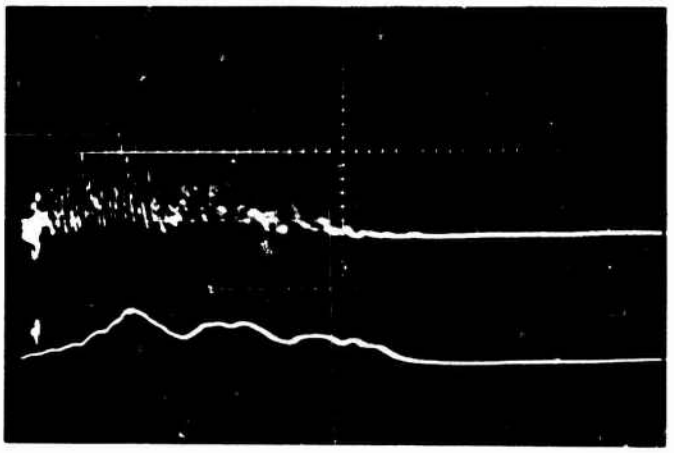

Steel Bar

10,000 lb/in^2/div

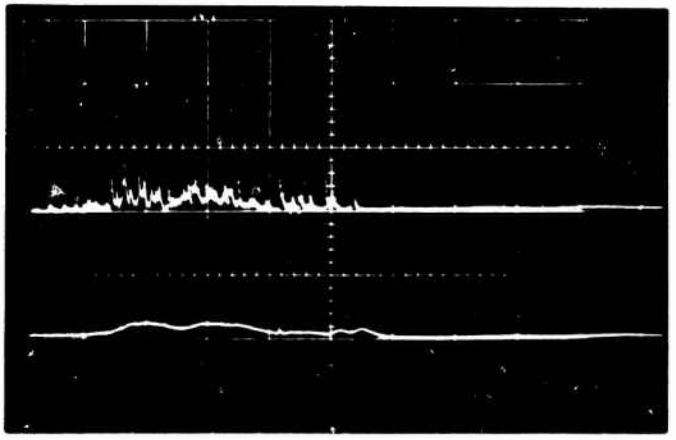

Steel Bar

11,111 lb/in^2/div

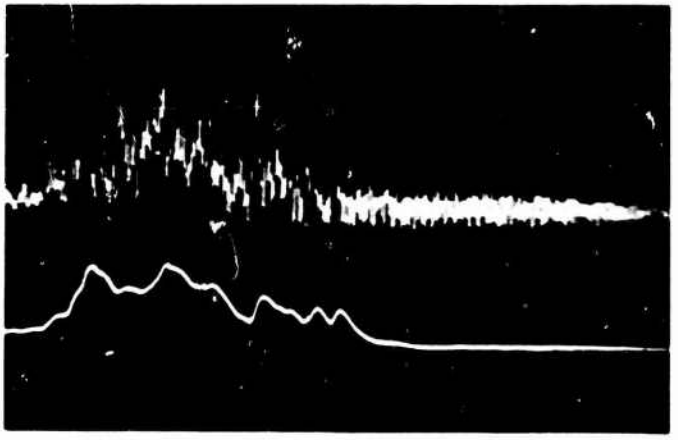

Steel Bar

11,111 lb/in^2/div

FIGURE B-29. Pressure-Time Data from a 120-Series Leaded Glass Surround. Charge-to-Mass Ratio 1.05. Sweep Rate 100 µsec/div.

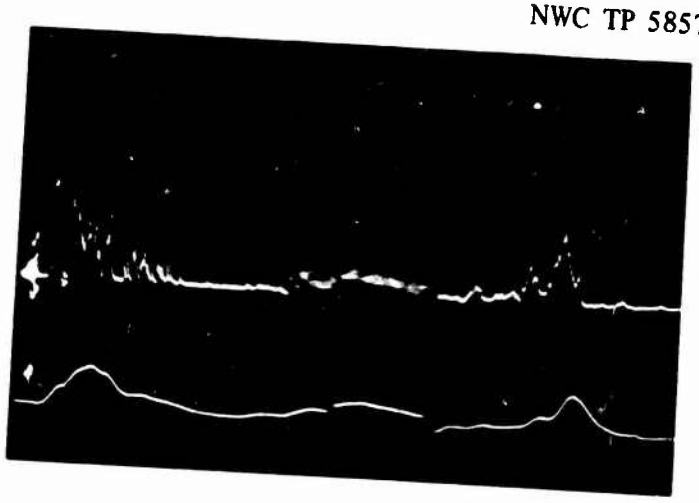

Steel Bar

10,000 lb/in^2/div

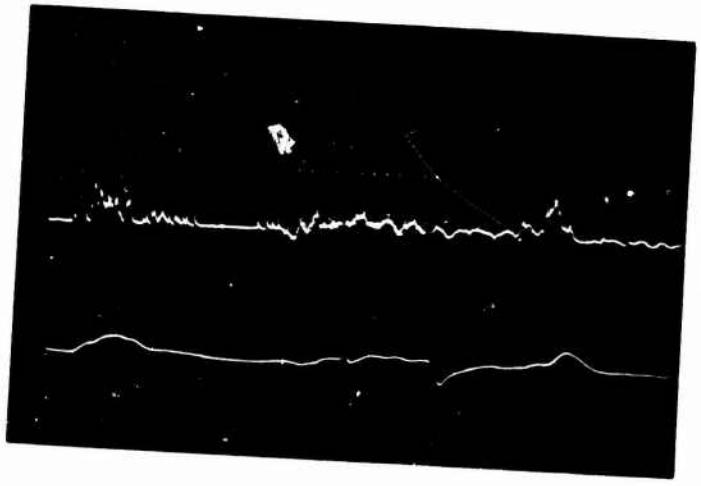

Steel Bar

5555 lb/in^2/div

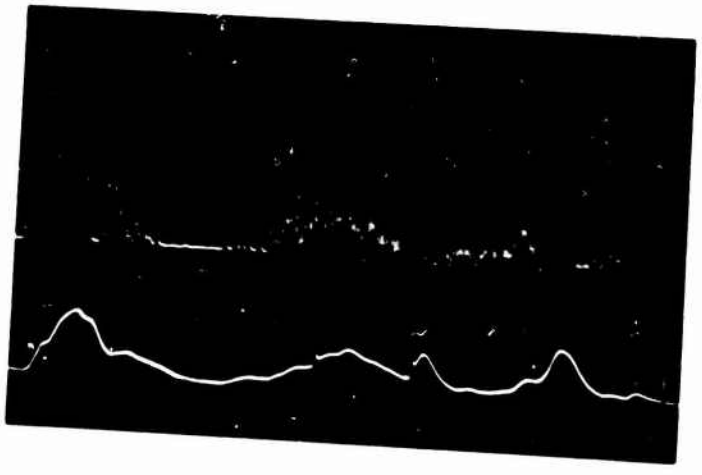

Steel Bar

22,222 lb/in^2/div

FIGURE B-30. Pressure-Time Data from a 64-Series Glass Surround. Charge-to-Mass Ratio 0.015. Sweep Rate 100 µsec/div.

Steel Bar

10,000 lb/in^2/div

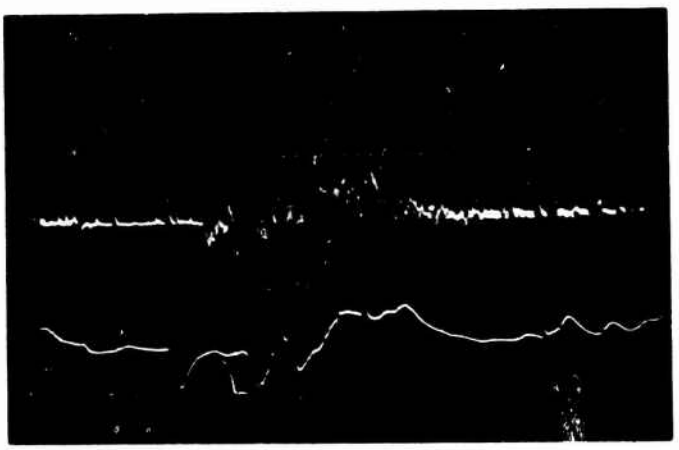

Steel Bar

5555 lb/in^2/div

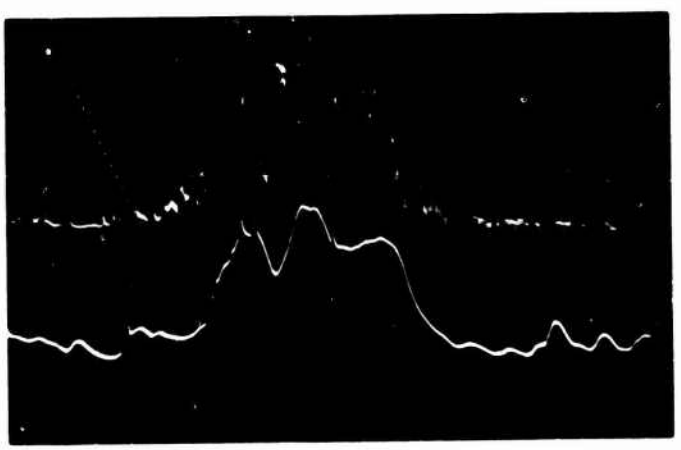

Steel Bar

22,222 lb/in^2/div

FIGURE B-31. Pressure-Time Data from a 80-Series Glass Surround. Charge-to-Mass Ratio 0.30. Sweep Rate 100 µsec/div.

Steel Bar

10,000 lb/in^2/div

Steel Bar

5555 lb/in^2/div

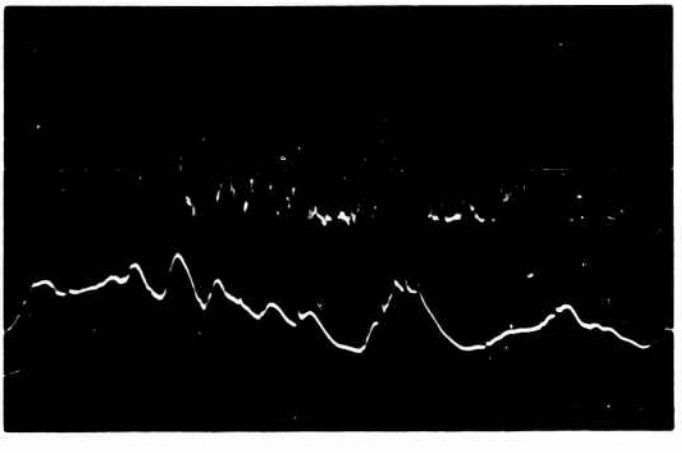

Steel Bar

22,222 lb/in^2/div

FIGURE B-32. Pressure-Time Data from a 95-Series Glass Surround. Charge-to-Mass Ratio 0.68. Sweep Rate 100 µsec/div.

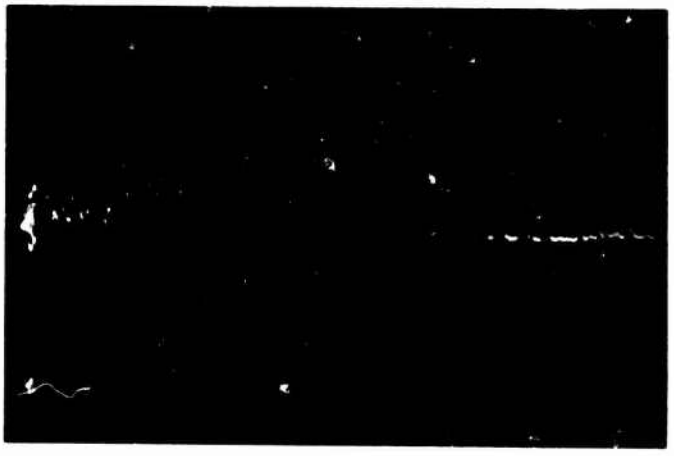

Steel Bar

2000 lb/in^2/div

Steel Bar

2222 lb/in^2/div

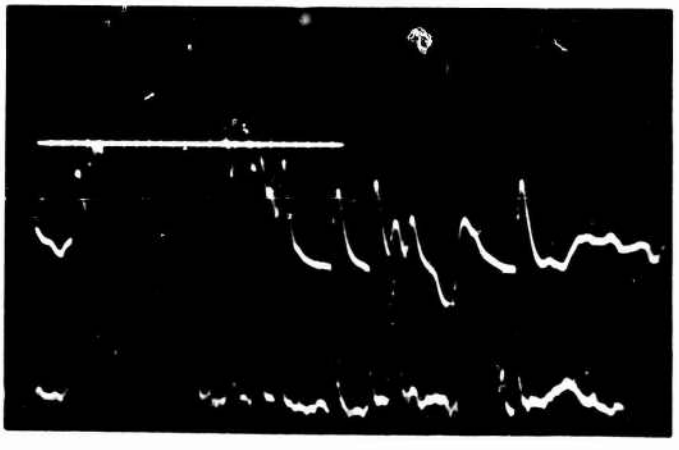

Steel Bar

5555 lb/in^2/div

Current Source

905 lb/in^2/div

FIGURE B-33. Pressure-Time Data from a 110-Series Glass Surround. Charge-to-Mass Ratio 0.97. Sweep Rate 100 µsec/div.

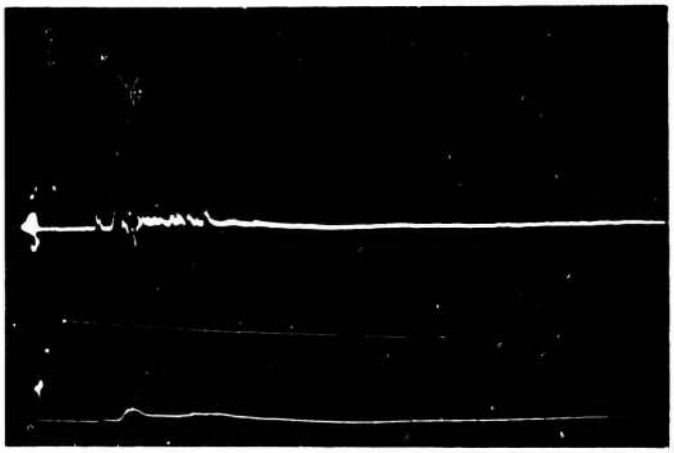

Steel Bar

10,000 lb/in^2/div

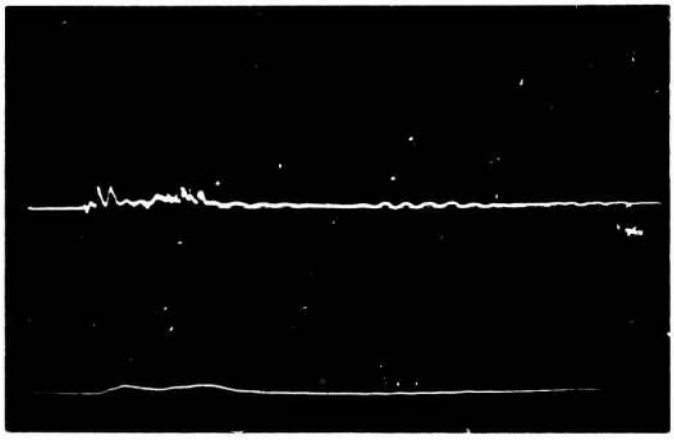

Steel Bar

11,111 lb/in^2/div

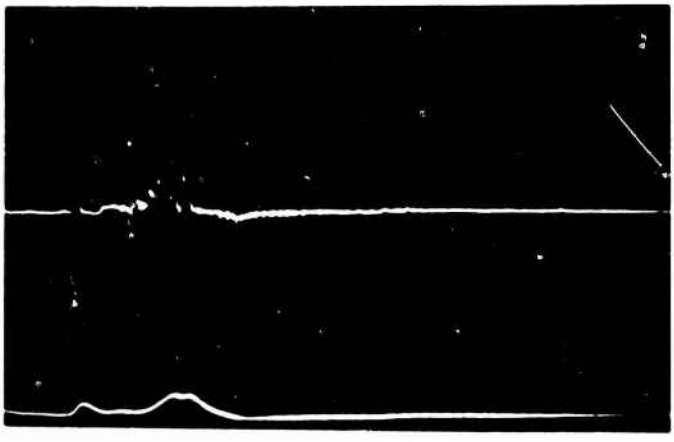

Steel Bar

11,111 lb/in^2/div

FIGURE B-34. Pressure-Time Data from a 120-Series Glass Surround. Charge-to-Mass Ratio 1.93. Sweep Rate 100 µsec/div.

INITIAL DISTRIBUTION

13 Naval Air Systems Command
- AIR-09E3A (1)
- AIR-350 (2)
- AIR-50174 (2)
- AIR-5108 (1)
- AIR-5108B (1)
- AIR-5109B1 (1)
- AIR-5109C2 (1)
- AIR-532 (1)
- AIR-5323 (1)
- AIR-5324 (1)
- AIR-53242 (1)

6 Chief of Naval Operations
- OP-03EG (1)
- OP-342 (1)
- OP-506 (1)
- OP-506F (1)
- OP-982 (1)
- OP-982E42 (1)

10 Naval Sea Systems Command
- SEA-0333 (1)
- SEA-09B4 (4)
- SEA-09G32 (2)
- SEA-6543 (1)
- SEA-6543C (1)
- PMS-40622 (1)

1 Chief of Naval Research, Arlington (ONR-461)

1 Commandant of the Marine Corps (Code AAW-1)

2 Marine Corps Development and Education Command, Quantico
- Mobility Support Division, Major Thorp (1)
- War Games Division, Marine Corps Landing Force Development Center (1)

1 Air Test and Evaluation Squadron 5

1 Naval Ammunition Depot, Earle

1 Naval Ammunition Depot, Hawthorne (Code 05, Robert Dempsey)

1 Naval Coastal Systems Laboratory, Panama City (Code 772)

1 Naval Explosive Ordnance Disposal Facility, Indian Head

1 Naval Intelligence Support Center (Code OOXA, Cdr. Jack Darnell)

1 Naval Ordnance Station, Indian Head (Technical Library)

1 Naval School Explosive Ordnance Disposal, Naval Ordnance Station, Indian Head

1 Naval Special Warfare Group, Atlantic (RDT&E)

1 Naval Special Warfare Group, Pacific (RDT&E)

12 Naval Surface Weapons Center, White Oak
- Code 0431, G. Klamm (1)
- Code ESE, S. Mason (1)
- Code GWA (1)
- Code KM (1)
- Code NS (1)
- Code T (1)
- Code W (1)
- Code WR-102, I. Kabik (1)
- Code WR-12, M. Stosz (1)
- Code WR-13, N. L. Coleburn (1)
- Code WWB (1)
- Code XWF (1)